EVALUATION OF A BRIDGE DECK WITH
CFRP PRESTRESSED PANELS UNDER FATIGUE LOAD CYCLES

by

P. Benson Shing
Kerri Anne Borlin
Gero Marzahn

Department of Civil, Environmental
& Architectural Engineering
University of Colorado
Boulder, CO 80309-0428

ACKNOWLEDGEMENTS

EXECUTIVE SUMMARY

This report summarizes a study conducted under an IBRC (Innovative Bridge Research and Construction) project sponsored by the FHWA. In this project, a bridge deck with CFRP (carbon fiber reinforced polymeric) prestressed panels and cast-in-place topping slab was designed and constructed by the Colorado Department of Transportation (CDOT) at the I-225 and Parker Road interchange southeast of Denver. To evaluate the performance of the CFRP prestressed deck, an experimental study was carried out on a model deck.

The main objectives of the study were to evaluate the strength and long-term performance of CFRP prestressed panels in a bridge deck, compare the behavior of bridge decks designed with the empirical and conventional methods of AASHTO, and a new limit-state design approach developed in this project, study the applicability of the AASHTO empirical method to topping slabs in bridge decks that have precast panels as stay-in-place forms, and examine the influence of lap splices between precast panels on deck cracking. To meet the last objective, part of the panels had lap splices and the rest did not. The design of the lap splices followed the normal practice of CDOT.

The model bridge deck was constructed and tested under static loads and fatigue load cycles in the Structures Laboratory of the University of Colorado. The deck was 16-ft wide and had a 30-ft long span, representing a 2/3-scale model of a three-girder deck.

The concrete slab in the deck was 6-in thick and had four distinct segments along the span. Each segment had a different design and construction. Segments A, B, and C had 3-in thick precast panels as stay-in-place forms and a 3-in topping slab. One side of the deck had CFRP prestressed panels, while the other had steel prestressed panels. Except for the scaling, both types of panels were designed in the same way as those in the I-225 bridge. The topping slab in

segment A was designed with the empirical method of the AASHTO LRFD Specifications, while that in segment B was designed with the conventional method of AASHTO. The topping slab in segment C was designed with a new limit-state method that accounts for girder deflections and the arching mechanism of the concrete slab. Segment D was entirely cast in place and was designed with the empirical method.

The topping slabs for Segments A and C of the deck, which were designed with the AASHTO empirical method and the new limit-state method, respectively, had comparable quantities of negative reinforcement. They were about 70% less than that in segment B, which was designed with the AASHTO conventional method. Segment D, which was entirely cast in place, had a total reinforcement that was 28% of that required by the AASHTO conventional method.

Results of this study indicate that CFRP bars are a viable alternative to steel tendons for precast panel construction. The portion of the bridge deck that had CFRP prestressed panels demonstrated the same performance as that with steel prestressed panels. The segments of the deck that had the topping slabs designed with the empirical method and the limit-state method exhibited the same performance as that designed with the conventional method, even though the latter required 70% more reinforcement in the topping slab. Furthermore, with the use of the empirical method, the segment (segment A) of the deck that had precast panels performed better than the full-depth cast-in-place segment (segment D) due to the enhanced strength and crack resistance introduced by the prestressed panels.

Implementation Statement

CFRP bars are a viable alternative to steel reinforcement for the construction of bridge decks. The CFRP bars used here had a modulus of elasticity comparable to that of steel, and had a very tensile high strength. The material also had a good bonding property with concrete, which makes it suitable for prestressed concrete construction. This material has already been introduced by CDOT into a bridge structure at the I-225/Parker Road interchange. Since CFRP bars are non-corrosive, the use of this material will slow down the deterioration of bridge decks and thereby, prolong the life-span of a bridge. However, the material is very costly, compared to steel, and the life-cycle cost of a bridge constructed with CFRP material should be further investigated. Furthermore, CFRP bars are more fragile than steel reinforcement, and they should be handled with care during construction. The aforementioned issues need to be resolved before the material could be widely adopted by bridge engineers.

The use of the AASHTO empirical method for the design of the topping slab of a precast panel deck does not seem to jeopardize the deck performance under fatigue load cycles. The empirical method can lead to a significant reduction of the top reinforcement in such a deck. It will not only save construction costs, but will also prolong the life-span of a bridge deck that has steel reinforcement by reducing corrosion problems. Therefore, it is recommended that the empirical method be allowed for the design of the topping slab for precast panel decks.

The limit-state design method proposed in this project will result in a reinforcement quantity that is comparable to the empirical method of AASHTO. The former is, however, a more rational approach based on a rigorous analytical procedure. With more calibration and evaluation, this method can be adopted in the design practice in the near future.

TABLE OF CONTENTS

1. INTRODUCTION

1.1. Background

Use of fiber reinforced polymers (FRP) for prestressing and reinforcing concrete structures has received increasing attention in the last decade. The benefits of using FRP tendons and bars are that they are non-corrosive, lightweight, non-conductive, magnetically neutral, and extremely strong in tension. The corrosion resistance of FRP reinforcement is highly beneficial to bridges, whose service life is often limited by the corrosion of the reinforcement.

Under the Innovative Bridge Research and Construction (IBRC) program of the FHWA, the Colorado Department of Transportation (CDOT) introduced FRP reinforcement in a bridge structure at the I-225/Parker Road interchange southeast of Denver. The bridge during construction is shown in Figures 1.1 and 1.2. In this project, precast prestressed concrete panels were used as stay-in-place forms for a bridge deck. As an exploratory project, some of the panels were prestressed with carbon fiber reinforced polymeric (CFRP) tendons and the rest with regular seven-wire steel strands. Furthermore, deformed glass fiber reinforced polymeric (GFRP) bars were used as temperature reinforcement for the panels prestressed with CFRP bars.

The primary objective of this project was to demonstrate the feasibility of using CFRP tendons in place of seven-wire steel strands for prestressed concrete panels. It was the first time CFRP bars were used in such fashion. The precast panels were supported on two cast-in-place, post-tensioned concrete box girders. A topping slab was added to the panels to form a composite bridge deck to carry the traffic. ACI 440H Draft Document (2000) was used as a guide for the design of the CFRP prestressed panels. The panel design was extremely conservative to account for the lack of well-proven design guidelines for FRP reinforced structures.

Figure 1.1 – I-225/Parker Road Bridge under Construction

Figure 1.2 – Precast Panels supported on Two Box Girders

Because of the lack of standard design provisions for FRP reinforced concrete structures, studies must be conducted to validate the load-carrying capacity of the deck panels and to examine the long-term performance of the bridge deck containing FRP reinforcement. Furthermore, the applicability of current AASHTO provisions to CFRP prestressed panels must be investigated and additional design requirements for FRP reinforcement must be identified from research results in the literature. These studies were conducted at the University of Colorado at Boulder as part of the IBRC project. The studies included the load tests of simply supported deck panels with and without topping slabs (Zylstra et al. 2001), and the evaluation of the long-term performance of such decks by testing a 30-ft. span and 16-ft. wide, 2/3-scale three-girder deck under fatigue loads. The latter study is presented in this report.

In addition to the experimental investigation, a new rational design methodology for bridge decks was proposed and investigated (Borlin 2001) in this project. Most highway bridges in the United States have slab-on-girder decks, in which steel or precast concrete girders support a reinforced concrete slab. The two components are tied together with shear connectors to allow for composite action. The main reinforcement in the deck slabs is placed perpendicular to the direction of traffic. For these decks, both the AASHTO Standard Specifications for Highway Bridges (AASHTO 1996) and the conventional method in the AASHTO LRFD Bridge Design Specifications (AASHTO 1998), result in two dense reinforcement mats, one in the top of the slab and one in the bottom.

Numerous studies (deV. Batchelor et al. 1972, 1978; Cao et al. 1996) have shown that the tensile stresses in the top of a deck induced by negative moments are usually extremely small. This phenomenon has been attributed to two factors: girder deflections and arching action.

By accounting for a lower negative bending moment in a deck induced by girder deflections and taking into account the increased moment resistance developed from the arching action, the quantity of reinforcement in a deck slab can be significantly reduced. Many advantages are associated with reduced reinforcement. First, the construction costs will be lowered, including both the material and labor costs. This is especially attractive for FRP reinforced bridge decks. For the case of steel reinforced bridge decks, the service life will be extended and typical maintenance problems associated with concrete spalling and reinforcement corrosion will be minimized.

In an effort to minimize the reinforcement used in a bridge deck, a method referred to as the Ontario Method was developed in the 1970's. The method considers the capacity of a deck provided by the arching action. It was officially adopted as part of the Ontario Highway Bridge

Design Code (1991), and later, after minor modifications, adopted into the 1994 AASHTO Specifications as the empirical method. These methods specify a minimum quantity of reinforcement to be provided in both directions in the top and bottom of a slab, given that a series of design conditions are met.

Although the Ontario and AASHTO empirical methods allow for a reduction in the reinforcement in a bridge deck, they lack an analytical approach to account for the true behavior of a deck, namely, the girder deflections, arching action, and punching shear, in a rational manner. Furthermore, the use of the empirical method is not allowed by AASHTO for bridge decks that have precast prestressed panels as stay-in-place forms. As part of the Colorado IBRC project, a rational limit-state design approach has been developed to account for the girder deflections and arching mechanism in bridge decks (Borlin 2001). The method can be applied to cast-in-place slab-on-girder decks as well as precast panel construction.

1.2. Objectives and Scope

In the study reported here, a 2/3-scale three-girder bridge deck was designed, constructed, and tested under static loads and fatigue load cycles. The test deck had both steel prestressed and CFRP prestressed panels. Furthermore, different segments of the deck were designed with different methods, namely, the AASHTO empirical method, the AASHTO conventional method, and the new limit-state design approach mentioned above. The main objectives of these tests were as follows.

1. Study the performance of a bridge deck that had CFRP prestressed panels designed in the same way as those in the I-225/Parker Road bridge under fatigue load cycles.

2. Evaluate and compare the performance of bridge decks designed with the empirical, conventional, and new limit-state methods.

3. Study the applicability of the AASHTO empirical method to cast-in-place topping slabs for decks that have precast panels as stay-in-place forms.

Furthermore, the influence of lap splices between precast panels on the cracking of a deck is investigated by having part of the deck with lap splices and the rest without.

1.3. Report Organization

This report is organized in the following fashion. In Chapter 2, an overview of the existing AASHTO provisions for the design of bridge decks is provided, and the new limit-state design method is presented. In Chapter 3, the different design methods are compared with a bridge deck design example.

Chapter 4 presents the design of the test deck, which is an extension of the design example presented in Chapter 3. The construction procedure of the test deck and the test program, including the test setup, loading procedure, and instrumentation plan, are presented in Chapter 5. Test results are presented and discussed in Chapter 6. Chapter 7 provides a summary and the conclusions of this study.

2. DESIGN OF BRIDGE DECKS

2.1 Introduction

The design of bridge decks can follow either the 16th Edition of the Standard Specifications for Highway Bridges (AASHTO 1996), which is predominantly based on the working stress design (WSD) philosophy, or the AASHTO LRFD Bridge Design Specifications (AASHTO 1998), which is based on the strength design approach. The WSD was prominent until the mid-1970's when the load factor design (LFD) method appeared. The LRFD method accounts for the variability in not only loads, but also structural element properties. In the AASHTO LRFD Specifications, bridge decks can be designed with the *conventional method*, which is similar to the strength design method in the 16th Edition of the Standard Specifications, or the *empirical method*. A brief description of these methods is given in Sections 2.2 and 2.3.

The conventional method adopted in the LRFD Specifications for the design of slab-on-girder bridge decks is very conservative. It is based on flexural design and considers the moment resistance created by the reinforcement to be the primary load resisting mechanism of the slab. There are a number of shortcomings associated with this method. First of all, it neglects the effects of arching action on the load-carrying capacity of the bridge deck. Furthermore, the conventional method fails to account for the influence of the differential girder deflections on the negative moment. Consideration of this factor would allow for a reduction in the quantity of top reinforcement, which resists the negative moment. Because of arching action, bridge decks seldom fail in moment, but rather in punching shear. Thus, the actual load-carrying capacity of the deck is much higher than anticipated.

A design method accounting for the true behavior of bridge decks can lead to more cost-efficient bridge decks. In specific, one should consider:

- the effects of girder deflections on the negative moment,

- the effects of arching action on the load-carrying capacity, and

- the consideration of punching shear as a possible mode of failure.

While the empirical method addresses the aforementioned issues, it is simply a set of design rules derived from experimental observations and does not lend itself to rational analysis tools. For this reason, a rational limit-state design method that accounts for the true behavior of bridge decks has been developed in this study (Borlin 2001). This method is presented in Section 2.4.

2.2 AASHTO 16th Edition

In the 16th Edition of the AASHTO Standard Specifications for Highway Bridges (AASHTO 1996), there are two design approaches, the Service Load Design (Allowable Stress Design) and the Strength Design Method (Load Factor Design). In consideration of the design of bridge decks, both methods have proven to give similar results in terms of the quantity of reinforcement required. The Strength Design Method requires that the strength of the member be sufficient enough to resist the factored applied loads and forces as stated in AASHTO Article 8.16.1. Under this method, the design strength of a bridge deck is calculated as the nominal strength multiplied by a strength-reduction factor.

In conventional design, strength is normally governed by flexure. Through considerable research, this design method has proven to carry a factor of safety of at least 10 for bridge decks. Since bridge decks rarely fail in bending because of the arching mechanism, consideration of flexure as the failure mechanism is over-conservative.

2.3 AASHTO LRFD Specifications

The AASHTO LRFD Bridge Design Specifications (AASHTO 1998) provide two different design methods for bridge decks. The first is the Conventional Method, and the other is the Empirical Method. A main focus of the LRFD method is on the predictability and variability of both loads and material properties and consequent use of the theory of reliability in determining the applicable load and resistance factors. The LRFD approach considers various limit states (i.e., service, fatigue & fracture, strength, and extreme event) and requires that the factored resistance outweigh the factored loads for each state. The LRFD approach for the design of bridge decks is detailed in Section 9 of the manual. It requires that fully elastic methods of analysis be used for the service limit state and that either elastic or inelastic methods of analysis be used for the strength limit state.

2.3.1 Conventional Method

The LRFD Conventional Method is similar to the 16th Edition's Strength Design Method, and it considers that the failure of a bridge deck is governed by flexure. The LRFD method differs from the 16th Edition, however, by providing a different procedure for determining the moment in a continuous deck. The 16th Edition allows for the application of a continuity factor of 0.8 to the calculated live load moment of a simply-supported slab. The resulting value is used for both the positive and negative live load moments in a continuous slab. The LRFD code, on the other hand, provides a more refined means for calculating the negative and positive live load moments in a continuous slab.

2.3.2   Empirical Method

The second bridge deck design method in the AASHTO LRFD Bridge Design Specifications is the Empirical Method. The Empirical Method is an alternate method of design included in the LRFD manual, which allows for the design of concrete slabs without analysis. This method stipulates a series of design conditions as presented in Article 9.7.2.4 of the design manual. If these conditions are all met, the minimum amount of steel reinforcement specified in the subsequent article can be utilized to determine the reinforcement layout.

This method is based primarily on research that was conducted in Canada to explore the contribution of internal arching action to the load-carrying capacity of bridge decks. In the late 1970's, the Ontario Ministry of Transportation & Communications conducted a number of tests on existing structures in an attempt to evaluate the compressive membrane action (Ontario 1979). Results of the study indicate that the strength of a deck can be significantly enhanced by the arching mechanism. This arching mechanism is created by the migration of the neutral axis away from the positive and negative moment cracks.

2.4   Proposed Limit-State Design Method

The performance of a bridge deck is often limited by serviceability conditions rather than its ultimate load capacity. For this reason, a limit-state design approach that emphasizes the serviceability conditions of a deck is proposed here. This approach is more rational than the current AASHTO provisions in that it considers the effects of differential girder deflections, the influence of the arching action on the total load-carrying capacity of a deck, and the punching shear capacity. The method can be easily implemented in code provisions in that it is not too different from the limit-state design concept that has been used in prestressed concrete structures for a long time.

The new design method is expected to achieve the same goal as the Empirical Method in the AASHTO LRFD Specifications in that it leads to a significant reduction in slab reinforcement. There are many advantages associated with reduced quantities of reinforcement in bridge decks. The most obvious advantage is the reduction in construction costs, including both material and labor. Another important advantage is the reduction in long-term maintenance costs associated with the deterioration of decks due to the corrosion of steel reinforcement and the spalling of concrete. The corrosion of steel reinforcement normally leads to the spalling of the concrete cover and is a major cause of deck deterioration. Therefore, reducing the quantity of steel reinforcement can prolong the lifespan of a deck.

The method can be applied to full-depth deck slabs as well as composite slabs with precast panels. Following is a description of the proposed method.

2.4.1 Basic Approach

The new limit-state design approach consists of the following steps.

- Determine the bending moments in a deck slab considering the influence of girder deflections.

- Determine the quantity of reinforcement based on serviceability conditions that are governed by allowable stresses and crack width.

- Check the load-carrying capacity of the design considering the arching action and punching shear mechanism.

To take advantage of the arching action, one must assure that such a mechanism can develop in the deck. The Empirical Method of AASHTO provides a set of conditions that can lead to adequate arching action. In the absence of more rational criteria, one can refer to these conditions as a guide.

The aforementioned steps are described with more details in the following sections.

2.4.2 Deck Analysis

The positive and negative bending moments in a deck slab are calculated with the consideration of girder deflections. Both the dead load and live load should be considered. However, one must realize that girder deflections have no impact on dead load moments since the majority of the dead load acting on a slab is its self-weight, which is introduced before the concrete hardens in the slab. In that case, the girders will deflect initially under the weight of the wet concrete; once the concrete hardens and the forms are removed, no additional girder deflections will be experienced; and thus, the dead load moments in the slab will be the same as those in a slab supported on rigid girders.

The calculation of live load moments, however, requires the consideration of girder deflections. A simplified analysis method developed by Cao and Shing (1999) provides a tool for determining the maximum negative bending moment in a continuous deck with consideration of girder deflections. It first requires the determination of the maximum negative moments in a slab on rigid girders. A reduction factor, accounting for the span-to-length ratio, the stiffness ratio for bending in both directions of a slab-on-girder deck, and the location of the load from the abutment, is then determined. By applying this reduction factor to the maximum positive moment in a simply-supported slab and adding this value to the negative moment previously computed with rigid girders, the maximum negative bending moment in a slab on flexible girders is determined.

The positive live load moment can be based on a simply-supported slab. This is conservative for continuous slabs with girder deflections. This method is described in detail in Appendix A.

2.4.3   Quantity of Reinforcement

With the moments in a deck slab calculated, one can determine the quantity of reinforcing steel required assuming that the thickness of a slab has been selected *a prior*. The quantity of reinforcement in the proposed approach will be based on serviceability conditions. The main serviceability considerations for a bridge deck are the fatigue effect of the traffic loads and the maximum crack width under service loads that affect the rate of corrosion of the reinforcing steel. While we can readily use the AASHTO provisions for the maximum allowable crack width, the provisions require no consideration of fatigue stress limits for concrete deck slabs due to studies conducted by deV. Batchelor et al. (1978) on the fatigue testing of model slabs using pulsating loads. As a result, the allowable stress and crack width requirements in the 16th Edition of the AASHTO Standard Specifications are conservatively adopted here to limit the stress levels in bridge decks. These requirements should be refined as more information on fatigue behavior of bridge decks becomes available.

The design process for full-depth cast-in-place decks and precast prestressed panel decks with cast-in-place topping slabs based on the aforementioned concepts is summarized below.

Full Depth Cast-in-Place Concrete Decks

For the design of full-depth cast-in-place concrete decks**,** the following allowable stresses for concrete and steel are proposed to be used here.

$$f_c \leq 0.40 f'_c \tag{2.1}$$

$$f_s \leq 0.60 f_y \tag{2.2}$$

where f'_c = 28-day compressive strength of concrete and f_y = yield strength of steel. The first equation is from the Allowable Stress Design Method of the 16th Edition of the AASHTO Standard Specifications, while the second equation is based on the crack-width requirement in

the Strength Design Method of the AASHTO Specifications. With the lack of better information, the above allowable stresses are deemed adequate.

For a given slab thickness, the minimum reinforcement ratio can be determined from the allowable stresses by considering the elastic behavior of a cracked section using simple bending theory. Once the size and spacing has been selected, the member must be checked with Equation 2.3 to ensure that there will be no excessive crack widths.

$$f_s \le \frac{z}{\sqrt[3]{d_c A}} \le 0.60 f_y \qquad (2.3)$$

where $z = 130$ KIPS/IN (crack width parameter for members in severe exposure conditions), $d_c =$ depth (IN) of concrete from extreme tension fiber to centroid of reinforcement, and $A =$ area (IN^2) of concrete having the same centroid as the tensile reinforcement divided by the number of bars. The above equation is also from the Strength Design Method of AASHTO.

Precast Prestressed Panels with Cast-in-Place Topping

The allowable stress design approach is currently the most commonly practiced method for precast prestressed panels. The allowable concrete and steel stresses for pretensioned members with bonded low-relaxation tendons are stated in the 16th Edition of the AASHTO specifications as follows.

$$f_{ti} \le 3\sqrt{f'_{ci}} \qquad (2.4)$$

$$f_{ci} \le 0.60 f'_{ci} \qquad (2.5)$$

$$f_{ts} \le 6\sqrt{f'_c} \qquad (2.6)$$

$$f_{cs} \le 0.60 f'_c \qquad (2.7)$$

$$f_{pj} \le 0.75 f_{pu} \qquad (2.8)$$

14

where f_{ti} = initial tensile stress (PSI) in concrete right after tendon release, f_{ts} = tensile stress (PSI) in concrete under service loads, f_{ci} = initial compressive stress (PSI) in concrete right after tendon release, f_{cs} = compressive stress (PSI) in concrete under service loads, f'_{ci} = initial compressive strength (PSI) of concrete, f'_c = specified 28-day compressive strength (PSI) of concrete, f_{pj} = jacking stress (KSI) in prestressing steel prior to stress transfer, and f_{pu} = ultimate strength (KSI) of prestressing steel. The prestress losses are determined by AASHTO Article 9.16.

Since construction is done in stages from precasting to the casting of the topping slabs, the designer should select the prestressing force, eccentricity of tendons, tendon size, and tendon spacing so that the concrete stresses are within the specified limits during each stage under the dead loads, construction loads, and total service loads.

The cast-in-place topping slab is designed in the same manner as a full-depth cast-in-place deck as far as the top reinforcement is concerned.

2.4.4 Strength Requirements

The strength of a deck, provided by the arching action and the punching shear resistance, should be assessed as a final check for the design. The arching action arises once cracking occurs in a restrained slab. A shift in the neutral axis toward the top of the deck at the midspan and the bottom at the supports creates the mechanism of an arch. A method is presented in Appendix B for the determination of the enhanced load capacity of a deck due to arching and beam actions. The method is proposed by Rankin and Long (1997) and it is simple enough for design purposes.

The punching shear capacity can be determined by following either Article 8.16.6.6.2 of the AASHTO 16th Edition or the general method outlined in Appendix C. The general method of

Appendix C presents a modification to the AASHTO equation to account for varying failure angles. A rational method for the determination of failure angles remains to be developed. The experimental results obtained by Tsui et al. (1986) from a model deck suggest a failure angle of 39 degrees and AASHTO adopts a more conservative approach by using a 45-degree failure angle.

2.4.5 Secondary Reinforcement

The final step in the design process involves the selection of secondary reinforcement. This can be based on the 16th Edition of the AASHTO code. According to AASHTO, distribution reinforcement is required at the bottom of a slab. Temperature and shrinkage reinforcement for reinforced concrete slabs can be determined per AASHTO Article 8.20. The article requires a minimum total area of 1/8 square inch of reinforcement per foot in each direction spaced at no more than three times the slab thickness or 18 inches. The requirement for prestressed panels is presented in AASHTO Article 9.24, requiring a minimum of 0.11 square inches of reinforcement per foot of slab transverse to the tendons.

3. COMPARISON OF DESIGN METHODS

To illustrate the applicability of the limit-state design procedure proposed in Chapter 2 for bridge decks, a design example is considered in this chapter. In this example, a deck designed with the new method is compared to those designed with the conventional method according to the 16th Edition of the AASHTO Standard Specifications (AASHTO 1996) and the empirical method given in the AASHTO LRFD Specifications (AASHTO 1998). For this purpose, a 2/3-scale deck consisting of a 6-in-thick cast-in-place concrete slab supported on three W14x99 steel girders equally spaced at 6 ft on center was selected as the base design. The deck had a simple span of 30 ft with a 2 ft overhang beyond the simple support on each end. A transverse section of the deck is shown in Figure 3.1.

The deck was to carry its self-weight and a scaled-down HS-25 design truck. An HS-25 truck has a wheel load of 20 kips. With a length scale factor of 2/3, this wheel load was scaled down to 8.89 kips to maintain a scaling factor of one for the stresses. This base design was used later on for the construction of a model deck that was tested under static and fatigue loadings as described in sequent chapters.

Normal density concrete was used with a design strength of $f'_c = 4,500$ psi. The mild reinforcement consisted of steel with a yield strength of $f_y = 60$ ksi. Based on the 16th Edition of the AASHTO Standard Specifications, a 2.5-in concrete cover was to be maintained over the top reinforcement of bridge decks exposed to deicing salts. For the 2/3-scale model, this was approximately a 1.5-in cover. Although only a 1-in cover was required over the bottom reinforcement, it was decided to use a 1.5-in cover for both the top and bottom steel.
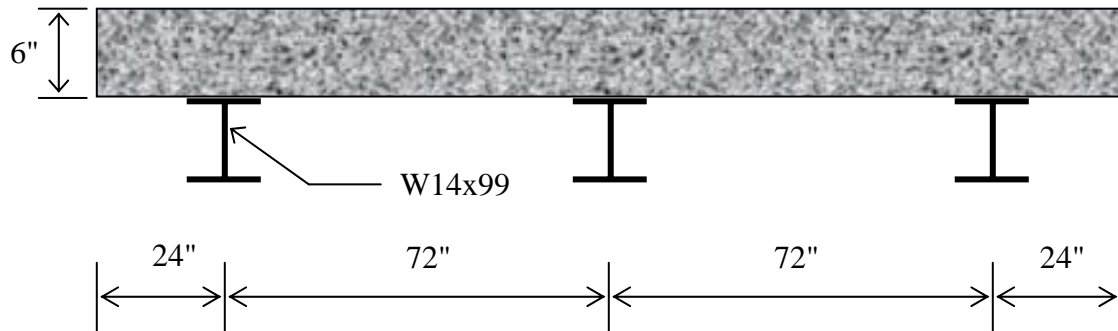
Figure 3.1 – Cross-section of a Full-Depth Cast-in-Place Deck

3.1 Limit-State Design

The deck was first designed with the limit-state method proposed in Section 2.4 of this report. The analysis methods presented in Appendices A, B, and C were used throughout the design.

Dead Load Moments

The only dead load acting on the slab was its self-weight of 150 lb/ft^3. To compute the dead load moments, the deck was modeled as a uniformly loaded slab, simply-supported on one end and fixed on the other. Hence, the maximum positive and negative moments due to the dead load were determined by the following equations.

$$M^+{}_{max} = \frac{9wS^2}{128} \tag{3.1}$$

$$M^-{}_{max} = \frac{wS^2}{8} \tag{3.2}$$

where w = dead load per unit length, and S = center-to-center spacing of supports (girders). These moments are illustrated in Figure 3.2. The computed positive dead load moment was equal to 2.3 kip-in/ft and the negative dead load moment was equal to 4.1 kip-in/ft.
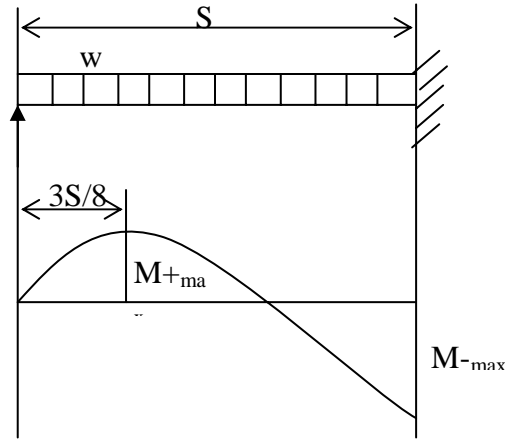

Figure 3.2 – Bending Moment Diagram for a Beam Fixed at One End and Simply-supported on the Other under a Uniformly Distributed Load

Live Load Moments

The maximum positive bending moment due to the live loads for a simply-supported slab was computed using the Westergaard's formula (Equation A.2 in Appendix A) with the Poisson's ratio assumed to be 0.2. The maximum negative bending moment due to the live loads was calculated using the Simplified Analysis Method with Equations A.1, A.7, and A.8 in Appendix A.

The distance of the load from the end support of the deck is important. A load at midspan between the supports will produce minimal negative moments as opposed to a load near the supports because of the girder flexibility. Table 3.1 shows a summary of the design factors and moments determined for loads placed at 6, 12 and 15 ft from a support. Figure 3.3 shows a

graphical representation of the effects of the distance, d, between the load and the support on the maximum negative moment, M_t.

The service load moments were determined for both the positive and negative reinforcement by combining the dead load and live load moments. At the midspan location between the supports, the service load moment for the positive reinforcement was 43.6 kip-in/ft and for the negative reinforcement was 17.1 kip-in/ft.

Table 3.1 – Negative Moments Due to Various Loading Positions as Determined from the Simplified Analysis Method

			Distance from Support (ft)		
			6	12	15
Design Factors		d/L	0.200	0.400	0.500
		K_{do}	0.404	0.404	0.404
		K_d	0.237	0.384	0.404
Moments (kip-ft)		M_1	-2.480	-2.480	-2.480
		M_o	3.440	3.440	3.440
		M_t	-1.663	-1.158	-1.090

Reinforcement Design

For the 4,500-psi concrete, the allowable compressive stress based Equation 2.1 was 1800 psi. Based on Equation 2.2, the allowable tensile stress for the Grade-60 steel was 36 ksi. The quantity of reinforcement was chosen to satisfy these requirements.

The quantity of reinforcement was determined through an iterative process by considering the elastic behavior of a cracked section using the simple bending theory. The initial value for the reinforcement ratio was determined by setting $\rho = \rho_e$, the balanced reinforcement ratio, which was determined from Equation 3.3.

$$\rho_e = \frac{n}{2r(n+r)} \tag{3.3}$$

where n = modulus ratio (E_s/E_c), E_s = modulus of elasticity of steel, E_c = modulus of elasticity of concrete, r = the stress ratio ($f_{s,all}/f_{c,all}$), $f_{s,all}$ = allowable stress in steel and $f_{c,all}$ = allowable stress in concrete. This value was calculated to be 0.00687.
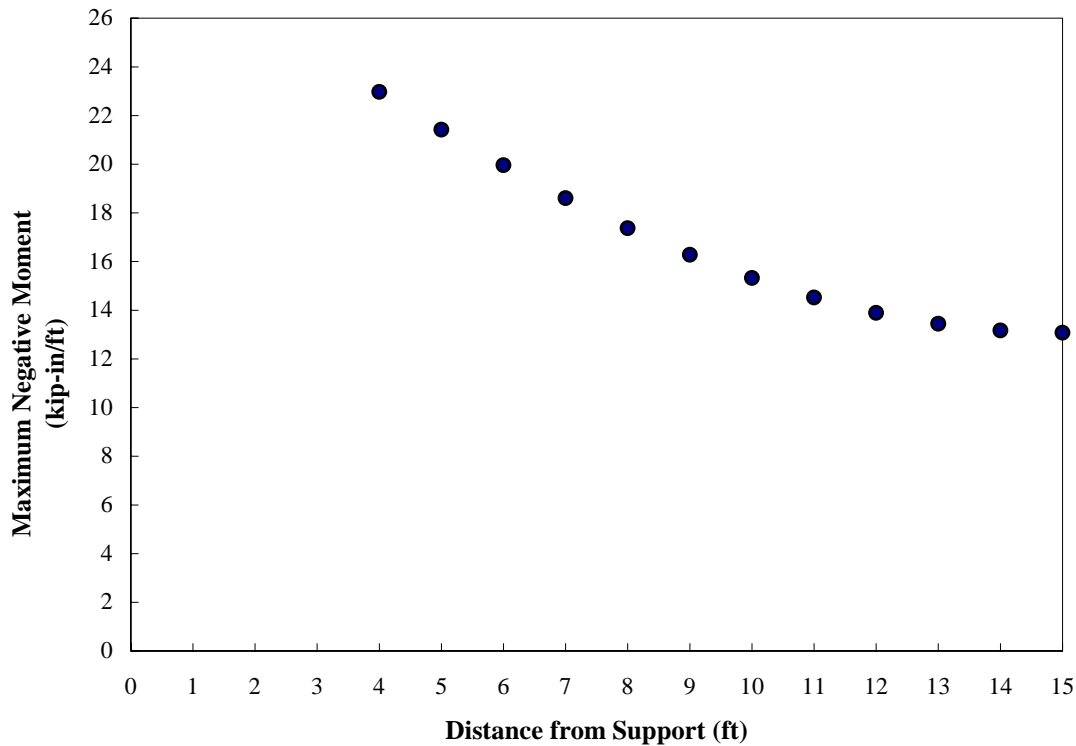

Figure 3.3 – Maximum Negative Moments Due to Various Loading Positions as Determined from the Simplified Analysis Method

With an initial value for the reinforcement ratio (ρ), the location of the corresponding neutral axis (kd) was determined by calculating k from Equation 3.4.

$$k = \sqrt{2\rho n + (\rho n)^2} - \rho n \tag{3.4}$$

The initial value of k was determined to be 0.2748.

It was assumed that the stress in the steel controls the design, which is typically the case for bridge design. With this assumption and a pre-determined value for k, Equation 3.5 was used to determine a new value for the reinforcement ratio.

$$\rho = \frac{M_s}{f_{s,all}jbd^2} \tag{3.5}$$

where M_s = moment due to service loads, b = width of design section, d = effective depth of slab, and j = 1– (k/3). Through an iterative procedure involving Equations 3.4 and 3.5, the minimum reinforcement ratio was determined.

This iterative technique was applied for both the positive and negative reinforcement. A minimum reinforcement ratio of 0.00543 was found for the positive reinforcement. Hence, No. 4 bars at 8-in spacing were chosen, resulting in a reinforcement ratio of 0.00556. A minimum reinforcement ratio of 0.00207 was found for the negative reinforcement. For this, No. 3 bars at 11.25-in spacing were chosen, resulting in a reinforcement ratio of 0.00217.

As a final check, the actual stresses in the steel and concrete were determined by the following equations according to the beam theory and compared to the previously computed allowable stresses.

$$f_s = \frac{M_s}{A_s jd} \tag{3.6}$$

$$f_c = \frac{2M_s}{jkbd^2} \tag{3.7}$$

Under the service loads, the maximum compressive stress in the concrete was found to be 909 psi, which was well below the 1800-psi allowable stress. The maximum tensile stress in the positive reinforcement was 35.2 ksi and in the negative reinforcement was 34.4 ksi, both below the 36-ksi allowable stress limit.

In addition, the maximum crack width was checked with Equation 2.3. For this case, d_c in Equation 2.3 was 1.5 in for both the positive and negative reinforcement, and A was 24 in^2 for the positive reinforcement and 33.8 in^2 for the negative reinforcement. This check yielded an allowable steel stress of 36 ksi for the positive reinforcement and 35 ksi for the negative reinforcement. The actual stresses as calculated above were below these limits.

Arching Capacity

The arching capacity was determined based on the method in Appendix B. First, the parameter R was found using Equation B.1, with $\varepsilon_c = 0.0011$, $L_r = 36$ in, and $d_1 = 2.73$ in. The resulting R was 0.0498. The arching moment ratio and the maximum arching moment resistance were then calculated by Equations B.8 and B.9, respectively.

The equivalent strip width of the slab was determined to be 56.9 in based on the AASHTO LRFD Specifications. It was calculated with a girder spacing of 9 ft for the full-scale deck and then reduced by a factor of 2/3 for the scaled deck. The resulting arching moment was found to be 1,215 kip-in for the equivalent strip. To account for the flexibility of the restraint, this value was conservatively reduced by 50%, resulting in an arching moment of 607 kip-in.

The positive and negative bending moment capacities were found from the following equation.

$$M_b = A_s f_y d \left(1 - 0.6 \frac{\rho f_y}{f'_c} \right) \tag{3.8}$$

where A_s = the area of reinforcement per equivalent strip width (EW) of slab, f_y = the yield strength of the reinforcement, d = the effective depth of the slab, and ρ = the reinforcement ratio.

The positive bending moment capacity was 368 kip-in for the equivalent strip, and the negative bending moment capacity was 148 kip-in. To determine the live load-carrying capacity,

the portion of the bending moment required to resist the dead load moment, which in this case was just the self-weight of the slab, must be subtracted. The positive dead load moment was 10.8 kip-in for the equivalent strip, and the negative dead load moment was 19.2 kip-in. By deducting these from the bending moment capacities, the positive bending moment capacity available to carry the live load was 357 kip-in and that available from the negative bending moment capacity was 129 kip-in.

The wheel load capacity P_p was calculated with Equations B.14, B.15, and B.16. The k factor for a wheel load in this case was 0.056, and the resulting P_p was 60.7 kips. The results are summarized in Table 3.2.

Punching Shear Capacity

According to the AASHTO LRFD Specifications, the width of the tire area was 20 in and the length was determined from the following equation.

$$l = \gamma \left(1 + \frac{IM}{100} \right) \frac{P}{2.5} \tag{3.9}$$

where IM = impact factor, P = wheel load, and γ = load factor. In this example, the impact factor was 33, P = 20 kips, and γ = 1.75. Based on this, the full-scale length was 18.6 in. When applying the 2/3 scaling factor, the tire dimensions were 13.3 in by 12.4 in. For simplicity, it was assumed to be a 13-in square.

Table 3.2 – Summary of Arching and Punching Shear Capacities for a Full-Depth Cast-in-Place Deck Designed with the Limit-State Method

Arching Capacity	P_p	60.7	Kips
	R	0.0498	
	M_r	3.00	
	M_b^+	357	kip-in/EW
	M_b^-	129	kip-in/EW
	M_a	607	kip-in/EW
	k	0.056	
Punching Shear Capacity	V_c	111	Kips

The punching shear capacity was calculated by Equation C.2 in Appendix C, where θ was assumed to be 39 degrees based on the experimental data of Tsui et al. (1986). The resulting punching shear strength was 111 kips. Had the AASHTO formula, which assumes a 45-degree failure angle, been used instead of the general formula, the resulting punching shear capacity would be 84.5 kips. The punching shear capacity is compared to the arching capacity in Table 3.2.

Secondary Reinforcement

Based on the 16th Edition of AASHTO, the total temperature and shrinkage reinforcement in a slab must be at least 0.125 in^2/ft of slab, or 0.0625 in^2/ft for each of the top and bottom layers. The maximum spacing is three times the slab thickness or 18 in. Per the scaling factor of 2/3, this requirement became 0.083 in^2/ft of slab for the total reinforcement with a maximum spacing of three times the slab thickness or 12 in. To meet the spacing requirement, No. 3 bars at 11-in spacing were chosen for both the top and bottom longitudinal reinforcement, resulting in a reinforcement area of 0.120 in^2 per foot of slab.

Based on the requirement of AASHTO, distribution reinforcement must be included in the bottom of the slab, transverse to the main steel reinforcement to distribute the concentrated live loads. The distribution reinforcement was determined by the following equation as a percentage of the primary positive moment reinforcement.

$$\frac{220}{\sqrt{S}} \leq 67\% \text{ of primary reinforcement} \tag{3.11}$$

where S = effective span length (FT). A value of 5.4 feet was determined for S, resulting in a requirement of 67% of the primary reinforcement. This led to 0.057 in^2/ft. This requirement was already met by the temperature and shrinkage reinforcement provided, so no additional reinforcement was necessary.

3.2   Conventional Design

The bridge deck was re-designed using the Strength Design Method according to the 16th Edition of the AASHTO Standard Specifications.

Moments

The positive and negative dead load moments were the same as those calculated in Section 3.1. The major difference in the design pertains to the calculations for the live load moments. The live load moment due to traffic loading was determined from the following equation.

$$M_{LL} = \left(\frac{S+2}{32}\right)(1+I)P \tag{3.11}$$

where M_{LL} = live load moment (KIP-FT), P = single wheel load (KIPS) of design truck, S = the effective transverse span length (FT) defined as the distance between the edges of the top flange

plus one half of the top flange width for continuous slabs supported on steel stringers, and I = impact factor as defined below:

$$I = \frac{50}{L + 125} \leq 0.30 \qquad (3.12)$$

where L = the longitudinal design span (FT) defined as the clear span plus the depth of the member limited to the distance between the centers of the supports. In this example, the truck load (P) was equal to 8.89 kips and the impact factor (I) was calculated to be 0.3. This moment was then multiplied by the continuity factor of 0.8 resulting in a live load moment of 38 kip-in/ft for both the positive and negative moments.

Using the Strength Design Method, the design moment was determined with the following formula.

$$M_u = 1.3 \left[M_{DL} + 1.67 M_{LL} \right] \qquad (3.14)$$

where M_{DL} = moment due to dead load and M_{LL} = moment due to live load (including impact). In this study, the resulting positive design moment was 85.4 kip-in/ft, and the negative design moment was 87.7 kip-in/ft.

Reinforcement Design

Using an iterative procedure based on the following equations and assuming an initial value for a, the required reinforcement ratio (ρ) was determined.

$$A_s = \frac{M_u}{\phi f_y \left(d - \dfrac{a}{2} \right)} \qquad (3.15)$$

$$a = \frac{A_s f_y}{0.85 f'_c b} \qquad (3.16)$$

where $\phi = 0.90$, A_s = area of steel, f_y = yield strength of steel, f'_c = 28-day compressive strength of the concrete, d = effective depth of reinforcement, and b = width of concrete section. Through this iteration, ρ was calculated to be 0.0063. Hence, No. 4 bars at 6-inch spacing were chosen for both the positive and negative reinforcement, resulting in a value for ρ equal to 0.0074.

Strength Check

Though not required here, the actual strength of the slab considering the arching and punching shear mechanism was calculated in the same way as in Section 3.1. The positive and negative bending moment capacities were calculated to be 483 kip-in for the equivalent strip. By subtracting the moment required to resist the dead load, the positive bending moment capacity available to carry the live load was 472 kip-in and the negative bending moment available was 464 kip-in. The arching moment capacity was found to be 480 kip-in. The live load capacity was calculated based on the sum of the loads resisted by both bending and arching and was equal to 78.6 kips. The punching shear capacity of the section was identical to that of the deck designed in Section 3.1.

Secondary Reinforcement

The secondary reinforcement was the same as that in Section 3.1.

3.3 Empirical Method

The deck was re-designed with the empirical method of the AASHTO LRFD Bridge Design Specifications (AASHTO 1998). According to the empirical method, the length of the overhang on each side of a deck should be at least five times the depth of the deck slab, which would result in a 2.5-ft overhang for the deck that had a 6-in slab. This is to ensure a sufficient boundary restraint for the arching mechanism to develop. However, the deck designed here had only a 2-ft overhang on each side. Violating this requirement would result in a more

conservative evaluation of the empirical method later on in this report. The empirical method requires four layers of isotropic reinforcement with a yield strength of at least 60 ksi, with two orthogonal layers at the top and two at the bottom. The minimum area of reinforcement for each bottom layer is 0.27 in^2/ft, and that for each top layer is 0.18 in^2/ft. A maximum spacing of 18 in is permitted by the specifications. Since the test deck was a 2/3-scale model, the reinforcement area was scaled accordingly to keep the reinforcement ratio the same. Therefore, each of the bottom layers had a reinforcement of 0.18 in^2/ft and each of the top layers had a reinforcement of 0.12 in^2/ft with a maximum spacing of 12 in.

For the reinforcement in the top of the deck, No. 3 bars at 10.5-in spacing were selected for the transverse direction, resulting in 0.126 in^2 of reinforcement per foot of slab and No. 3 bars at 11.0-in spacing were selected for the longitudinal direction, resulting in 0.120 in^2 of reinforcement per foot of slab. For the reinforcement in the bottom of the deck, No. 3 bars at 7.25-in spacing were selected for both the transverse and longitudinal directions, resulting in 0.182 in^2 of reinforcement per foot of slab.

Strength Check

To check the actual load-carrying capacity of the slab considering the arching and punching shear mechanisms, the positive bending moment capacity was calculated to be 227 kip-in for the equivalent strip, and the negative bending moment capacity was 158 kip-in. By subtracting the moment required to resist the dead load, the positive bending moment capacity available to carry the live load was 216 kip-in and the negative bending moment capacity available was 139 kip-in. The arching moment capacity was found to be 646 kip-in. The live load capacity was calculated based on the sum of the loads resisted by both bending and arching

and was equal to 55.6 kips. The punching shear capacity of the deck was again the same as that for the previous designs.

3.4   Comparison of Designs

Table 3.3 shows a summary of the reinforcement in decks designed with the proposed limit-state, AASHTO empirical and AASHTO conventional methods. It can be seen from the table that the positive reinforcement for the empirical method is less than that from either the proposed or AASHTO conventional methods. However, the proposed method only requires about 75% of the positive reinforcement required by the conventional method. The most important difference associated with these three design methods is the required quantity of negative reinforcement. Both the proposed and empirical methods require only about 30% of the top reinforcement required by the AASHTO conventional method. In fact, the proposed method requires slightly less reinforcement than the empirical method. From this table, it is apparent that bridge decks designed by the AASHTO conventional method are extremely over-designed. However, it should be pointed out that the quantity of reinforcement with the proposed method shown here is at a mid-span location, and it will increase a little toward the supported end of the slab.

Table 3.3 – Primary Reinforcement Summary for Full-Depth Cast-in-Place Decks

Design Method	Bottom Reinforcement (Postive Moment Resistance)			Top Reinforcement (Negative Moment Resistance)		
	Bar #	Spacing (in)	A_s (in^2/ft)	Bar #	Spacing (in)	A_s (in^2/ft)
Limit-State Method	4	8.00	0.300	3	11.25	0.117
Empirical Method	3	7.25	0.182	3	10.50	0.126
AASHTO Conventional Method	4	6.00	0.400	4	6.00	0.400

Table 3.4 shows a summary of the strength capacities of the decks designed with the proposed limit-state, AASHTO empirical and AASHTO conventional methods. According to the AASHTO Strength Design, the positive ultimate design moment is 405 kip-in for the equivalent strip, and the negative moment is 416 kip-in. From Table 3.4, it can be seen that, based on the moment resistance alone, only the deck designed with the AASHTO conventional method can resist this moment. However, the live load capacity (P_p) developed by the arching action ranges from 55.6 to 78.6 kips, and the punching shear capacity (V_c) is 111 kips. These load capacities are more than adequate in consideration of the 8.89-kip wheel load of a scaled design truck. The moment values given in the table are per equivalent strip width.

Table 3.4 – Strength Capacity Summary for Cast-in-Place Decks

Design Method	Bending Moment Capacity				Arching Capacity				Punching Shear Capacity
	Positive		Negative						
	M_b	ϕM_b	M_b	ϕM_b	M_a	P_b	P_a	P_p	V_c
	k-in	k-in	k-in	k-in	k-in	kips	kips	kips	kips
Proposed Method	368	**331**	148	**133**	**607**	27.0	33.7	**60.7**	**111**
Empirical Method	227	**204**	158	**142**	**646**	19.7	35.9	**55.6**	**111**
AASHTO Conventional Method	483	**434**	483	**434**	**480**	51.9	26.7	**78.6**	**111**

Table 3.4 shows that the strengths of the decks are governed by the arching capacity. However, it must be pointed out that the arching strengths were estimated with a great degree of conservatism assuming very flexible side restraints.

4. DESIGN OF TEST DECK

The bridge deck at the I-225/Parker Road interchange has post-tensioned reinforced concrete box girders. On top of the girders, 3-1/5-in-thick precast concrete panels were placed as stay-in-place forms and a 5-in-thick cast-in-place topping slab was poured to result in an 8-1/2-in composite slab. Some of the panels were pretensioned with CFRP bars as one objective of the IBRC project. To evaluate the strength and long-term performance of the composite slab that has CFRP prestressed panels, a model bridge deck was built and tested under static and fatigue loads. However, unlike the actual deck that has post-tensioned concrete box girders, the test deck had the same base design as the 2/3-scale deck considered in Chapter 3. The test deck had a composite slab made of 3-in-thick precast panels and a 3-in topping, as shown in Figure 4.1. The 6-in composite slab approximately represented a 2/3-scale model of the actual bridge slab. Since a minimum thickness of 3 in was required for the precast panels from the construction standpoint, an exact scaling was not possible here.
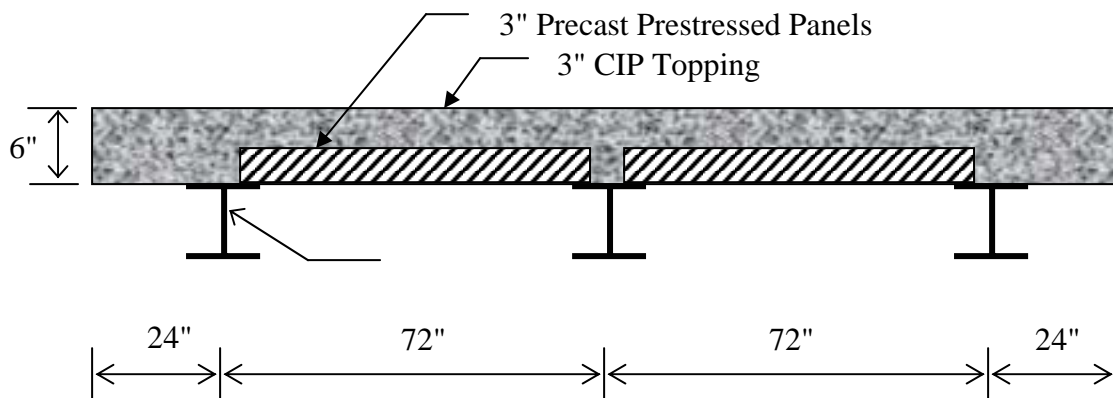

Figure 4.1 – Cross-Section of Precast Prestressed Panel Deck with Cast-in-Place Topping

In addition to the aforementioned objective, the test deck was designed and constructed for the following investigations: (a) evaluating and comparing the performance of bridge decks

designed with the empirical, conventional, and proposed limit-state methods; (b) studying the applicability of the AASHTO empirical method to cast-in-place topping slabs in bridge decks that have precast panels as stay-in-place forms; and (c) examining the influence of lap splices between precast panels on deck cracking.

To fulfill the above goals, a segment of the test deck had full-depth cast-in-place concrete, and the remainder had a composite section with precast prestressed panels as stay-in-place forms and a cast-in-place reinforced concrete topping. Half of the precast panels contained steel reinforcement to serve as control panels and the other half contained FRP reinforcement. Furthermore, the deck was divided into segments that were designed with the limit-state method proposed in Chapter 2, the AAHTO empirical method, and the AASHTO conventional method, respectively.

Similar to the model deck designed in Chapter 3, normal density concrete was used for the test deck with a design strength of f'_c = 4,500 psi. The mild steel reinforcement used had a yield strength of f_y = 60 ksi. A 1.5-in concrete cover was used for both the top and bottom reinforcement. The deck span was 30 feet with a 2-ft overhang on each side. It was designed to carry its self-weight and a scaled-down HS-25 design truck that had a wheel load of 8.89 kips. The precast panels for the composite slab were also designed to support a 117 lb/ft^2 construction load.

4.1 Design Overview

The deck consisted of four segments, each having a different design. Figure 4.2 shows a plan view of the deck and the design methodology used for each segment of the deck. Segment A had a composite slab with a topping slab designed with the AASHTO empirical method. It must be mentioned that the use of the empirical method for the topping slab with precast panels

as stay-in-place forms is currently not permitted by AASHTO. Its inclusion in this study was to evaluate its potential applicability. Segment D had a full-depth cast-in-place slab that was deigned with the empirical method. It had the same design as the deck considered in Section 3.3. Segment B had a composite slab designed with the AASHTO conventional method, and Segment C had a composite slab designed with the limit-state approach proposed in Chapter 2. The simple supports were located right at the edges of Segments A and D with a 24-in overhang at each end.

The panels on the north side were control panels that had 3/8-in-diameter seven-wire steel strands for prestressing and No. 3 steel bars as mild reinforcement, while those on the south side had 8-mm Leadline CFRP bars for prestressing and No. 4 GFRP bars from Marshall Industries as temperature/shrinkage reinforcement. As shown in Figure 4.2, only three of the panel-to-panel joints had full lap splices. The remaining joints did not have any splicing bars. For the joints between the precast panels and full-depth cast-in-place slab, splicing bars were only provided by the precast panels.

Figures 4.3 and 4.4 show plan views of the top and bottom reinforcement. Figures 4.5 and 4.6 show transverse section views of the full-depth cast-in-place portion of the deck and the precast prestressed panel portion of the deck. Finally, Figure 4.7 shows a plan and cross-sectional view of the precast prestressed panels with splicing bars. The splicing bars shown are frequently used for this type of construction by the Colorado Department of Transportation.

It should be pointed out that the precast panels were all designed with an allowable stress approach regardless of the design method used for the composite slab.
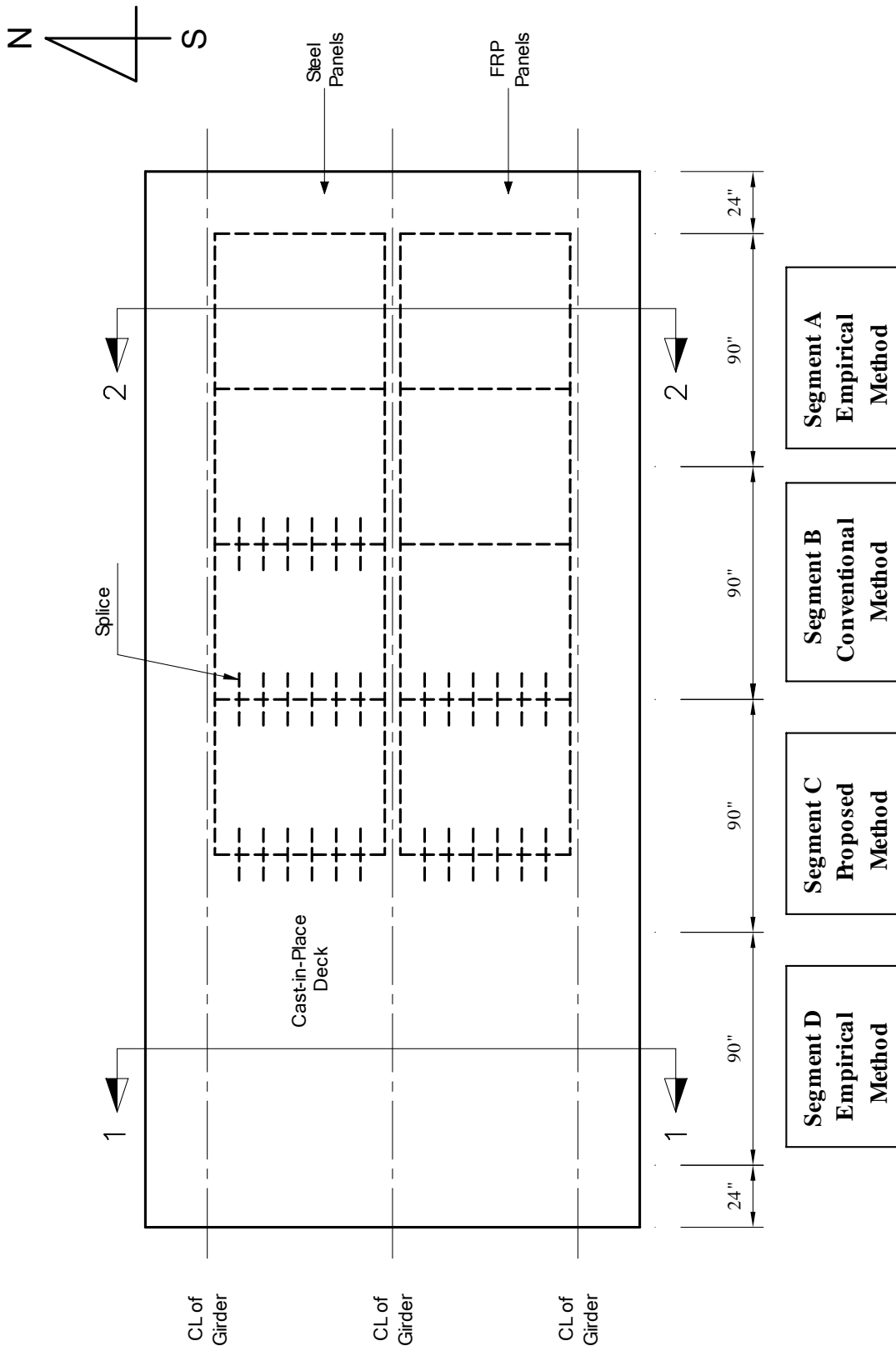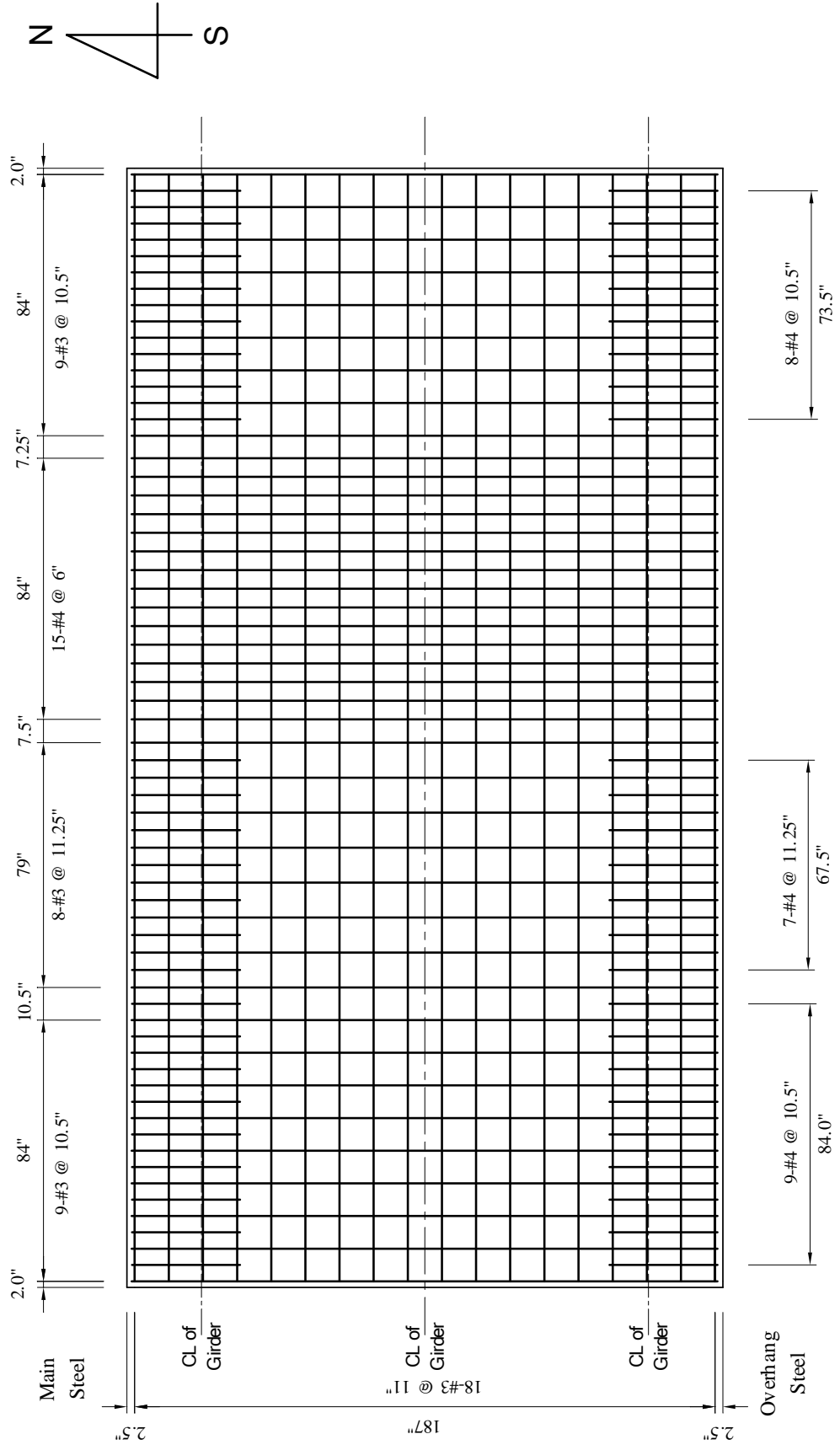
Figure 4.2 – Plan View of Deck

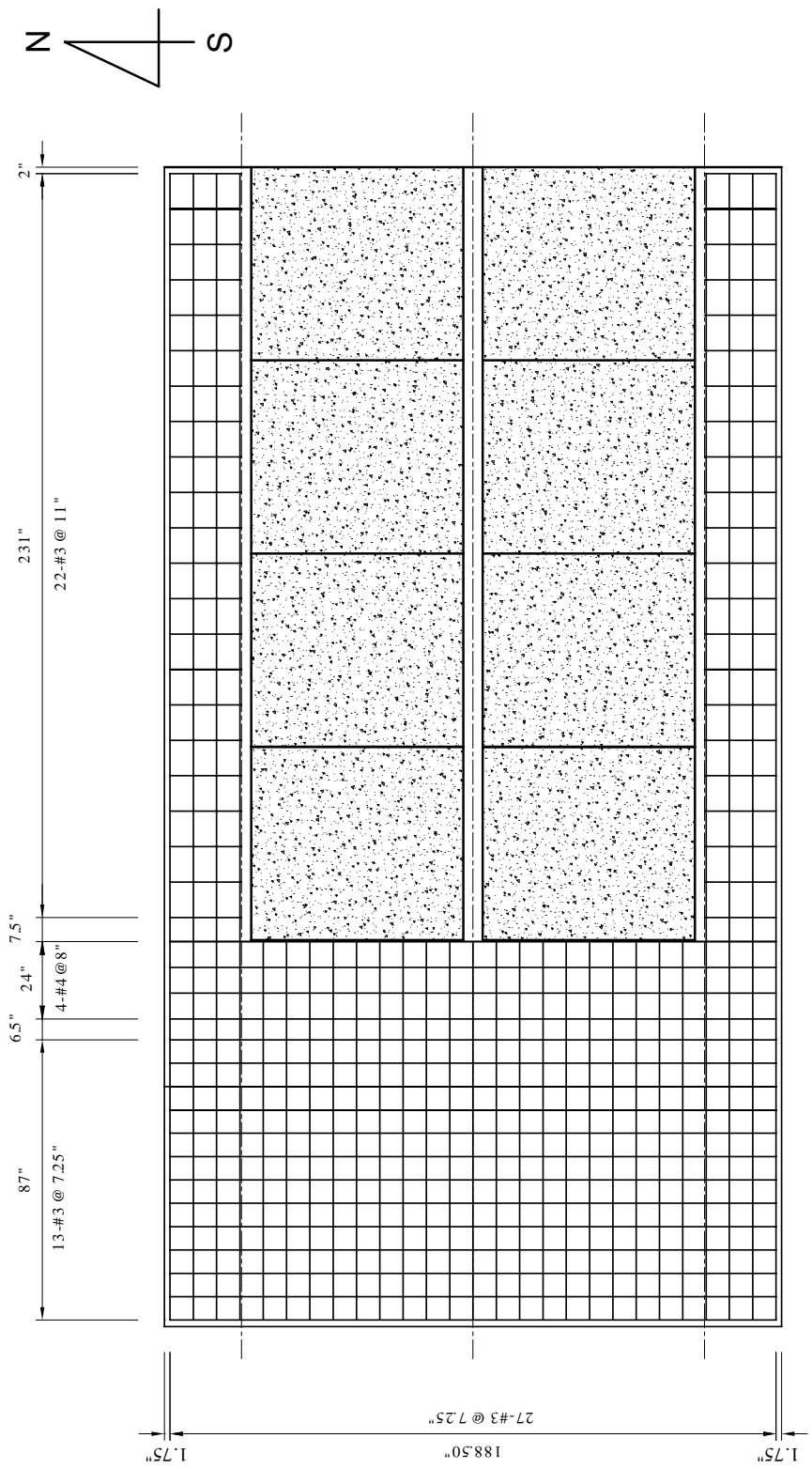Figure 4.3 – Plan View of Top Reinforcement (Support to Support only)

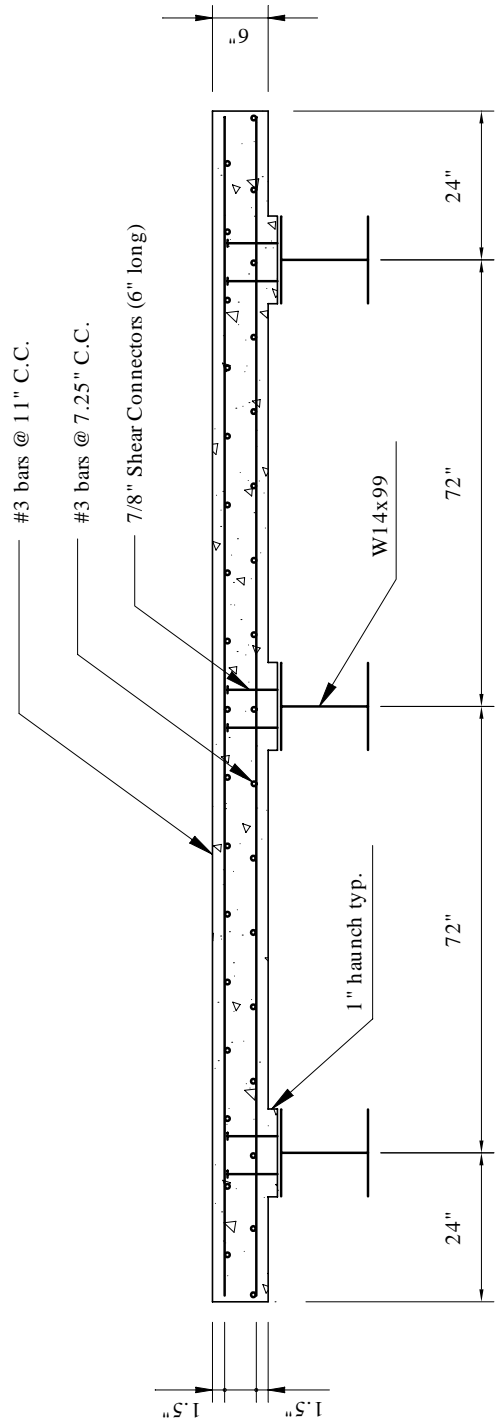Figure 4.4 – Plan View of Bottom Reinforcement (Support to Support Only)

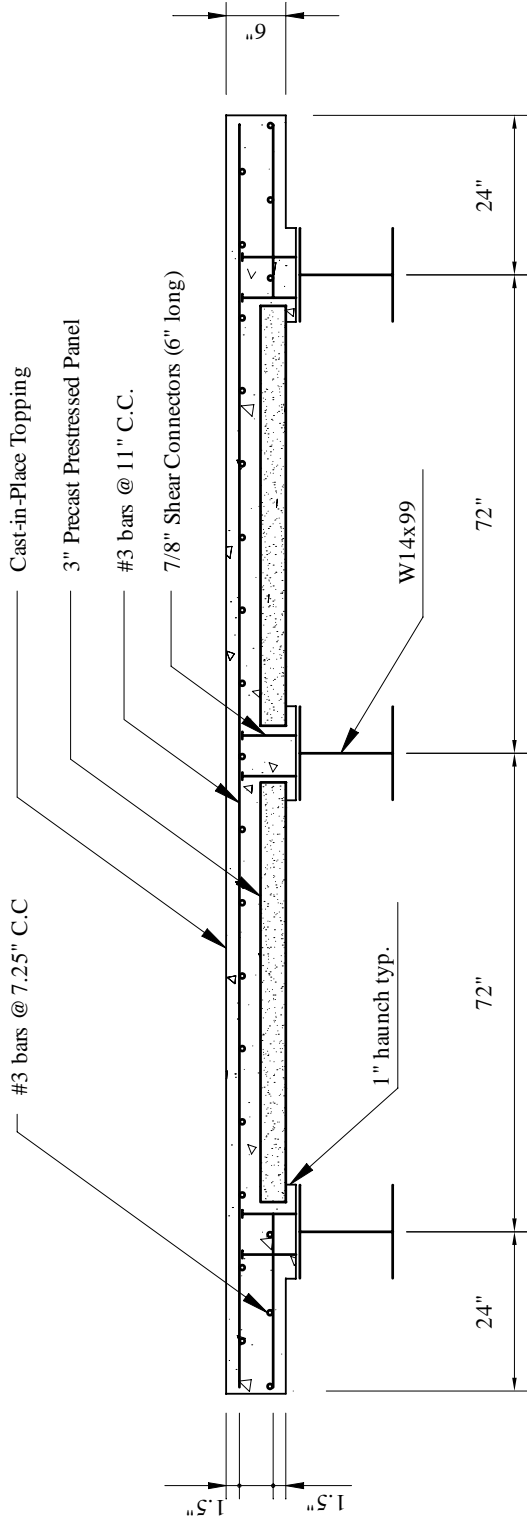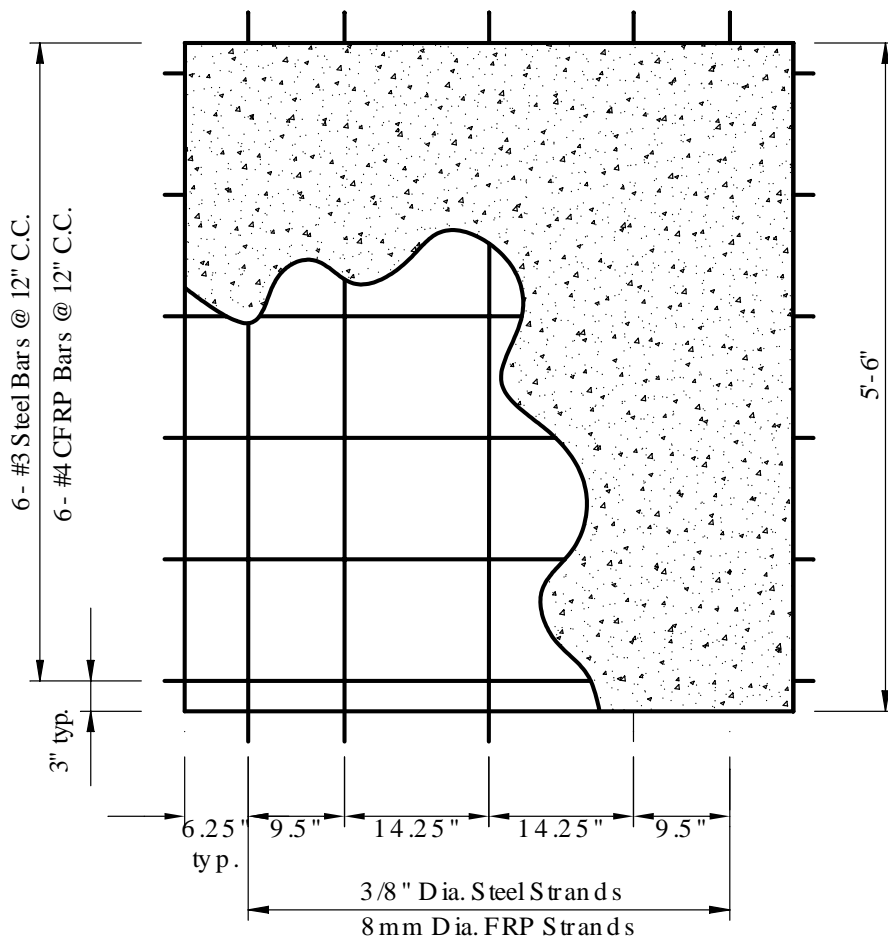SECTION 1-1

Figure 4.5 – Cross-Section of Full-Depth Cast-in-Place Deck

39

Cast-in-Place Topping

3" Precast Prestressed Panel

#3 bars @ 11" C.C.

7/8" Shear Connectors (6" long)

#3 bars @ 7.25" C.C

W14x99

1" haunch typ.

6"
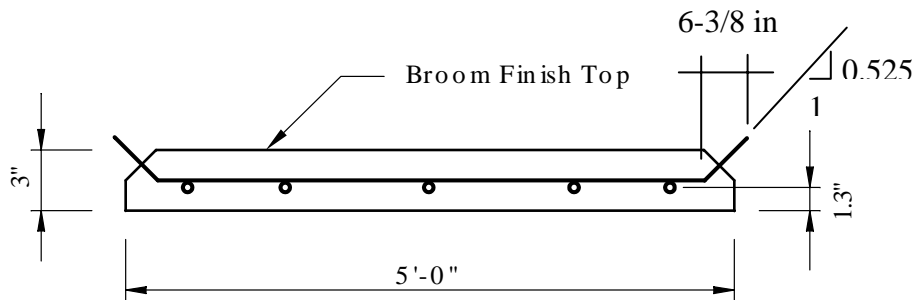
24"

72"

72"

24"

1.5"

1.5"

SECTION 2-2

Figure 4.6 – Cross-Section of Precast Panel Deck

40

Plan View

Section View

Figure 4.7 – Precast Panel Design

As shown in Figure 4.3, the empirical method resulted in a significant reduction in the top reinforcement, whereas the proposed method led to a reinforcement level that was slightly higher than that required by the empirical method. As shown in Chapter 3, for the full-depth cast-in-place segment designed with the empirical method (Segment D), the total reinforcement was significantly less than what would have resulted if it was designed with the conventional method.

While the design of Segment D is presented in Section 3.3, the design of the other segments that had a composite slab is described below.

4.2 Design of Segment C using the Limit-State Method

Segment C that had precast panels as stay-in-place form was designed with the proposed limit-state method. The panels were 5'-0" x 5'-6" x 3" in dimension and the reinforced concrete topping slab was 3-in thick. In addition to service loads, the precast panels must be able to support a construction live load of 117 lbs/ft^2. Normal density concrete with a design strength of f'$_c$ = 4,500 psi was used for both the precast panels and cast-in-place topping slab. At the time of stress transfer, the concrete in the panels was specified to have a strength of f'$_{ci}$ = 4,000 psi. All mild reinforcement had f$_y$ = 60 ksi.

The design of the precast panels followed the allowable stress approach in the 16th Edition of the AASHTO Standard Specifications, and the design of the cast-in-place topping slab was also based on an allowable stress approach but using the Simplified Analysis Method presented in Appendix A for a more refined analysis that accounts for girder deflection. The composite deck was finally checked for the flexural strength, the arching strength using the method presented in Appendix B, and the punching shear strength using the method presented in Appendix C.

The panels on the north side had standard seven-wire strands, while those on the south side had Leadline CFRP bars for prestressing. The panels had the same design and construction materials as the actual full-size panels in the I-225/Parker Road interchange, except that the test panels had smaller diameter prestressing strands and bars due to the scaling.

4.2.1 Panels with Steel Strands

The prestressing strands were specified as 3/8-in diameter seven-wire low-relaxation strands. The strands had an ultimate strength of f_{pu} = 270 ksi and a modulus of elasticity of E_p = 27,000 ksi. Total time-dependent losses were assumed to be 20% of the initial prestress.

The AASHTO allowable concrete stresses were determined from Equations 2.4 through 2.7 in Chapter 2. The section properties for both the panel alone and the composite panel/cast-in-place slab were calculated and summarized in Table 4.1.

Per Equation 2.8 in Chapter 2, the jacking stress in the steel tendons was set to 203 ksi, which was 75% of the ultimate strength of the tendons. The area of one 3/8-in strand was 0.085 in^2 and the calculated jacking force was 17.3 kips/strand. Hence, it was decided to use a jacking force of 17 kips. An initial prestress loss of 3% was assumed for elastic shortening, resulting in an initial prestressing force of 16.5 kips/strand. Through an iterative procedure, five strands were selected and centered in the panel with a 9.5-in spacing between the outer two on each side of the panel and a 14.25-in spacing between the three interior strands as shown in Figure 4.7. This spacing was to conform to the setup of the precaster, in which strand spacing was fixed at integer multiples of 4.75 in.

To check the elastic shortening loss assumption, the initial prestressing force was determined by Equation 4.1 for a unit panel width and found to be equal to 16.7 kips/strand.

$$P_i = \left[\frac{P_j}{E_p A_p} + \frac{M_{panel} e}{I_{panel} E_{ci}} \right] \left[\frac{A_{panel} E_{ci} A_p E_p}{\left(1 + \dfrac{e^2}{r_{panel}^2}\right) E_p A_p + A_{panel} E_{ci}} \right] \qquad (4.1)$$

where P_j = jacking force per unit width, E_p = modulus of elasticity of prestressing tendons, M_{panel} = moment per unit width due to the self-weight of the panel, e = tendon eccentricity, I_{panel} = moment of inertia of unit width of panel, E_{ci} = modulus of elasticity of concrete at initial strength, A_{panel} = area of unit width of panel, A_p = area of prestressing tendons per unit width of slab, and r_{panel} = radius of gyration of unit width of panel.

This shows a 2% elastic shortening loss, which was close to our assumed 3%. Next, by assuming a time-dependent loss of 20%, the effective prestressing force per strand was calculated to be 13.4 kips.

The stresses in the concrete due to the initial prestress, just after the release of the tendons, were determined at the top of the panel (f_{tp}) and bottom of the panel (f_{bp}) by the following equations, respectively:

$$f_{tp} = \frac{-P_{i,p}}{A_{panel}} \left(1 - \frac{ec_t}{r_{panel}^2} \right) \qquad (4.2)$$

$$f_{bp} = \frac{-P_{i,p}}{A_{panel}} \left(1 + \frac{ec_b}{r_{panel}^2} \right) \qquad (4.3)$$

where $P_{i,p}$ = the initial prestressing force per panel width, A_{panel} = the area of the panel, e = the eccentricity of the tendons in the panel, c_t = the distance from the top of the panel to the neutral axis, c_b = the distance from the bottom of the panel to the neutral axis, and r_{panel} = the radius of gyration of the panel.

Table 4.1 – Section Properties of Precast Panel Deck with Cast-in-Place Topping

	PANEL	CIP	TOTAL		Description
B	12.0	12.0		in	design width
I	27.0	27.0	54.0	in^4	moment of inertia
A	36.0	36.0	72.0	in^2	area of concrete
Y	1.5	4.5	3.0	in	distance from neutral axis to bottom of panel
Ay	54.0	162.0	216.0	in^3	
Z	1.5	1.5		in	distance from neutral axis of panel to composite neutral axis
Az^2	81.0	81.0	162.0	in^4	
I$_c$			216.0	in^4	composite moment of inertia
c$_t$	1.5	1.5	3.0	in	distance from neutral axis to top of member
c$_b$	1.5	1.5	3.0	in	distance from neutral axis to bottom of member
c$_{tp}$			0.0	in	distance from neutral axis to top of panel
S$_{tp}$	18.0			in^3	panel section modulus with respect to top (I/c$_t$)
S$_b$	18.0			in^3	panel section modulus with respect to bottom (I/c$_b$)
S$_t$			72.0	in^3	composite section modulus with respect to top [(I$_c$/c$_t$)(E$_p$/E$_s$)]
S$_{tp}$			0.0	in^3	composite section modulus with respect to top of panel (I$_c$/c$_{tp}$)
S$_b$			72.0	in^3	composite section modulus with respect to bottom (I$_c$/c$_b$)

The stresses in the concrete due to the effective prestress were determined at the top of the panel (f_{tp}) and bottom of the panel (f_{bp}) by the following equations, respectively:

$$f_{tp} = \frac{-P_{e,p}}{A_{panel}}\left(1 - \frac{ec_t}{r_{panel}^2}\right) \tag{4.4}$$

$$f_{bp} = \frac{-P_{e,p}}{A_{panel}}\left(1 + \frac{ec_b}{r_{panel}^2}\right) \tag{4.5}$$

where $P_{e,p}$ = the effective prestressing force per panel width.

Table 4.2 shows a summary of the actual and allowable stresses in the concrete for the steel reinforced panel deck. From the table, it can be seen that the entire concrete panel should always be in compression, except for the bottom of the prestressed panel under final service loads. The maximum compressive stress experienced by the deck should be around 729 psi, which was well below the allowable stress limits. Under the final service loads, the tension in the bottom of the deck should be 329 psi, which also met the allowable limit of 402 psi.

Table 4.2 – Summary of Concrete Stresses (psi) for Steel Reinforced Panel Deck

Stresses	At Release		Construction		Final		
	f_{tp}	f_{bp}	f_{tp}	f_{bp}	f_{tp}	f_{bp}	f_t
Prestress	-464	-464	-371	-371	-371	-371	
Panel Weight	-63	+63	-63	+63	-63	+63	
Total	**-527**	**-401**					
Allowable	*-2400*	*-2400*					
Slab Weight					-63	+63	
Construction			-295	+295			
Total			**-729**	**-13**			
Allowable			*-2700*	*-2700*			
Live Load					0	+574	-574
Total					**-497**	**+329**	**-574**
Allowable					*-2700*	*+402*	*-2700*

Secondary Reinforcement

The secondary reinforcement in the panel was selected to be No. 3 bars at 12-in spacing meeting the 0.11 in^2/ft requirement of AASHTO. The final panel design is shown in Figure 4.7.

4.2.2 Panels with CFRP Bars

In this case, 8-mm-diameter Leadline CFRP bars were chosen. Based on information provided by the manufacturer, the guaranteed ultimate strength of the prestressing bars was f_{fu} = 409 ksi, and the modulus of elasticity was E_f = 21,320 ksi. For temperature and shrinkage control, GFRP bars were used. The manufacturer provided ultimate strength of the GRFP bars was f_{fu} = 121 ksi, and the modulus of elasticity was E_f = 6,000 ksi. In the design, time-dependent losses were assumed to be 15% of the initial prestress because of the lower relaxation loss in CFRP tendons.

The basic design procedure for the panels with CFRP bars was essentially identical to that with steel tendons. However, to account for the distinct mechanical properties of FPR bars, some changes were introduced. As will be described in subsequent sections, these changes were based on the recommendations in the ACI 440H Draft Document (2000) for the design of FRP reinforced structures, the paper by Mahmoud, Rizkalla and Zaghloul (1999), and the report by Dolan et al. (2000).

For FRP prestressing tendons, it was again decided to use a jacking force of 17 kips/strand. The area of one 8-mm strand was 0.0715 in^2. Hence, the jacking stress was 238 ksi, which was about 58% of the guaranteed strength of CFRP strands. An initial prestress loss of 3% was assumed for elastic shortening, resulting in an initial prestressing force of 16.5 kips/strand. Through an iterative procedure, five strands were selected and centered in the panel with a 9.5-in spacing between the outer two on each side of the panel and a 14.25-in spacing between the three interior strands.

To check the elastic shortening loss assumption, the initial prestressing force was then determined by Equation 4.1 for a unit panel width and found to be equal to 16.8 kips/strand.

This shows a 1% elastic shortening loss, which was close to the assumed 3%. Next, by assuming a prestress loss of 15%, the effective prestressing force per strand was calculated to be 14.3 kips.

The stresses in the concrete due to the prestressing force were then computed from Equations 4.2 through 4.5. Table 4.3 shows a summary of the actual and allowable stresses in the concrete for the FRP reinforced panel deck.

From the table, it can be seen that the entire concrete panel should always be in compression, except for the bottom of the panel under final service loads. The maximum compressive stress experienced by the deck should be around 755 psi, which was well below the allowable stress limits. Under the final service loads, the tension in the bottom of the deck was determined to be 303 psi, which also met the allowable limit of 402 psi.

Secondary Reinforcement

For FRP prestressed panels, temperature and shrinkage reinforcement using GFRP bars produced by Marshall Industries was designed based on the following equation with a maximum spacing of 3 times the slab thickness or 12 in, which came from the ACI 440H Draft Document (2000) pertaining to FRP reinforcement.

$$\rho_{f,ts} = 0.0018 \left(\frac{60}{f_{fu}} \right) \left(\frac{29000}{E_f} \right) \geq 0.0014 \tag{4.6}$$

where f_{fu} = the ultimate guaranteed strength (KSI) of the FRP reinforcement and E_f = the modulus of elasticity (KSI) of the FRP reinforcement.

The minimum reinforcement ratio calculated was 0.0058, so 13-mm (#4) bars at 12-in spacing were selected, resulting in a reinforcement ratio of 0.0057. Although this was slightly lower than the minimum, it was considered acceptable.

Table 4.3 – Summary of Concrete Stresses (psi) for FRP Reinforced Panel Deck

Stresses	At Release		Construction		Final		
	f_{tp}	f_{bp}	f_{tp}	f_{bp}	f_{tp}	f_{bp}	f_t
Prestress	-467	-467	-397	-397	-397	-397	
Panel Weight	-63	+63	-63	+63	-63	+63	
Total	**-530**	**-404**					
Allowable	*-2100*	*-2100*					
Slab Weight					-63	+63	
Construction			-295	+295			
Total			**-755**	**-39**			
Allowable			*-2700*	*-2700*			
Live Load					0	+574	-574
Total					**-523**	**+303**	**-574**
Allowable					*-2700*	*+402*	*-2700*

4.2.3 Cast-in-Place Topping Slab

For the entire cast-in-place topping slab, mild steel was used for reinforcement. This is the case in the actual bridge deck at the I-225/Parker Road interchange to avoid the complication of handling FRP bars at the construction site. With the limit-state approach, the reinforcement in the topping slab was the same as the negative reinforcement in the full-depth cast-in-place deck designed in Section 3.1. As shown in Table 3.3 of Chapter 3, the reinforcement included No. 3 bars at 11.25-in spacing perpendicular to the direction of traffic. The temperature and shrinkage reinforcement was No. 3 bars at 11-in spacing. It should be noted that this does not meet the

minimum requirement of 0.25 in^2/ft in the 16th Edition of AASHTO. In an effort to minimize the top steel, we elected not to follow the above requirement in this example.

4.2.4   Strength Requirements

According to the limit-state approach, a final strength check is required. The arching capacity was determined using the method presented in Appendix B. First, the parameter R was determined by Equation B.1, with $\varepsilon_c = 0.0011$, $L_r = 36$ in, and $d_1 = 2.73$ in. The resulting R was 0.0498. The arching moment ratio and the maximum arching moment resistance were then calculated by Equations B.8 and B.9. To account for the flexibility of the support restraint, the final arching moment capacity was conservatively reduced by a factor of 50%. The equivalent strip width was determined from the AASHTO LRFD manual. This value, when reduced by a factor of 2/3 for scaling, was 56.9 in as described in Section 3.1.

Slab with Steel Strands

The average stress in the prestressing steel at ultimate load was evaluated by to be 261 ksi with the following equation from the AASHTO Standard Specifications.

$$f_{ps} = f_{pu}\left[1 - \left(\frac{\gamma}{\beta_1}\right)\left(\frac{\rho f_{pu}}{f'_c}\right)\right]$$ (4. 7)

where f_{pu} = guaranteed design strength of prestressing steel, γ = factor for type of prestressing steel (0.28 for low-relaxation steel and 0.4 for ordinary stress-relieved steel), β_1 = stress block length factor, ρ = ratio of prestressing steel, and f'_c = 28-day compressive strength of concrete.

This stress was subsequently reduced to 193 ksi when checked against the following development length requirement of AASHTO.

$$f_{ps} = \frac{l_x}{D} + \frac{2}{3}f_{pe}$$ (4.8)

where l_x = distance from end of prestressing strand to center of prestressed panel, D = nominal

diameter of strand, and f_{pe} = effective stress in prestressing strand after losses.

The positive moment capacity of the composite slab was then computed based on the

following equation.

$$M_n = A_p f_{ps} d \left(1 - 0.6 \frac{\rho f_{ps}}{f'_c} \right)$$
(4.9)

where A_p = area of prestressing steel per unit width.

The positive bending moment capacity was 336 kip-in for the equivalent strip, and the

negative moment capacity of the composite deck was 148 kip-in, which is the same as that for

the full-depth cast-in-place deck designed by the proposed method. To determine the live load-

carrying capacity, the portion of the bending moment required to resist the dead load moment,

which in this case was just the self-weight of the slab, must be subtracted. The arching moment

capacity was found to be 617 kip-in. The live load capacity was calculated based on the sum of

the load resisted by both bending and arching per Equation B.14 and was equal to 61.2 kips. The

punching shear capacity of the section was identical to that of the full-depth cast-in-place deck.

The results are summarized in Table 4.4.

Slab with CFRP Bars

The bending moment capacity of the FRP prestressed deck was determined by the

method proposed by Dolan et al. (2000). In this method, the value of the reinforcement ratio with

respect to the brittle reinforcement ratio is considered. The brittle reinforcement ratio is the ratio

that causes simultaneous failure of both the concrete and the tendons and is determined by the

following equation.

$$\rho_{br} = 0.85\beta_1 \frac{f'_c}{f_{fu}}\left(\frac{\varepsilon_{cu}}{\varepsilon_{cu} + \varepsilon_{pu} - \varepsilon_{pe}}\right) \tag{4.10}$$

where f_{fu} = guaranteed strength of the FRP reinforcement, ε_{cu} = ultimate strain in the concrete = 0.003, ε_{pu} = the total strain capacity of the tendon, and ε_{pe} = the effective prestressing strain. The strain ε_{pu} is given from the manufacturer's specifications and typically ranges from 1.2% to 6.0%. For Leadline CRFP tendons, $\varepsilon_{pu} = f_{pu}/E_f = 1.9\%$. The actual reinforcement ratio is compared to this brittle ratio, and the moment capacity is calculated accordingly.

Table 4.4 – Strength Capacity Summary for the Composite Slab in Segment C

	Bending Moment Capacity				Arching Capacity				Punching Shear Capacity
	Positive		Negative						
	M_b	ϕM_b	M_b	ϕM_b	M_a	P_b	P_a	P_p	V_c
	k-in	k-in	k-in	k-in	k-in	kips	kips	kips	kips
North Side (Steel Strands)	336	**302**	148	**133**	**617**	26.9	34.3	**61.2**	**111**
South Side (CFRP Bars)	320	**288**	148	**133**	**613**	26.0	34.1	**60.1**	**111**

Under-Reinforced ($\rho < 0.5\rho_{br}$)

Under this condition, the member is largely under-reinforced and will fail by rupturing of the tendon, while the concrete will remain linearly elastic. The nominal moment is given by the following equation.

$$M_n = \rho b d^2 f_{fu} \left(1 - \frac{k}{3} \right)$$
(4.11)

where

$$k = \sqrt{(\rho n)^2 + 2\rho n} - \rho n$$
(4.12)

in which n = modulus ratio as defined by the following equation:

$$n = \frac{E_f}{E_c}$$
(4.13)

where E_f = modulus of elasticity of FRP reinforcement.

Normal Reinforced $(0.5\rho_{br} < \rho < \rho_{br})$

Under this condition, the tendon will rupture, and the stresses in the concrete will be largely non-linear. The nominal moment is given by the following equation.

$$M_n = \rho b d^2 f_{fu} \left(1 - \frac{\rho}{1.7} \frac{f_{fu}}{f'_c} \right)$$
(4.14)

Over-Reinforced $(\rho > \rho_{br})$

The nominal moment capacity is based on a rectangular compression block with $a = \beta_1 c = \beta_1 k_u d$, where a = depth of the equivalent rectangular stress block and c = distance from the extreme compression fiber to the neutral axis. Under this condition, compressive failure of the concrete is the governing failure mechanism, and the tendons will not rupture. The nominal moment is given by the following equation.

$$M_n = 0.85 f'_c b \beta_1 k_u d^2 \left(1 - \frac{\beta_1 k_u}{2} \right)$$
(4.15)

The factor k_u is calculated by the following.

$$k_u = \sqrt{\rho\lambda + \left(\frac{\rho\lambda}{2}\left(\frac{1-\varepsilon_{pe}}{\varepsilon_{cu}}\right)\right)^2} - \frac{\rho\lambda}{2}\left(1 - \frac{\varepsilon_{pe}}{\varepsilon_{cu}}\right) \qquad (4.16)$$

in which λ = material property constant calculated with Equation 4.17.

$$\lambda = \frac{E_f \varepsilon_{cu}}{0.85 f'_c \beta_1} \qquad (4.17)$$

Check of Development Length

As for normal prestressing steel, the development length for FRP is the sum of the transfer length and flexural bond length. Transfer length is the tendon length required to fully transfer the prestressing force to the concrete. Flexural bond length is the additional embedment length required to develop the ultimate tensile strength of the tendon. For FRP, Dolan et al. have proposed an equation for determining the development length for FRP prestressed reinforcement. This equation is based on the ACI equation for prestressing steel, but with the rupture strength (f_r) replacing the stress at the nominal flexural strength (f_{ps}). A more refined equation has been developed by Mahmoud et al. (1999) to include the effects of not only the tendon diameter and initial prestress, but also the compressive strength of the concrete.

$$L_d = \frac{1.89 f_{pi} d_b}{\alpha_t f'_{ci}{}^{0.67}} + \frac{1.89\left(f_{fu} - f_{pe}\right)d_b}{\alpha_f f'_c{}^{0.67}} \qquad (4.18)$$

where L_d = required development length (IN), f_{pi} = initial prestress (KSI) in the tendons, f_{fu} = guaranteed ultimate strength (KSI) of the prestressing tendons, f_{se} = effective prestress (KSI) in the tendons after all losses, f'_{ci} = initial strength (KSI) of concrete at time of tendon release, f'_c = 28-day compressive strength (KSI) of concrete, d_b = nominal diameter (IN) of prestressing tendon, and α_t and α_f are coefficients determined from regression analysis specific to particular CFRP products.

54

For Leadline CRFP tendons, $\alpha_t = 1.9$ and $\alpha_f = 1.0$. Based on the above equation, the required development length was 74.5 in; however, only the distance across half of the panel was available for development, resulting in an available development length of 33 in. By rearranging Equation 4.18, the effective f_{fu} was calculated to be 218 ksi.

In this study, $\varepsilon_{pe} = f_{pe}/E_f = 0.009$, resulting in a brittle reinforcement ratio of 0.00181. The reinforcement ratio was 0.00132, which categorized the slab as normal-reinforced. Under this condition, the nominal moment capacity was calculated to be 320 kip-in for the equivalent strip with Equation 4.14. The negative moment capacity of the composite deck was 148 kip-in. The arching moment capacity was found to be 613 kip-in. The live load capacity was calculated to be 60.1 kips.

The punching shear capacity was 111 kips. The results are summarized in Table 4.4. As one can see, the capacities of the slabs with CFRP and steel prestressed panels are almost identical.

4.3   Design of Segments A and B

Segments A and B had the same panel design as Segment C. The cast-in-place topping slab in Segment A had reinforcing details identical to the top reinforcement in Segment D, which was designed with the empirical method, while that in Segment B had the same reinforcing details as the top reinforcement in a full-depth cast-in-place slab that was designed with the conventional method in Section 3.2. The load capacity of Segment A was expected to be similar to that of Segment C, and Segment B was expected to be slightly stronger than Segments A and C in flexure and arching as it had more top reinforcement.

5. DECK CONSTRUCTION AND TESTING PROCEDURE

This chapter describes the construction of the test deck designed in Chapter 4, and the static and fatigue test procedure used to evaluate its performance. As mentioned in Chapter 4, the objectives of the tests were to evaluate the strength and long-term performance of the composite slab that has CFRP prestressed panels, compare the behavior of bridge decks designed with the empirical, conventional, and proposed limit-state methods, study the applicability of the AASHTO empirical method to topping slabs in bridge decks that have precast panels as stay-in-place forms, and examine the influence of lap splices between precast panels on deck cracking.

5.1   Deck Fabrication

The deck design is shown in Figures 4.2 through 4.7. The entire deck was 34-ft long and was to be simply supported at two ends with a 30-ft span. The W14x99 steel girders were made of A36 steel and were supplied by a steel fabricator with 6-in-long 7/8-in-diameter shear studs attached to the top flanges. Each girder had two rows of shear studs that were 3.5-in apart. The studs were spaced at 6-in on center along each girder. The girders were connected by three diaphragms made of C7x9.8 single-channel sections. The diaphragms were spaced at 15-ft apart with one at the middle of the span. They were bolted to clip angles welded to the webs of the girders at mid-height. The girders were assembled in the laboratory and supported over two wide-flange steel beams that had a round bar welded on top to provide a simple support. The assembly is shown in Figure 5.1.
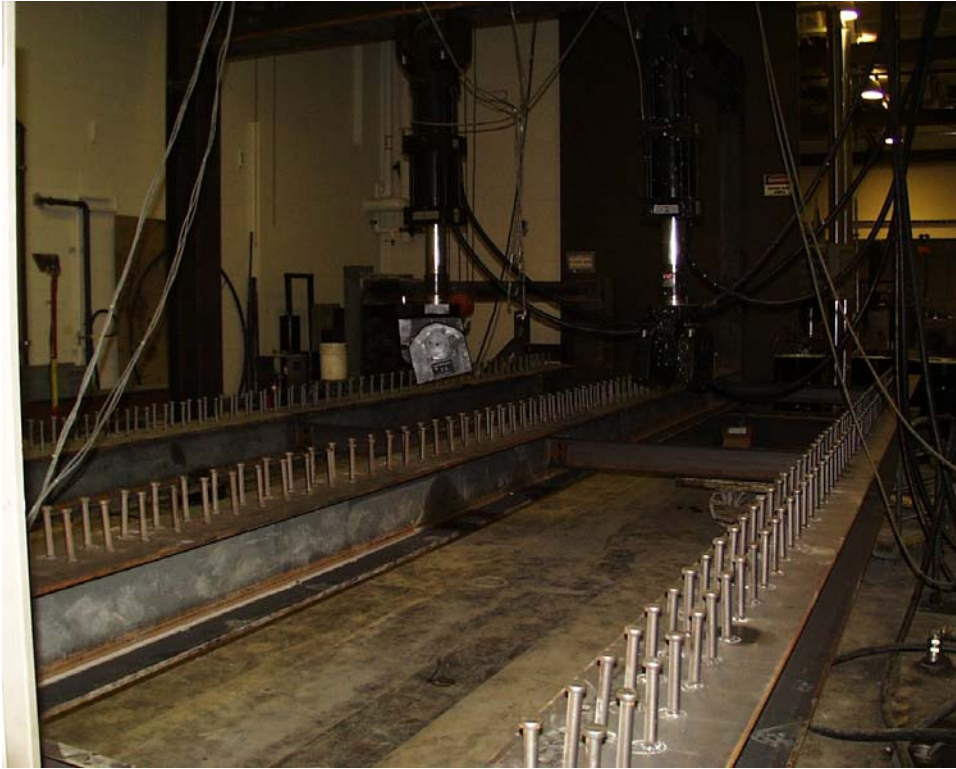
Figure 5.1 – W14x99 Bridge Girders

5.1.1   Precast Panels

The precast panels whose design is shown in Figure 4.7 were cast by a precaster. Four of the panels had Grade-270 3/8-in-diameter steel strands and the remaining four had 8-mm (0.315-in) Leadline CFRP bars. The pretensioning of the CFRP bars followed a procedure recommended by the supplier. Each steel/CFRP strand was pretensioned with a jacking force of 17 kips. The panels with steel strands were cast on April 5, 2001, and those with CFRP tendons were cast on April 10, 2001. The concrete mixes for the panels, which were based on a standard mix adopted by the precaster, are shown in Table 5.1. The concrete strength was specified to be 6,000 psi at 28 days and 4,351 psi at stress release. Originally, the panels were to be constructed with a high-performance concrete mix that had a design strength of 4,500 psi and a high fly ash content to reduce temperature and shrinkage cracks. However, this mix had a low early strength

and was found to be problematic for prestressed panels (Zylstra et al. 2001). For this reason, it was not used for these panels, but it was used for the topping slab. The casting procedure is shown in Figure 5.2.

Table 5.1 – Concrete Mixes for Precast Panels

	Panels with Steel Strands (cast on April 5, 2001)	Panels with CFRP Tendons (cast on April 10, 2001)
	lbs/yd^3	lbs/yd^3
Portland Cement Type III with Low Alkali	603	576
Water	239	252
Sand	1,207	1,207
Gravel	1,512	1,510
WRDA-19	92.5 oz/ yd^3	86 oz/ yd^3
WRDA-64	12 oz/ yd^3	12 oz/ yd^3

As shown in Figure 5.2, each panel had two spirals halfway embedded in concrete. They were intended to serve as dowels to enhance the shear transfer between the precast panels and cast-in-place topping slab as well as for lifting purpose. They were made of 10-mm diameter GFRP bars for panels with Leadline bars, and No. 3 epoxy coated steel bars for panels with 3/8-in diameter steel strands. Since they protruded more than 3 inches beyond the surface, the spirals were later cut short in the laboratory, as shown in Figure 5.5, before the casting of the 3-in-thick topping slab.

The panels were heat cured in the casting bed. The panels with steel strands reached a maximum curing temperature of 120 ^{o}F (49 ^{o}C) in ten hours, and those with CFRP tendons reached 163 ^{o}F (73 ^{o}C) in 6 hours. Two batches of 4-in-by-8-in cylinders were cast for each type of panels. One batch was heat cured with the panels and air cured afterwards, and the other was moisture cured in a curing room at room temperature. The 28-day compressive strengths obtained from these specimens are given in Table 5.2.

| Reinforcement | Casting |

Surface Roughened with ¼-in amplitude

Figure 5.2 – Construction of Precast Panels

Table 5.2 - 28-Day Compressive Strength of Precast-Panel Concrete

Panels with Steel Strands		Panels with CFRP Tendons	
Heat Cured	Moist Cured	Heat Cured	Moist Cured
7,400 psi	6,200 psi	6,700 psi	5,800 psi

The Leadline CFRP bars had a guaranteed ultimate strength of 409 ksi and a modulus of elasticity of 21,320 ksi. The No. 4 GFRP bars used for mild reinforcement had a guaranteed ultimate strength of 121 ksi and a modulus of elasticity of 6,000 ksi. No. 3 Grade 60 epoxy coated steel bars were used as mild reinforcement for the panels prestressed with 3/8-in steel strands.

5.1.2 Cast-in-Place Deck

After the panels were cast, they were delivered to the laboratory and placed on top of three W14x99 girders with 1-in wood shims in between to allow concrete to flow under the panels to produce a haunch on top of the girders. The panel installation is shown in Figure 5.3. Afterwards, No. 3 and No. 4 steel epoxy coated reinforcing bars were laid as shown in Figure 5.4. The splices between the panels are shown in Figure 5.5. Segment D of the deck (see Figure 4.2 for design) was entirely cast in place, as shown in Figure 5.6. Finally, the deck was cast by a commercial construction crew with concrete provided by a premix supplier on June 14, 2001. The casting process is shown in Fig. 5.7. The mix design for the cast-in-place concrete is shown in Table 5.3. It was the same high-performance concrete mix that was specified for the I-225/Parker Road bridge.

Table 5.3 – Mix Design for the Cast-in-Place Deck

	lbs/yd^3
Portland Cement Type I/II	470
Water	244
Sand	1,250
Gravel	1,780
Fly Ash, Class C	90
Silica Fume	25
Air Entraining Agent	2.9 oz/ yd^3
MRWR, DC-55	70.2 oz/ yd^3

The topping slab was moist cured for seven days. It was covered by plastic sheets, and sprayed with water from time to time.

Figure 5.3 – Installation of Precast Panels

Figure 5.4 – Top Reinforcement

Figure 5.5 – Panel Splicing

Figure 5.6 – Cast-in-Place Portion of Deck (Segment D)

Figure 5.7 – Casting of the Deck

Two batches of 4-in-by-8-in cylinders were cast. One batch was cured in air and the other was moist cured in a curing room. The compressive strengths of the cylinders are given in Table 5.4.

Table 5.4 – Compressive Strength of Cast-in-Place Concrete

Age	Air Cured	Moist Cured
28 dyas	4,500 psi	4,900 psi
56 days	4,800 psi	5,900 psi
84 days	4,600 psi	6,400 psi

5.2 Test Setup

The test setup was designed for both static and fatigue tests. To simulate a moving truck load, the fatigue test was conducted with two rocking curve beams as shown in Figure 5.8. The beams were made of W21x101 steel sections, and were bent into a circular arc with a radius of 600 ft. They were spaced at a center-to-center distance of 5 ft. The flange width of each beam was 12.3 in. Half-inch thick rubber pads were placed between the beams and the concrete surface of the deck to assure a more uniform load transfer.
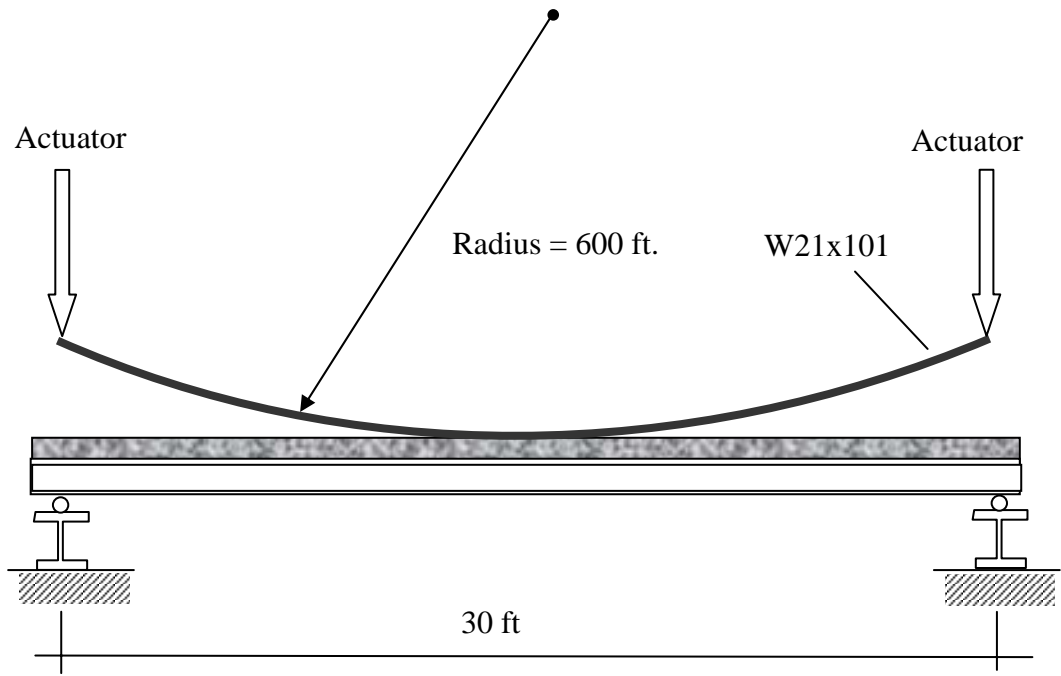
(a) Elevation View
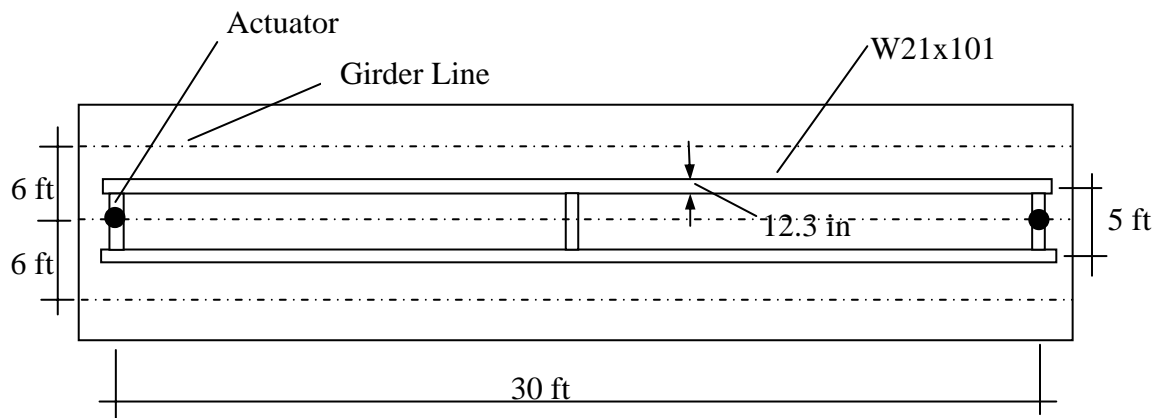
(b) Plan View

Figure 5.8 – Setup for Fatigue Test

The dimensions of the curve beams were selected based on the footprint of an HS-25 truck tire and the 2/3-scale of the test deck. According to the AASHTO LRFD Specifications (Equation 3.9), the tire area of an HS-25 truck is 20-in long and 18.6-in wide. This leads to a

scaled tire area of 13.3 in x 12.4 in. For this reason, a 12.3-in-wide steel beam section was chosen. The radius of curvature of the beams was determined by the total stroke of the actuators, which was 10 in. The contact length between a curve beam and the surface of the deck was estimated with the elastic contact theory to be close to the scaled length of a tire. Since it depends on the beam curvature, bending stiffness of the beam, and the stiffness of the rubber pads, it is difficult to estimate the contact length in an accurate manner. The distance of the wheels in a single axle of an HS-25 truck is 6 ft. For a 2/3-scale model, this leads to a wheel spacing of 4 ft. However, a 5-ft spacing was chosen to impose a more severe loading condition on the deck. A picture of the test setup is shown in Figure 5.9.

Static load tests were conducted before and after the fatigue load test to measure any change in the load resistance properties of the deck caused by fatigue load cycles, and to examine the final ultimate load resistance of the deck. As shown in Figure 5.10, a pair of static loads were applied to each of the four segments of the deck at a time by attaching the two actuators to a load frame that was orthogonal to the one used for the fatigue test, as shown in Figure 5.9. The loads were applied with 2-in-thick, 13-in-x-13-in steel plates, and there was a ½-inch-thick rubber pad between the plates and the deck to assure a more uniform load application.
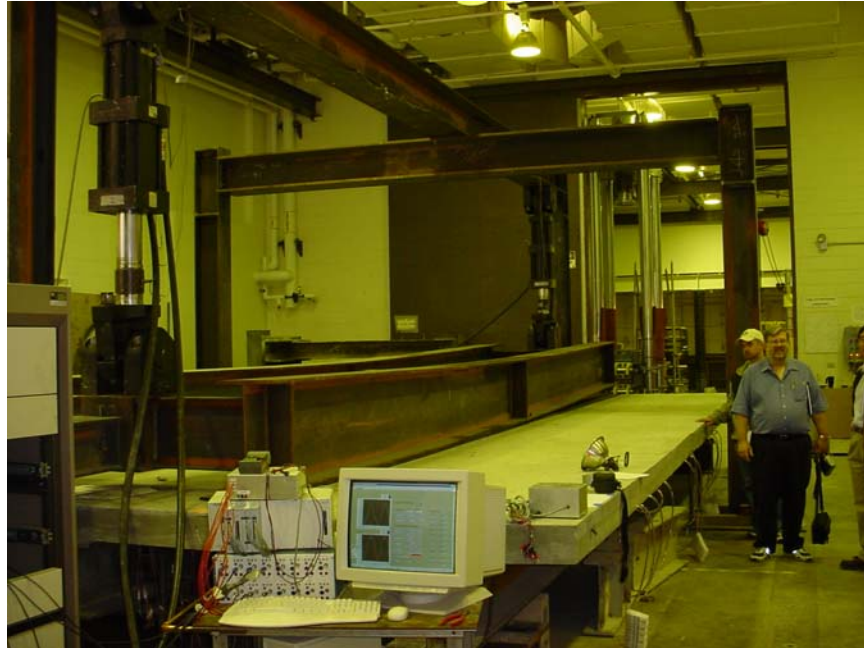
Figure 5.9 – Picture of Fatigue Test Setup
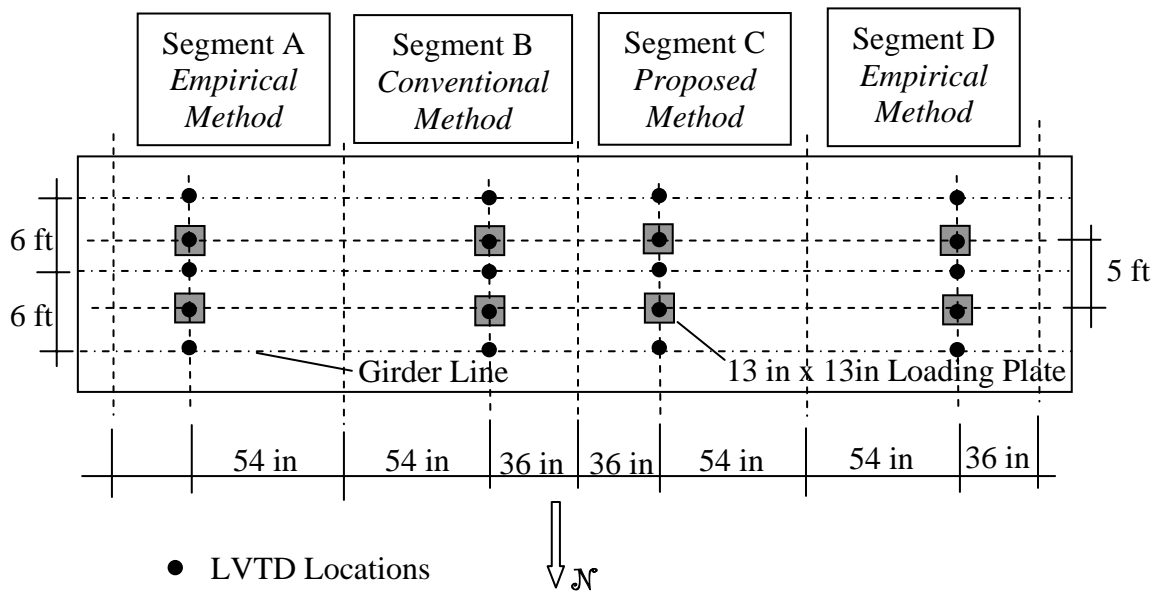
Figure 5.10 – Loading and LVDT Positions for Static Load Tests

5.3 Test Procedure and Instrumentation

5.3.1 Fatigue Test

In the fatigue test, the curve beams were rocked back and forth with a pair of actuators as shown in Figure 5.9. Each of the actuators had a load capacity of 110 kips. The actuators were under load control and driven by a sine wave function with a frequency of about 0.14 Hz. They were synchronized with a 180-degree phase angle. This resulted in a moving load that had a linear velocity of about 8.6 ft/sec. The actuators were controlled by electronic servo-hydraulic controllers, one of which had a function generator to generate a sine wave and a load cycle counter.

The total weight of the curve-beam assembly was measured to be around 7 kips. It was taken into account in determining the actuator loads. Two levels of load amplitudes were applied in the fatigue test that had a total of 160,000 load cycles or 320,000 load passes. For the first 62,000 cycles, the load in each actuator varied from 40.5 kips in compression to 2.5 kips in tension. With the self-weight of the curve beams, this resulted in a total compressive load of 22.5 kips exerted by each beam. The travel span of the load was calculated to be 28.7 ft. For the 2/3-scale deck, the scaling factor for load is 4/9. Therefore, including the impact factor, the wheel load of a scaled HS-25 truck was 11 kips. The fatigue load amplitude was, thereby, two times the design truck load.

For the remaining 98,000 cycles, the amplitude of the load in each actuator varied from 63.3 kips in compression to 2.5 kips in tension. This resulted in a total compressive load of 34 kips exerted by each beam, which was 3 times the design truck load. The travel span of the load was calculated to be 29.1 ft.

5.3.2   Static Tests

Before and after the fatigue test, static load tests were conducted with a pair of actuators on each segment of the deck as shown in Figure 5.10. As discussed in Chapter 4, each segment of the deck had a different design. Testing each segment with a pair of static loads required moving the load frame from one location to the other. The exact positions of the loads along the deck, as shown in Figure 5.10, were determined by the locations of the anchoring holes in the laboratory floor that were used to secure the load frame.

Before the fatigue test began, each segment of the deck was loaded simultaneously with two actuators up to a load of 22 kips in each actuator. Strain and deflection readings were taken. After the fatigue test was completed, these tests were repeated with a maximum load of 30 kips in each actuator. After this, the deck was loaded with one actuator at a time, up to the maximum capacity of the actuator or the failure of the deck, to examine the ultimate load resistance of the concrete slab.

5.3.3   Instrumentation

Strain gages and LVDT's (Linear Variable Differential Transformers) were installed to measure the strains and deflections of the deck at various locations. As shown in Figures 5.10 and 5.11, a group of sensors was installed in each segment of the deck. Figure 5.10 shows the positions of the LVDT's, which were all located along the same line as the applied static loads. Two of the LVDT's were directly under the applied loads and three were under the girders. The LDVT's were moved from one segment of the deck to another as the loading positions changed.

Figures 5.11 and 5.12 show the exact locations and numbering of the strain gages. The strain gages in the cast-in-place portion of the deck were glued onto rebars as shown by Sections A-A and C-C in Figure 5.12. Two bars were installed at each location to obtain two strain

readings along the depth of the slab. In regions where there were precast panels, only one bar could be used at each location as shown by Section B-B in Figure 5.12. To have two strain readings at each location in this region, a surface gage was attached to the bottom of the slab. Figure 5.13 shows the attachment of strain gages to rebars, which were later embedded in concrete at the designated locations. Each bar had two strain gages along its circumference, and was oriented in such a way that one gage was at the top and the other at the bottom to average out the localized bending effect of the bar.

All data were collected by a 16-channel data-acquisition system. The two gages on each bar were wired in such a way that only the averaged readings were recorded by a data-acquisition channel. During the static load tests, only the LVDT's and gages in the segment that was loaded were connected to the data-acquisition system. Because of the limited number of data channels, each static test was conducted two times. The first was to collect load-deflection information, and the second to collect strain readings.
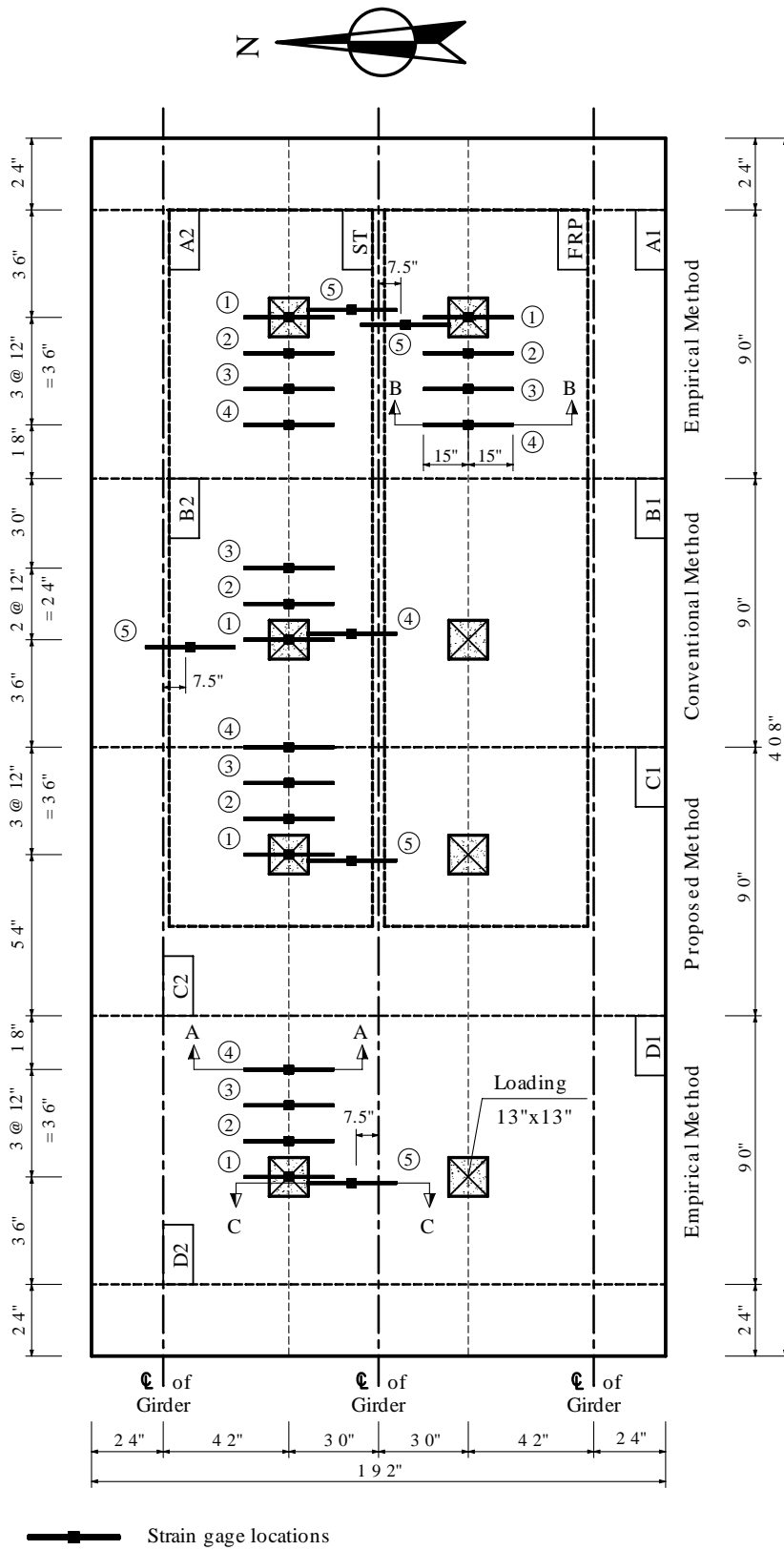
Figure 5.11 – Strain Gage Scheme

70
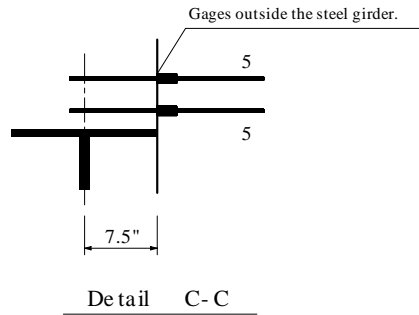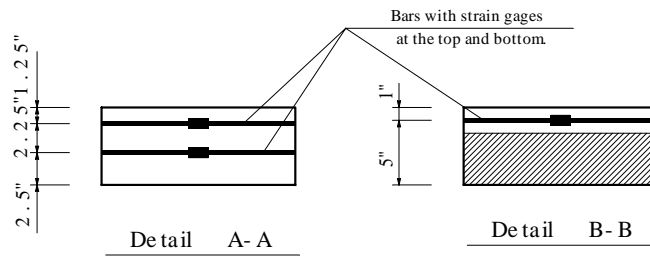
Figure 5.12 – Strain Gauge Locations along the Depth of the Slab

Figure 5.13 –Bars with Strain Gages

6. RESULTS OF DECK TESTS

The test deck was subjected to static loads and fatigue load cycles. The purpose of the static load tests was to compare the performance of the deck before and after fatigue load cycles, and to evaluate the ultimate load resistance of the concrete slab. Results of these tests are presented in this chapter. As shown in Figure 5.11, in segments A, B, and C of the deck, the south side was constructed with panels that had CFRP prestressing tendons, and the north side had steel prestressed panels. To distinguish these two regions, the south side of the deck is designated as region "1" and the north side is designated as region "2" in the following discussions. Hence, as an example, "A1" stands for the south side of segment A. However, segments D1 and D2 were all cast in place and were, therefore, identical.

6.1 Initial Static Load Tests

Before fatigue load cycles began, static load tests were conducted in September 2001 on each segment of the test deck to obtain baseline measurements on its response to static loads. In each segment, loads were applied simultaneously by a pair of actuators at locations shown in Figure 5.10. The load in each actuator was increased gradually from zero to 22 kips, which was two times the wheel load of a scaled HS-25 truck. Strain and LVDT readings were taken at small load increments. Because of the limited number of data channels in the data-acquisition system, each test was run two times. In the first run, load-deflection data were taken, and in the second run, load-strain data were taken. Once a segment was tested, the actuators were moved to a different location to test the next segment. Results of these tests are presented in the following sections.

6.1.1 Deck Deflections

As shown in Figure 5.10, the deflections of the deck in each segment were measured by five LVDT's positioned along the same line as the applied loads. Two of the LVDT's were attached to the concrete slab right underneath the loads, and the remaining three were attached to the interior and exterior girders. The load-deflection curves obtained in the initial static tests are shown in Figures 6.1 through 6.4. The tests were under load control. The two actuators were loaded simultaneously by turning the control knobs in the two analog controllers independently. The actuator loads were well synchronized with a maximum discrepancy of about 2%. The loads plotted in the following graphs are the average loads from the two actuators.

Figures 6.1 and 6.2 show the load-deflection responses at the south and north load points for all four segments of the deck. It can be seen that the response of segment D is much softer than that of segment A. This is because segment A had prestressed panels while segment D was entirely cast in place. As a result, segment D was expected to crack much earlier than segment A. Figure 6.2 shows that the response of segment D at the north load point started to deviate from that of segment A at about 7 kips, which can be identified as the cracking load. However, this change started much earlier and was more gradual at the south load point, as shown in Figure 6.1, indicating that the south side of segment D had progressive cracking started early on. Figure 6.1 shows that Segments B and C had very similar load-deflection behaviors. The two segments had similar constructions except that segment B had more top reinforcement and that a small part of C was entirely cast in place. Furthermore, segments B and C deflected a lot more than segments A and D because of the more significant girder deflections near the mid-span.
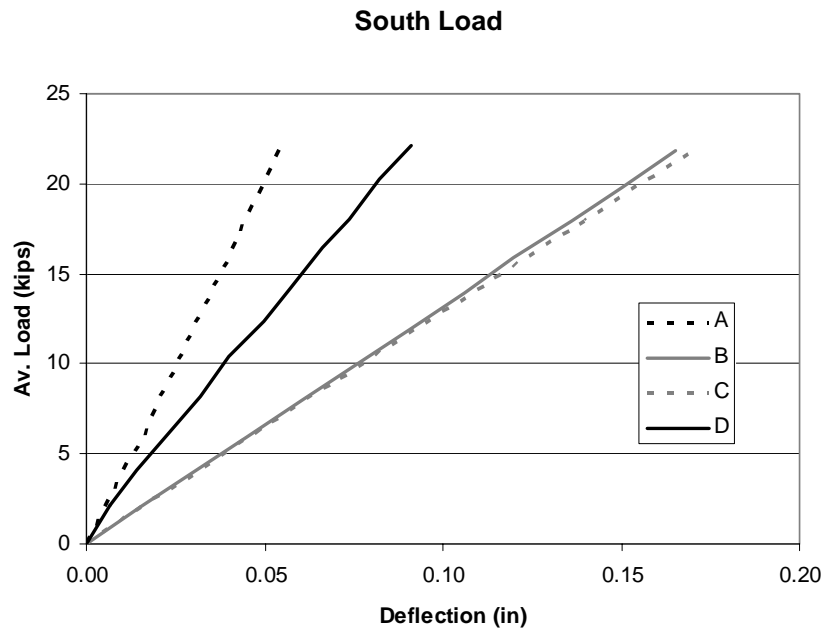
South Load

Figure 6.1 – Deflection of Slab at South Load Points in Initial Static Tests
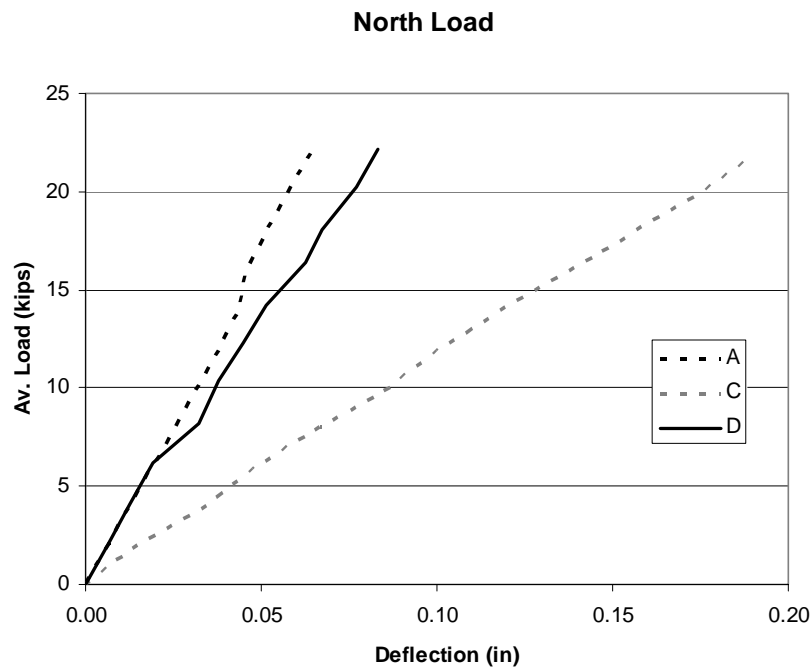
North Load

Figure 6.2 – Deflection of Slab at North Load Points in Initial Static Tests

Figure 6.3 shows the deflections of the interior girder. It can be seen that the girder deflected a lot more in segments B and C than in segments A and B. This is because the latter

segments were closer to the end supports. The deflections of the north exterior girder (NG) and south exterior girder (SG) are shown in Figure 6.4. Unfortunately, readings from several LDVT's were not good, and therefore, not included in the figure. In general, one can see that the deflection of an exterior girder was slightly less than that of the interior girder in segment A, and this difference is a lot more significant in segments B and C. This confirms the fact that differential girder deflection is more significant at the middle of a deck span than at the supports. This is accounted for in the Simplified Analysis Method presented in Appendix A.
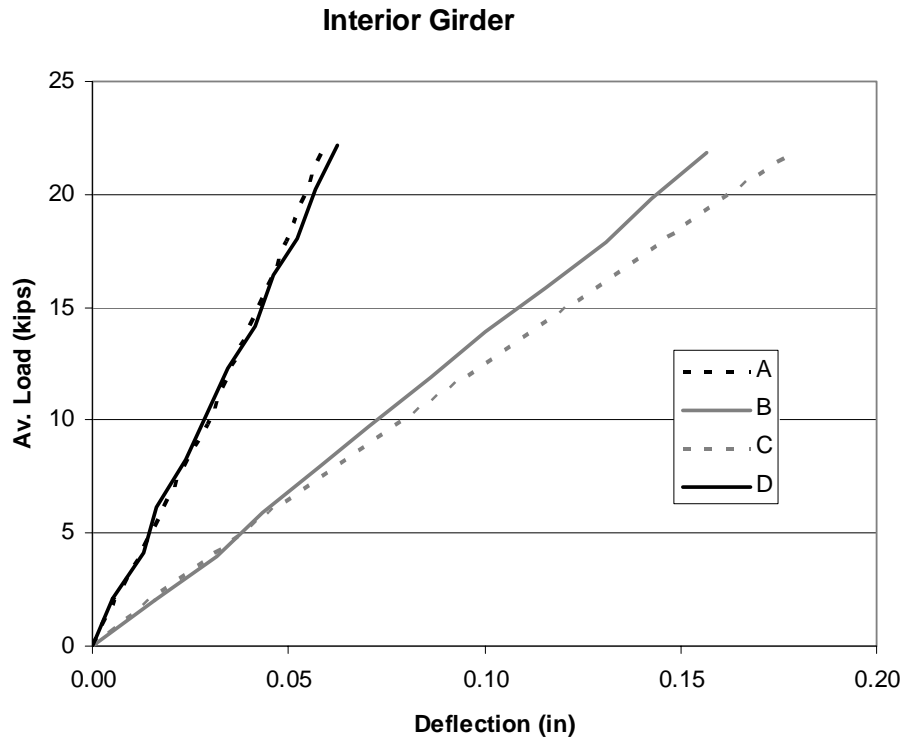
Interior Girder

Figure 6.3 – Deflection of Interior Girder in Initial Static Tests
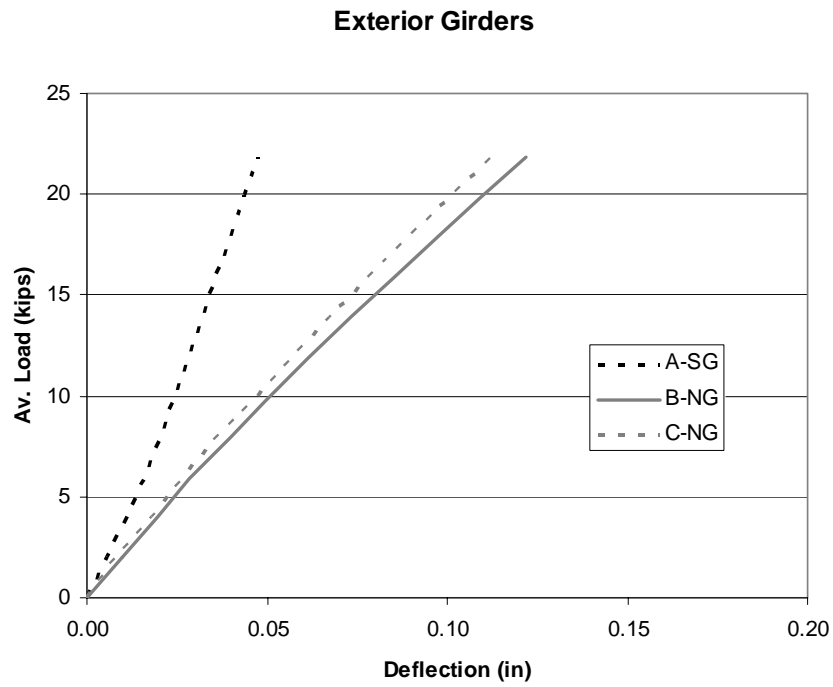
Exterior Girders

Figure 6.4 – Deflection of Exterior Girders in Initial Static Tests
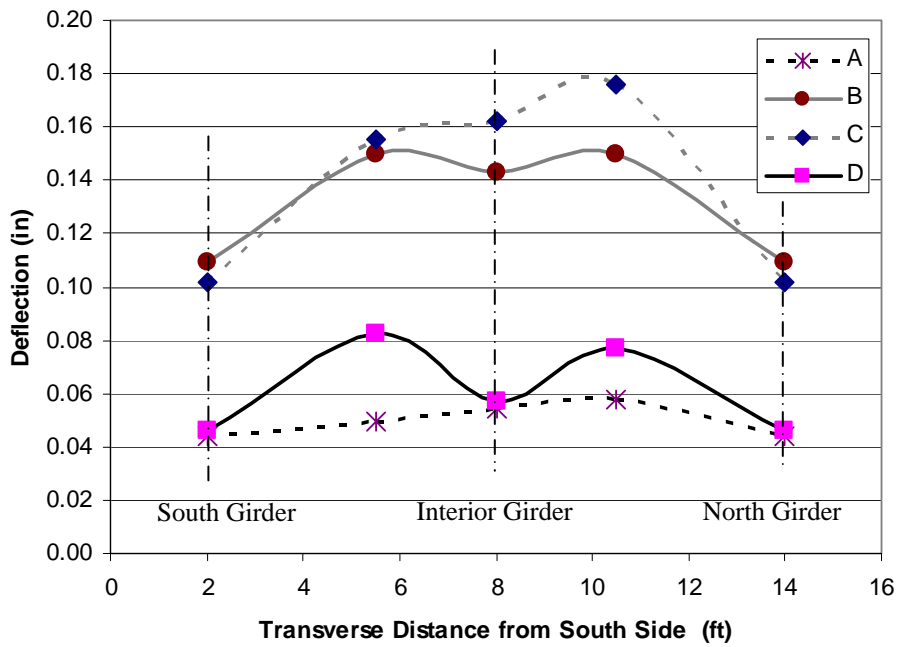
Figure 6.5 – Deflection Profiles under 20-kip Load in Each Actuator

The deflection profiles along the transverse direction of the test deck under a 20-kip load in each actuator are shown in Figure 6.5. Some of the missing data points required for this plot are reconstructed by enforcing symmetry between the south and north sides of the deck, and by assuming that the ratio of deflections between the interior and exterior girders in segment D is identical to that in segment A. It can be clearly seen from the constructed curves that the differential deflections between the exterior and interior girders are greater in segments B and C than in segments A and D. At the load points, segments with prestressed panels deformed less than segment D that had no prestressed panels. Furthermore, the limited data (from segments A and C) show that the side with steel prestressed panels (north side) deflected a little more than that with CFRP prestressed panels (south side) at the load points.

6.1.2 Strain Measurements

The strain gage readings obtained from the initial static load tests are shown in Figures 6.6 through 6.9. The gages are numbered according to the locations shown in Figure 5.11. For example, "S1-Top-A2" in Figure 6.6 stands for the strain gage reading at the top of location 1 in deck segment A2. Gage readings that do not appear to be correct are not shown in the figures. It must be noted that in segments A, B, and C, the top gages were glued onto steel bars that were embedded one inch below the top surface of the deck, as shown in Figure 5.12, while the bottom gages were directly glued onto the bottom concrete surface. For this reason, the tensile strains measured by the bottom gages were generally higher than the compressive strains measured by the top gages because the bottom gages were farther away from the neutral axis, which was located at the centroid of a deck section before the section was cracked. In segment D, the top and bottom gages were all glued onto steel bars that were embedded 1.25 in from the top and 2.5 in from the bottom, respectively, as shown in Figure 5.12.

Based on an assumption that the strain varies linearly along the depth of the concrete slab, the strains at the top and bottom surfaces of the deck can be calculated from the two strain readings obtained at each location. The strains calculated at the top of gage 1 locations in segments A and B are shown in Figure 6.10. It can be seen that the strains at the top and bottom faces are fairly symmetrical. This indicates that the neutral axis of bending was located near the mid-height of the concrete slab and, therefore, no cracking should have occurred in these locations.

Figure 6.9 shows that the tensile strains at the bottom of segment D were substantially higher than the compressive strain at the top, indicating that the bottom of segment D was cracked in the positive moment region.

Segments A1 & A2 -Initial Test
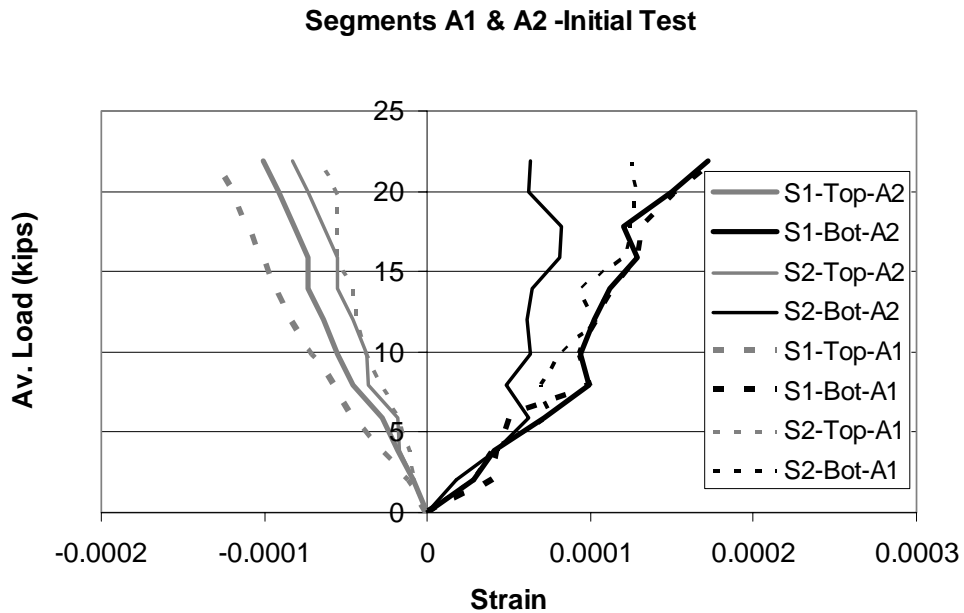
Figure 6.6 – Strain Readings from Segment A in Initial Static Test

Segment B2-Initial Test
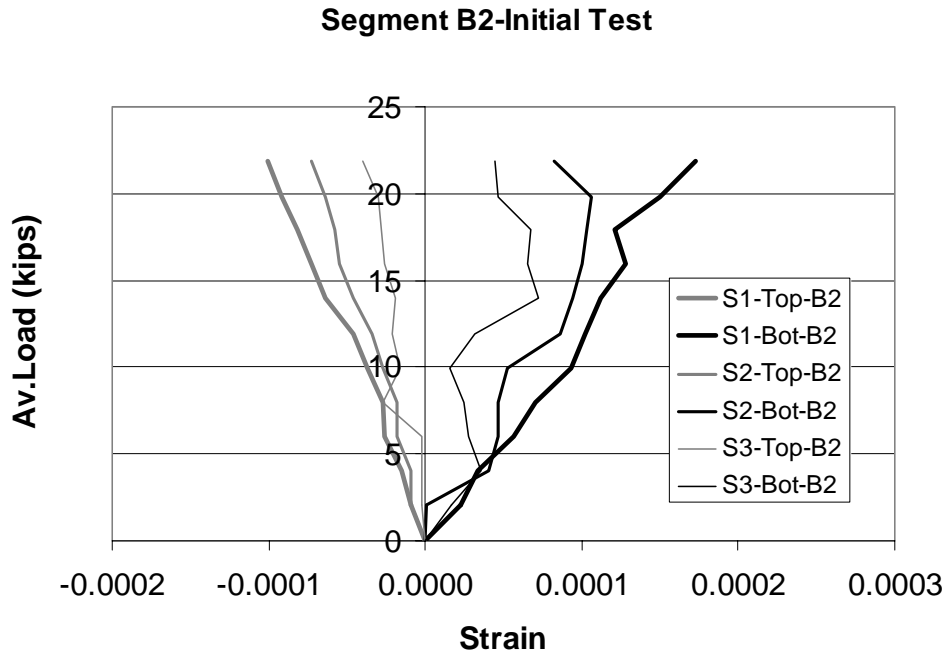
Figure 6.7 – Strain Readings from Segment B2 in Initial Static Test

Segment C2-Initial Test
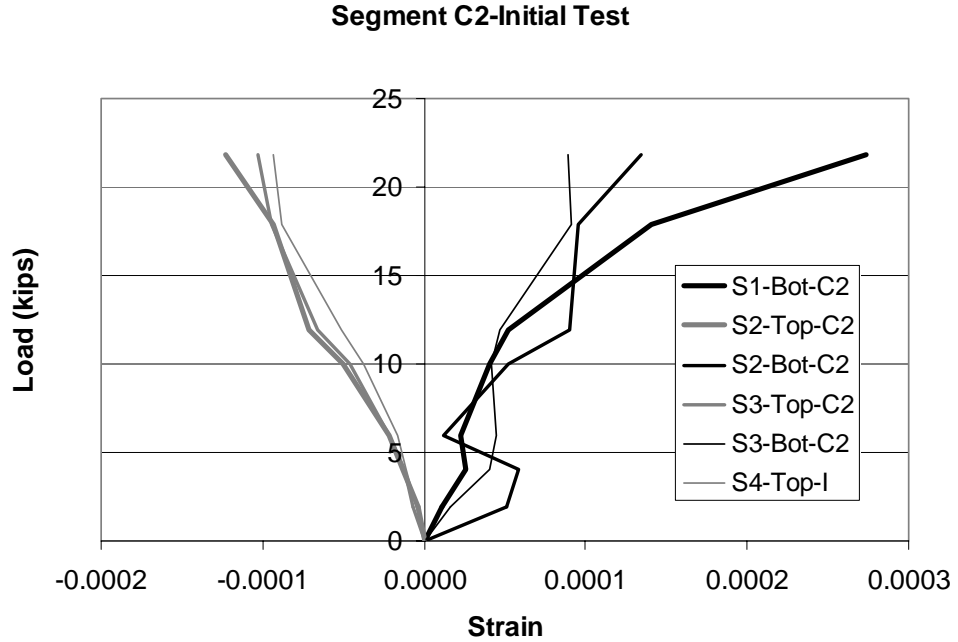
Figure 6.8 – Strain Readings from Segment C2 in Initial Static Test

Segment D2-Initial Test
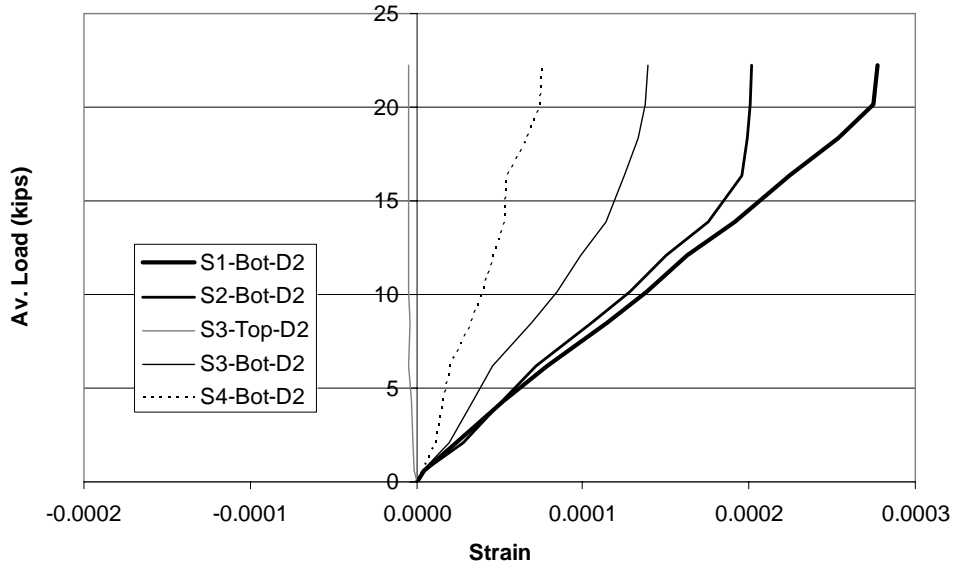
Figure 6.9 – Strain Readings from Segment D2 in Initial Static Test

Calculated Top Strain
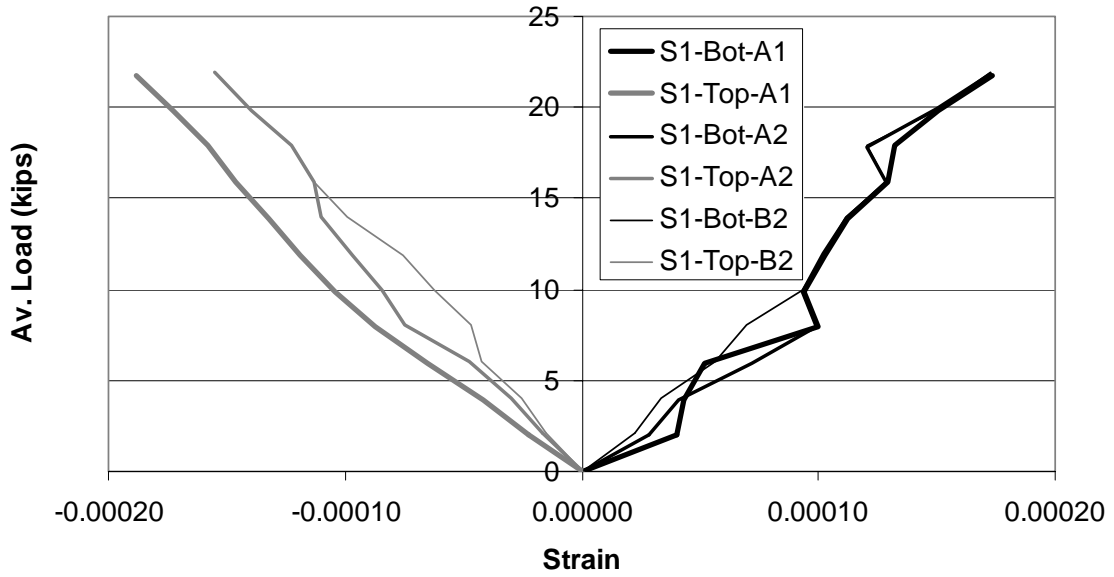
Figure 6.10 – Comparison of Calculated Top Strains to Bottom Strains

Considering that the minimum 28-day compressive strength of the heat-cured concrete used for the precast panels is 6,700 psi, as given in Table 5.2, we can calculate the modulus of rupture and modulus of elasticity of the concrete based on the formulas given in ACI-318 (1999). They are 0.614 and the 4,666 ksi, respectively. This leads to a cracking strain of 0.0001316. With the prestressing and self-weight alone, the bottom of the panels was subjected to a net precompression of 245 psi, as shown in Table 4.2. Hence, the net cracking strain due to load application should be around 0.0001841. Comparing the strains in Figures 6.6 and 6.7 to the estimated cracking strain, we can see that segments A and B should not have cracked even though they were on the verge of cracking under a 22-kip load. Nevertheless, Figure 6.8 shows that segment C2 might have cracked right underneath the load. This could be due to the propagation of flexural cracks from segment D.

Figure 6.6 shows that except for the bottom gage 1 and top gage 2 locations, strains in A1 appear to be higher than those in A2. The former had CFRP prestressing strands. However, Figure 6.5 shows that A2 had more deflection right underneath the load.

For the cast-in-place concrete, the average 84-day compressive strength of the air-cured samples is 4,600 psi, as shown in Table 5.4. Using the ACI formulas, we can estimate the modulus of rupture and modulus of elasticity to be 0.509 and 3,866 ksi. This leads to a cracking strain of 0.0001317. Comparing this to the strains shown in Figure 6.9, we can see that segment D had certainly cracked. This explains the large difference in the tensile and compressive strains measured.

Negative Moment Region-Initial Test
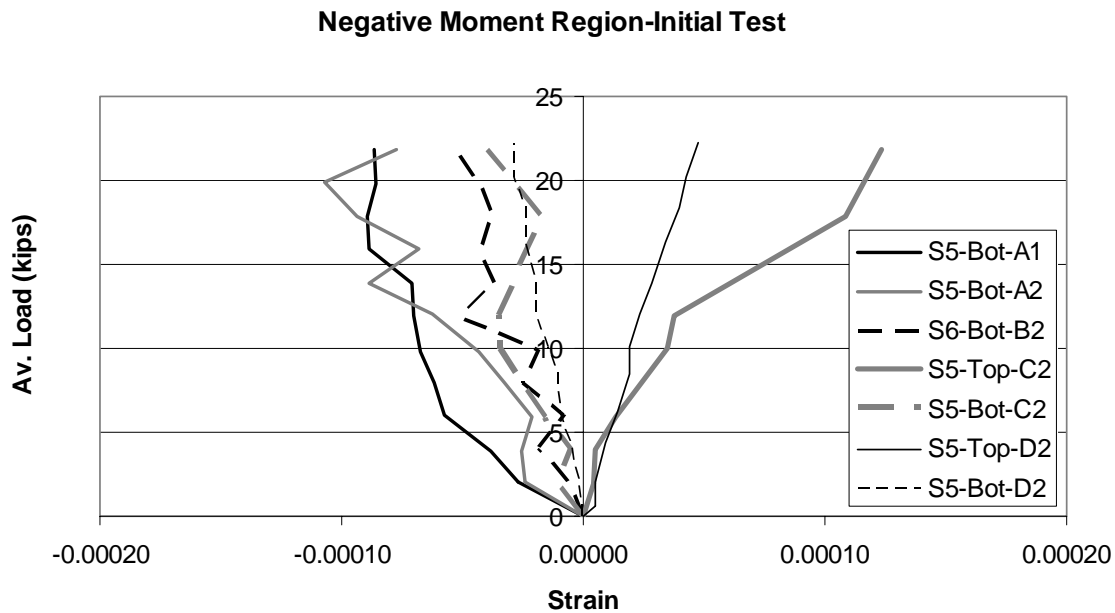
Figure 6.11 – Strain Readings from Negative Moment Regions in Initial Static Tests

The strains in the negative moment regions are plotted in Figure 6.11. It can be seen that the tensile strain at the top of segment C was unexpectedly high and the strains in segment D were unexpectedly low. These measurements could have some errors. In general, strains in a negative moment region near the mid-span should be lower than those near the end supports. This is due to the fact that near the midspan, there should be a larger differential deflection between the interior and exterior girders, as shown in Figure 6.5, which leads to a larger reduction of the negative moment as explained in Appendix A. This is confirmed by the strains measured in segments A and B, which are also shown in Figure 6.11. No cracking was observed at the top of the slab near the interior girder during the initial static load tests.

6.2 Fatigue Load Cycles

The static load tests were followed by fatigue load cycles applied by a pair of curve beams that were rocked back and forth by two actuators, as described in Sections 5.2 and 5.3.

The fatigue test was started in November 2001 and finished in August 2002. From November 7, 2001 to March 22, 2002, 62,000 load cycles (124,000 passes) were applied to the deck with a maximum load of 22.5 kips exerted by each beam. From April 15, 2002 to August 14, 2002, 98,000 load cycles (196,000 passes) were applied with a maximum load of 34 kips in each beam. These add up to a total of 160,000 load cycles or 320,000 load passes. The test ended on August 14.

During the fatigue load cycles, strain readings were taken on March 22, 2002 and May 29, 2002, respectively, and crack propagation in the concrete deck was monitored and recorded from time to time. Figure 6.12 shows the strain reading obtained on March 22, after 62,000 load cycles, at the top gage 3 location in segment A2. The peak load in the fatigue cycles was the same as the maximum load applied in the initial static load tests. Comparing Figures 6.12 and 6.6, one can see that the peak strain (S3-Top-A2) obtained under the fatigue cycles was slightly higher than that (S1-Top-A2) in the initial static load test. The two gage locations can be compared because the fatigue load was a moving load.
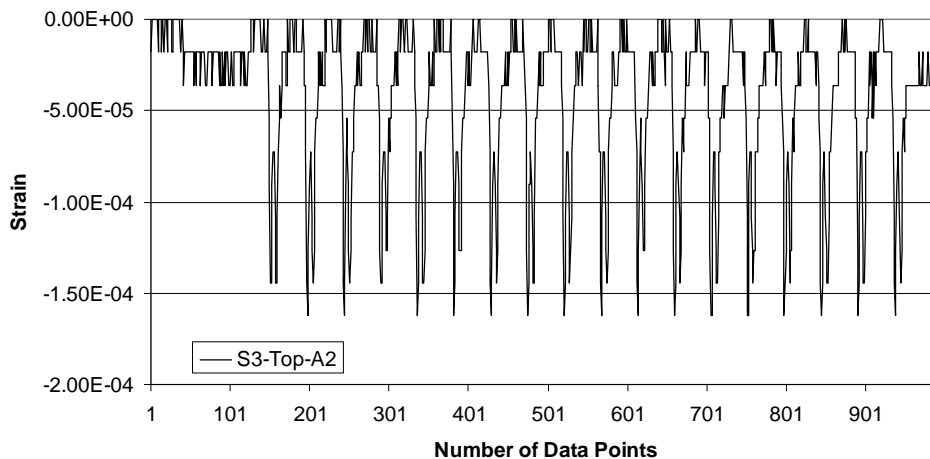
Figure 6.12 – Strain at Top Gage 3 Location in Segment A2 after 62,000 Cycles

Figure 6.13 shows the strain reading at the bottom gage 1 location in segment D2 after 62,000 load cycles. Again, the peak strain is comparable to the maximum strain obtained in the initial static load test, which is shown in Figure 6.9.
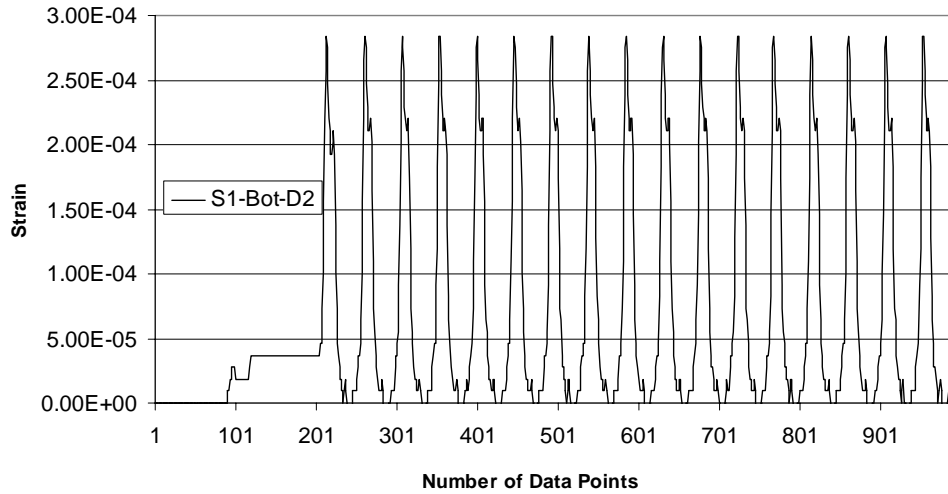
Figure 6.13 - Strain at Bottom Gage 1 Location in Segment D2 after 62,000 Cycles

Figure 6.14 shows the strain readings obtained at the bottom of segments A2 and D2 on May 29, 2002, after 62,000 load cycles with a 22.5-kip peak load in each beam and 5,790 cycles with a peak load of 34 kips had been applied. It can been seen that the peak strain in segment D2 was more than two times the maximum strain obtained in the initial static test (see Figure 6.9). This indicates that cracks had probably grown wider due to the progressive debonding of the reinforcing bars. This was highly possible under fatigue load cycles since segment D had already cracked in the initial static load test. On the other hand, strain in segment A2 remained relatively low (i.e., less than 0.0002), indicating that no cracking had occurred at the bottom of segment A2.
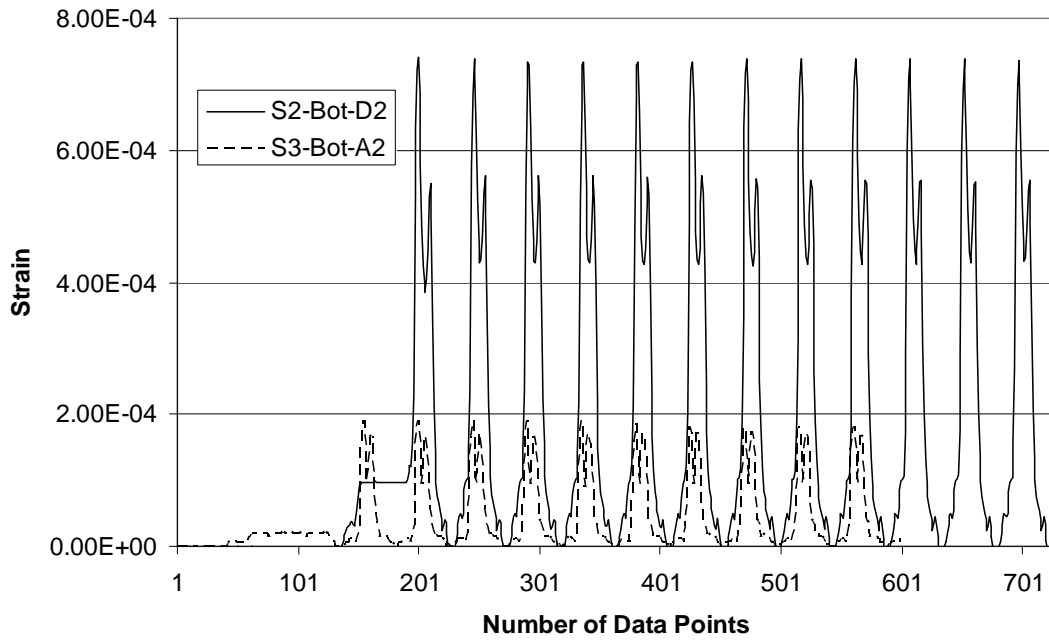
Figure 6.14 – Strains in Segments A2 and D2 after 67,790 Cycles

The crack patterns recorded during the fatigue test are shown in Figures 6.15 through 6.17. It can be seen that cracks were localized at the top and bottom of segment D within the first 60,900 cycles. Later on, a longitudinal crack propagated at the top along the entire length of the deck right above the interior girder, and cracks at the bottom propagated from segment D to C.
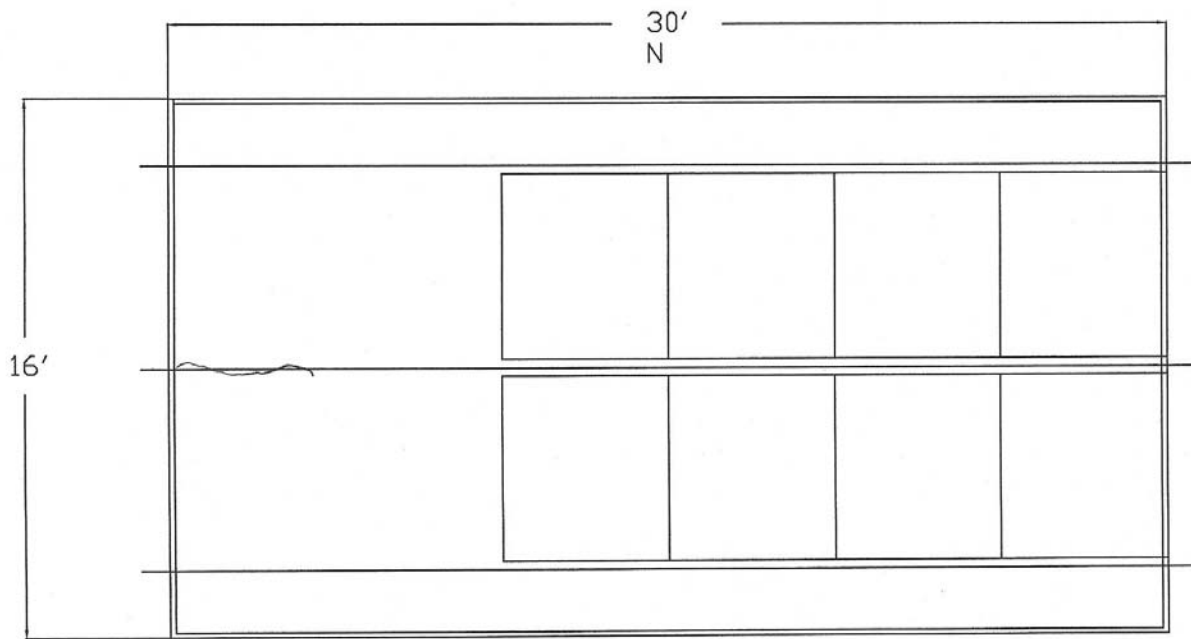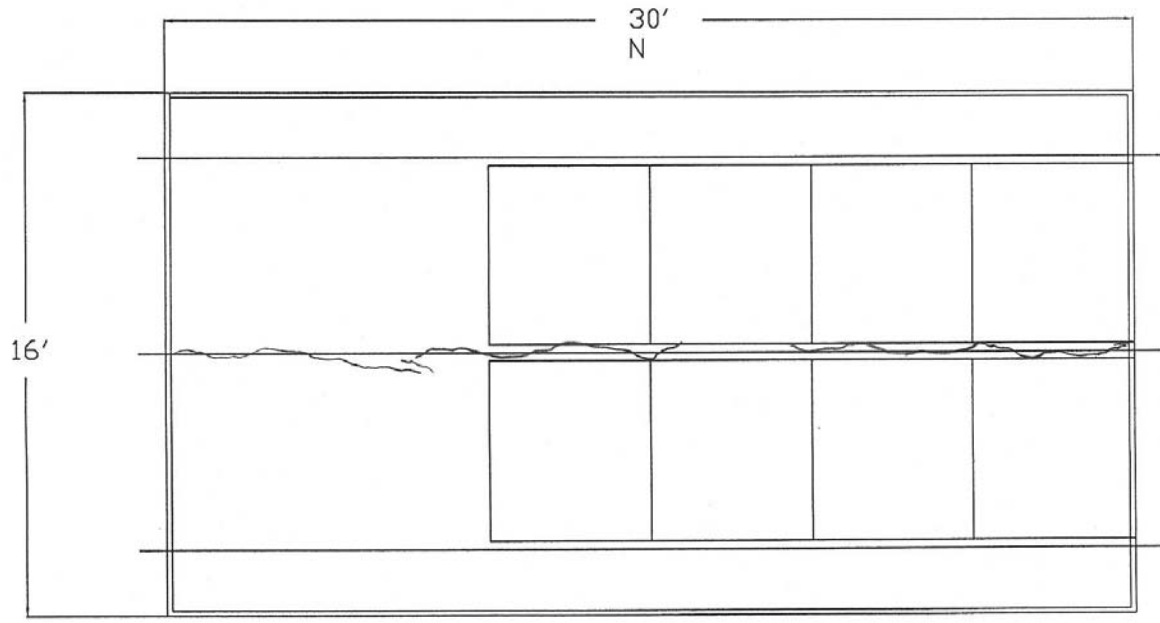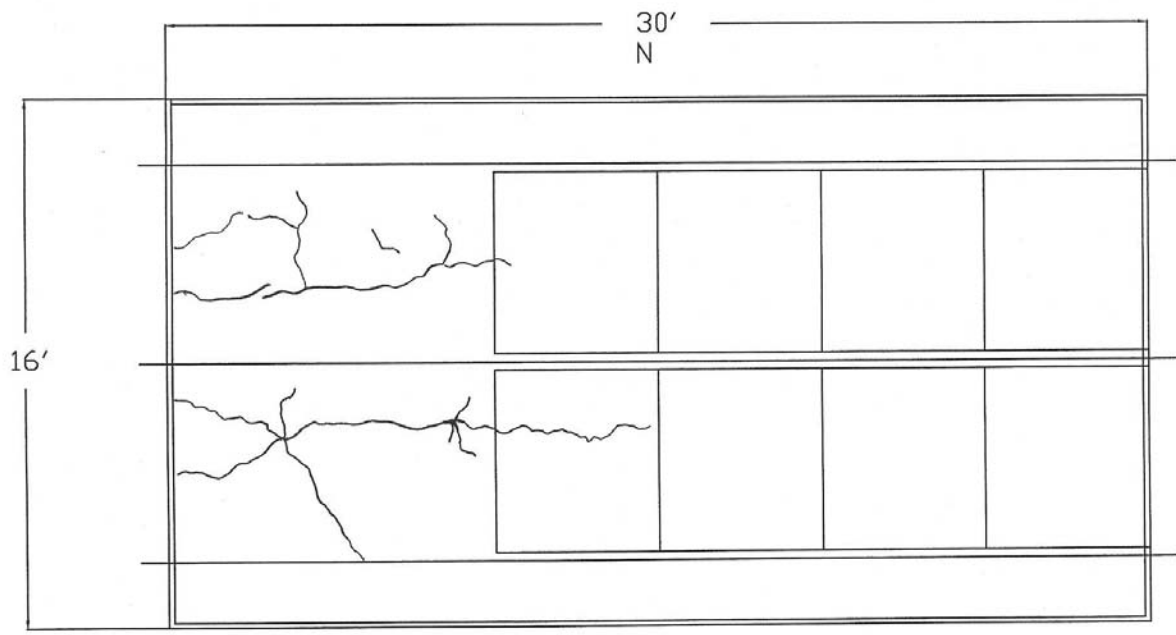
Top Surface
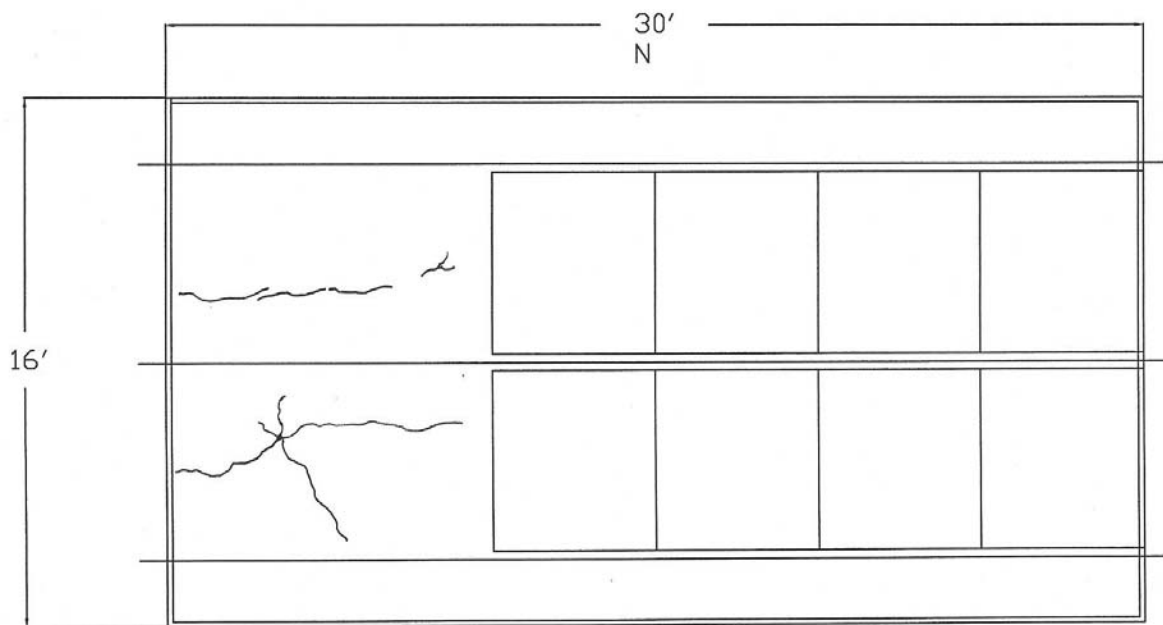
Bottom Surface

Figure 6.15 – Crack Patterns Recorded on March 15, 2002 (60,900 Cycles)
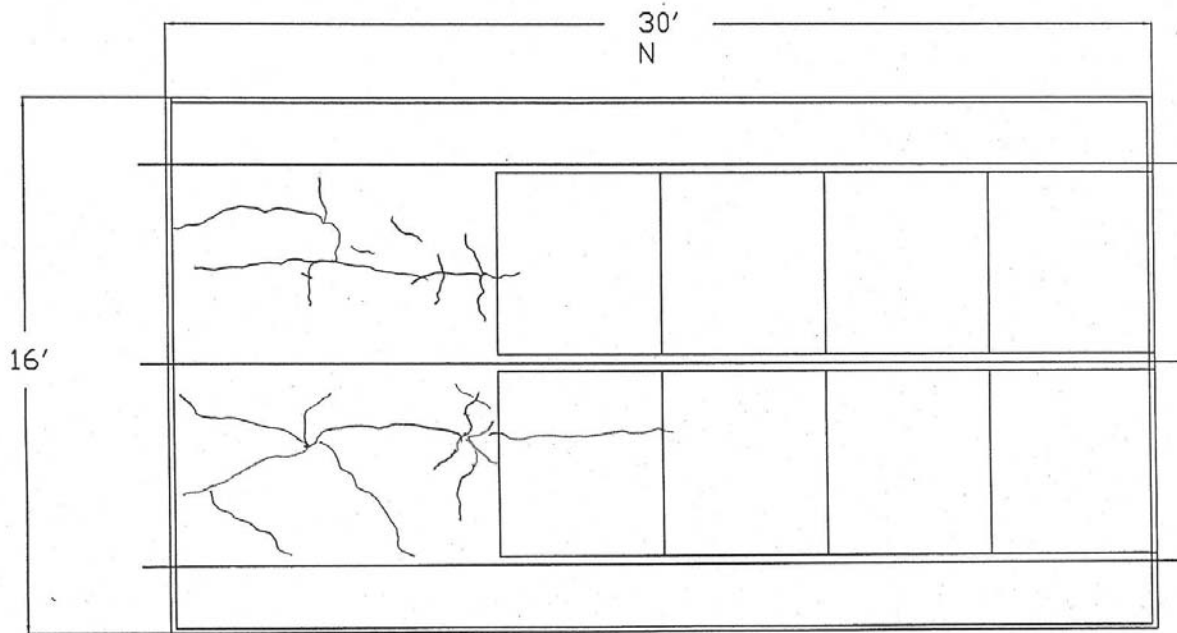
Top Surface

Bottom Surface

Figure 6.16 - Crack Patterns Recorded on June 4, 2002 (77,000 Cycles)
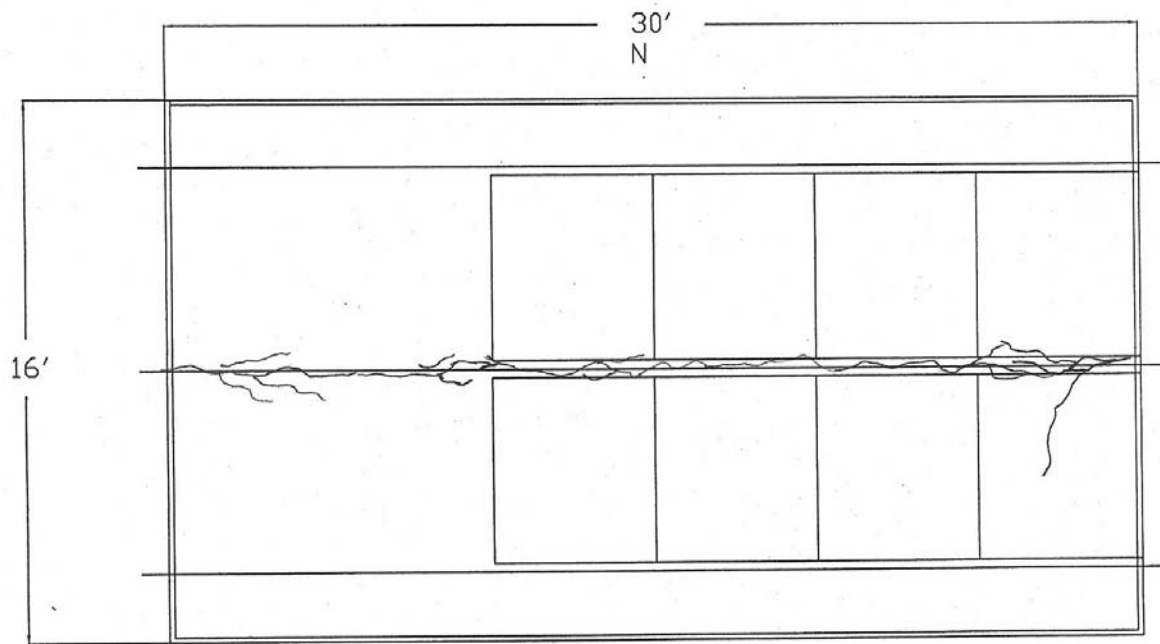
Top Surface

Bottom Surface

Figure 6.17 – Crack Patterns Recorded on August 14, 2002 (160,000 Cycles)

6.3 Final Static Load Tests

The final static load tests were conducted in October 2002, after 160,000 load cycles (320,000 load passes), to observe any change in the load-strain behavior of the deck and to evaluate the ultimate load resistance of the concrete slab. In these tests, each segment of the deck was first loaded with two actuators simultaneously, similar to the initial static load tests, up to a maximum load of 30 kips. After this, each side (north/south) of the deck was loaded one at a time with a single actuator up to failure or the maximum calibrated load capacity of the actuator, which was about 107 kips, whichever came first.

The strain readings obtained in the double actuator tests are compared to those obtained in the initial static tests. Figures 6.18 through 6.22 compare the strains obtained at gage 1 locations in the initial and final static tests. In these figures, "I" and "F" stand for the initial and final tests, respectively. It can be seen that segments A and B did not exhibit any significant change in the load-strain response. Unfortunately, there is not sufficient data to make a comparison for segment C because of bad gage readings. However, the strains shown in Figure 6.21 indicate that C2 did not have any major cracking. These results confirm the crack patterns observed and shown in Figures 6.15 through 6.17. Figure 6.22 shows that the strain at the bottom gage 1 location in segment D2 increased in the final static test indicating the widening of the bottom crack due to the progressive debonding of the reinforcing bars.
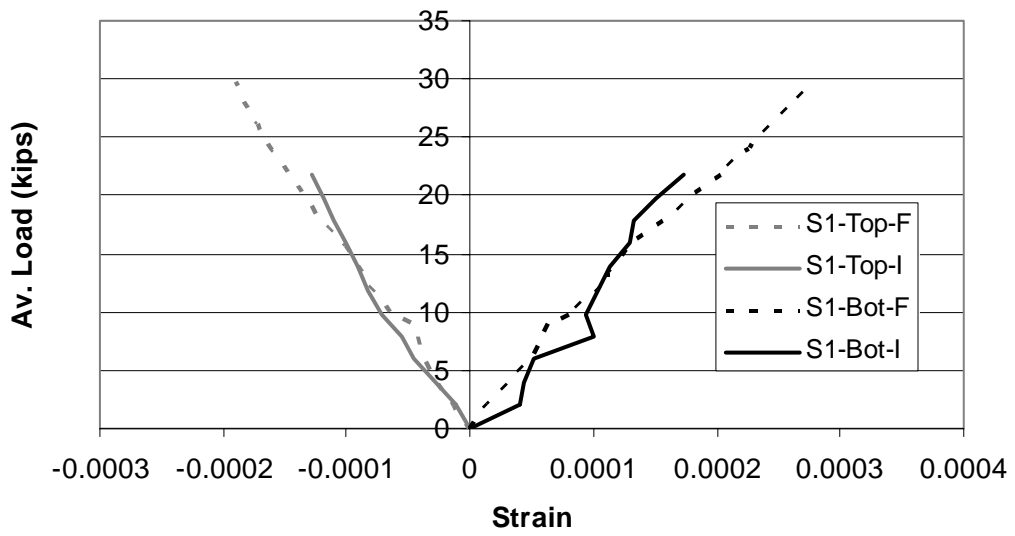
Segment A1-Two Loads

Figure 6.18 – Strain Readings from Segment A1 in Final Two-Actuator Test
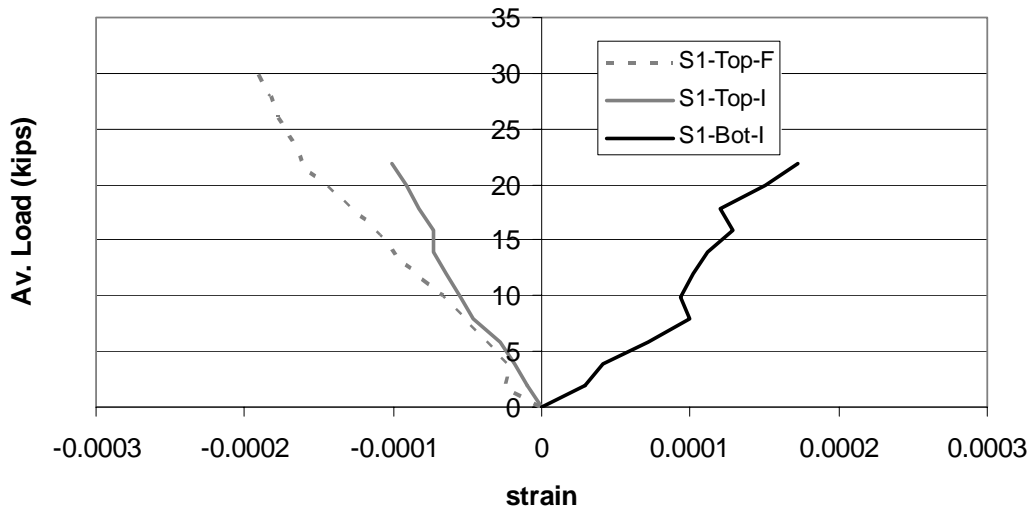

Segment A2-Two Loads

Figure 6.19 – Strain Readings from Segment A2 in Final Two-Actuator Test
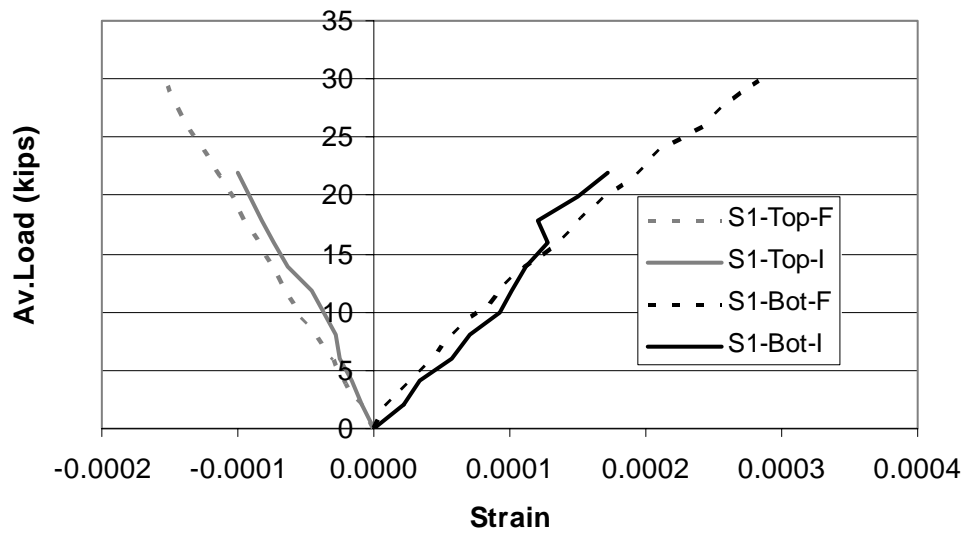
Segment B2-Two Loads

Figure 6.20 – Strain Readings from Segment B2 in Final Two-Actuator Test
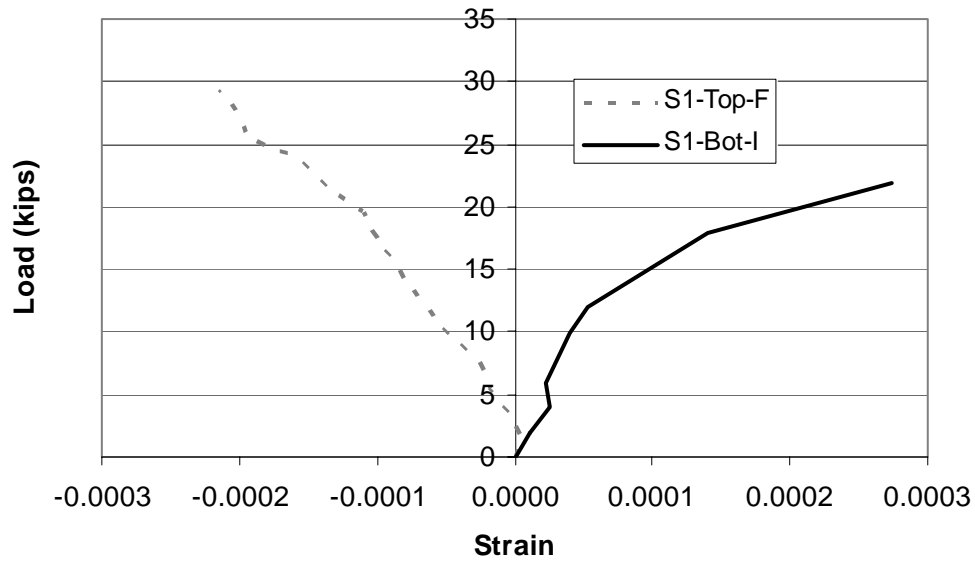
Segment C2-Two Loads

Figure 6.21 – Strain Readings from Segment C2 in Final Two-Actuator Test
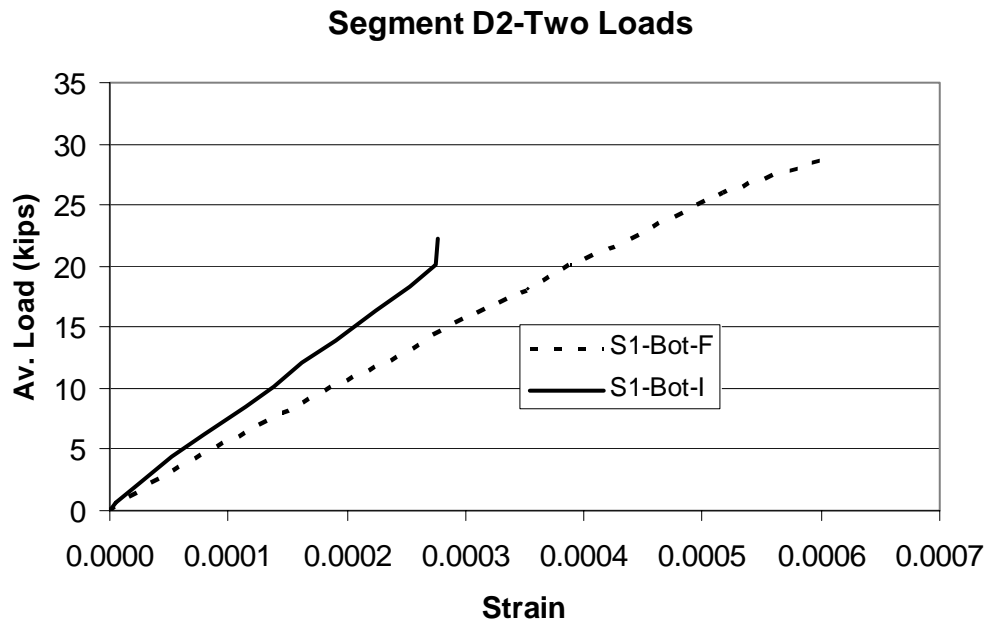
Segment D2-Two Loads

Figure 6.22 – Strain Readings from Segment D2 in Final Two-Actuator Test

The linear load-strain relations in Figures 6.18 and 6.20 indicate that segments A1 and B2 did not crack at the bottom gage 1 locations up to a maximum tensile strain of 0.0003.

After reaching 30-kip loads in the two actuators, the deck was unloaded and loaded again with one actuator at a time up to 107 kips or failure, whichever came first. Both segments D1 and D2 had a punching shear failure at about 102 kips. A typical crack pattern for the punching shear failure is shown in Figure 6.23. However, the load carrying capacities of Segments A, B, and C were beyond the load capacity of the actuators, and were, therefore, not reachable in the tests.

The strain readings obtained from the single-actuator tests are shown in Figures 6.24 through 6.28. It is interesting to observe from Figures 6.24 through 6.27 that the strains measured at top gage 1 locations in segments A, B, and C started to decrease as the load increased beyond 40 kips. This indicates that the neutral axis had a significant upward shift due to the cracking of the prestressed panels, subjecting the top gages, which were 1 inch below the top surface of the

deck, to tension. As shown in Figure 6.28, no such change can be observed in segment D, which was entirely cast in place. This difference can be explained by the fact that the concrete in the prestressed panels had a significant contribution to flexural tension, and the loss of this tensile resistance due to cracking caused a significant shift of the neutral axis. The strains at bottom gage 1 locations in segments A1 and B2 (Figures 6.24 and 6.26) indicate that cracking occurred at a strain level of about 0.0003 right before a 40-kip load was reached.

Figure 6.23 – Punching Shear Crack
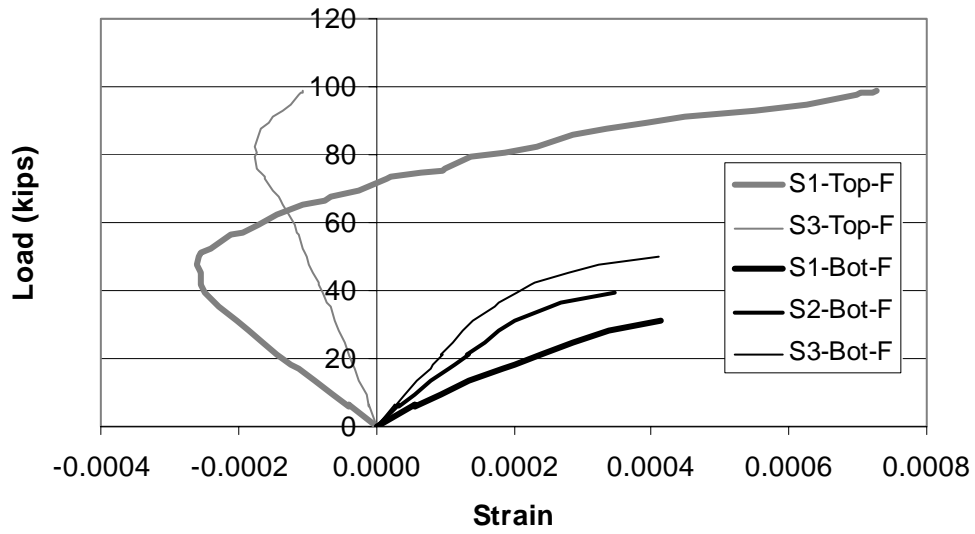
Segment A1-Single Load

Figure 6.24 - Strain Readings from Segment A1 in Final One-Actuator Test

Segment A2-Single Load

Figure 6.25 - Strain Readings from Segment A2 in Final One-Actuator Test

Segment B2-Single Load

Figure 6.26 - Strain Readings from Segment B2 in Final One-Actuator Test
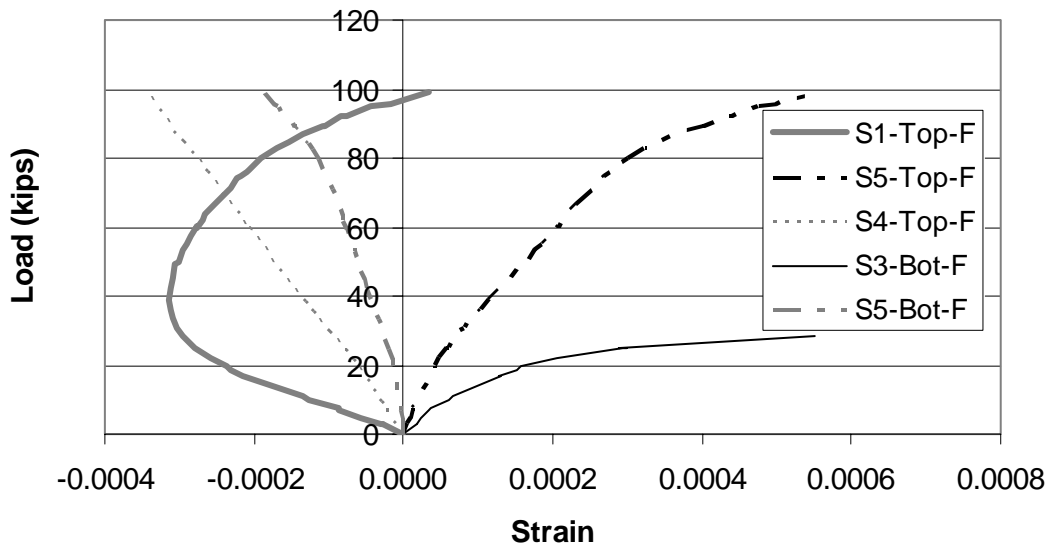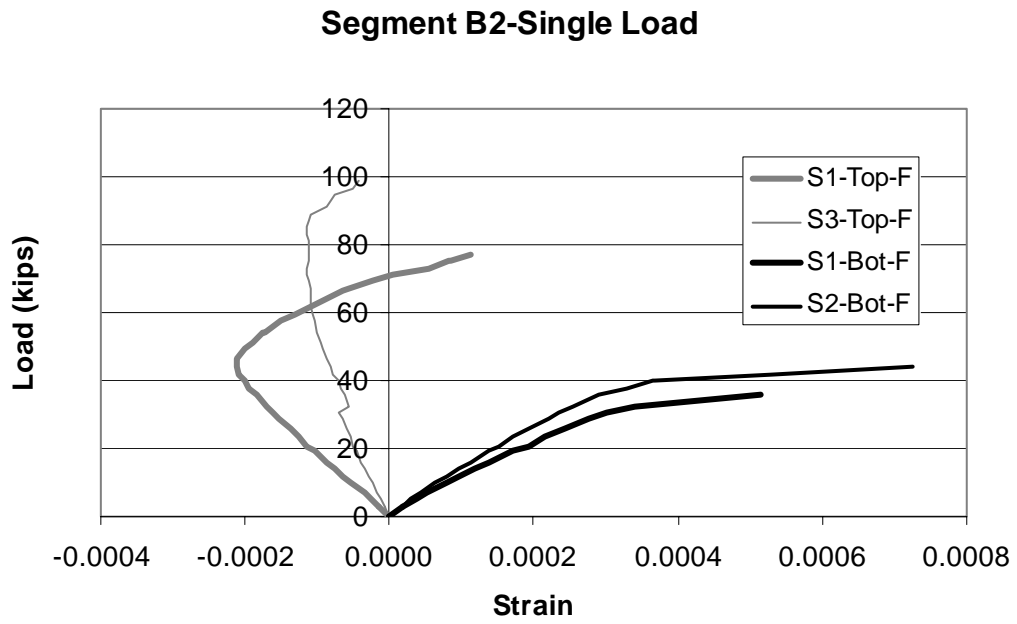
Segment C2-Single Load

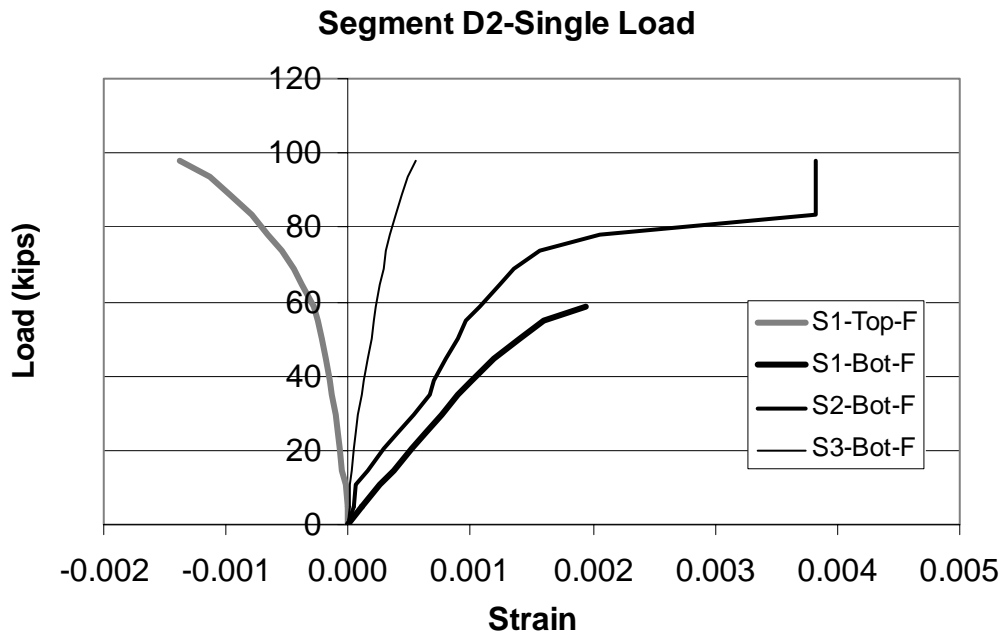Figure 6.27 - Strain Readings from Segment C2 in Final One-Actuator Test

Figure 6.28 - Strain Readings from Segment D2 in Final One-Actuator Test

6.4 Concluding Remarks

The following conclusions can be obtained from the test results.

1. Segments A, B, and C of the bridge deck, which had precast panels, demonstrated a better performance than segment D, which was cast in place. The prestressing force in the precast panels delayed/prevented the cracking of the deck and, therefore, improved its endurance under fatigue load cycles.

2. The deck developed a significant arching mechanism that led to a very high load resistance. Segment D had punching shear failures at a load of about 102 kips, which is slightly under the theoretical prediction of 111 kips evaluated with the method presented in Appendix C. The punching shear capacities of segments A, B, and C were higher than the prediction. This indicates the contribution of the prestressing force, which is ignored in the theoretical formula in Appendix C, to the punching shear strength. In summary,

after 160,000 of fatigue load cycles, the strength of the deck was still at least 10 times the design truck load.

3. Segments A, B, and C showed comparable performances. Segments A and B, whose top reinforcement was selected according to the empirical method and the conventional method of AASHTO, respectively, had no bottom cracks, while segment C, whose top steel was selected with the proposed limit-state method, had bottom cracks developed in the positive moment regions. These cracks were, however, extensions of the cracks developed in segment D.

4. There was no visible difference in the performances of the south and north sides of the deck, which had CFRP prestressed panels and steel prestressed panels, respectively.

5. No reflection cracks were observed on the top surface of the deck right above the joints between the precast panels. The absence of lap splices at some panel joints did not seem to promote reflection cracks.

In general, the precast panel portion of the deck performed well under fatigue load cycles. No delamination between the panels and the cast-in-place topping slab was observed. A small separation between the concrete slab and the steel girders was observed at the west end of the deck, as shown in Figure 6.29, at the conclusion of the fatigue test.

Figure 6.29 – Small Separation between the Concrete Slab and a Steel Girder

7. SUMMARY AND CONCLUSIONS

7.1 Summary

In an IBRC (Innovative Bridge Research and Construction) project sponsored by the FHWA, a bridge deck with CFRP (carbon fiber reinforced polymeric) prestressed panels was designed and constructed by the Colorado Department of Transportation (CDOT) at the I-225 and Parker Road interchange southeast of Denver. To evaluate the long-term performance of these panels as compared to conventional steel prestressed panels, a model bridge deck was constructed and tested under static loads and fatigue load cycles in the Structures Laboratory of the University of Colorado. The deck was 16-ft wide and had a 30-ft long span, representing a 2/3-scale model of a three-girder deck.

The span of the deck was along the east-west direction. The concrete slab in the deck was 6-in thick and had four distinct segments along the span. Each segment had a different design and construction. Segments A, B, and C had 3-in thick precast panels as stay-in-place forms and a 3-in topping slab. The south side of the deck had CFRP prestressed panels, while the north side had steel prestressed panels. The latter was introduced in the test for comparison purpose. Except for the scaling, both types of panels were designed in the same way as those in the I-225 bridge. The topping slab in segment A was designed with the empirical method of the AASHTO LRFD Specifications, while that in segment B was designed with the conventional method of AASHTO. The topping slab in segment C was designed with a new limit-state method (Borlin 2001) that accounts for girder deflections and the arching mechanism of the concrete slab. Segment D was entirely cast in place and was designed with the empirical method.

The main objectives of the study were to evaluate the strength and long-term performance of the composite slab that has CFRP prestressed panels, compare the behavior of

bridge decks designed with the empirical, conventional, and proposed limit-state methods, study the applicability of the AASHTO empirical method to topping slabs in bridge decks that have precast panels as stay-in-place forms, and examine the influence of lap splices between precast panels on deck cracking. To meet the last objective, part of the panels had lap splices and the rest did not. The design of the lap splices followed the normal practice of CDOT.

The topping slabs for Segments A and C of the deck, which were designed with the AASHTO empirical method and the new limit-state method, respectively, had comparable quantities of negative reinforcement. They were about 70% less than that in segment B, which was designed with the AASHTO conventional method. Segment D, which was entirely cast in place, had a total reinforcement that was 28% of that required by the AASHTO conventional method.

7.2 Conclusions

From the load resistance standpoint, CFRP bars seem to be a viable alternative to steel tendons for precast panel construction. The portion of the bridge deck that had CFRP prestressed panels demonstrated the same performance as that with steel prestressed panels. In the example considered in this report, the limit-state design method developed in this project resulted in a reinforcement quantity that is comparable to the empirical method of AASHTO. The former is, however, a more rational approach based on a rigorous analytical procedure.

The test results show that the segments of the deck that had the topping slabs designed with the empirical method and the limit-state method exhibited the same performance as that designed with the conventional method, even though the latter required 70% more reinforcement in the topping slab. Furthermore, with the use of the empirical method, the segment (segment A) of the deck that had precast panels performed better than the full-depth cast-in-place segment

(segment D) due to the enhanced strength and crack resistance introduced by the prestressed panels.

In particular, the following observations are obtained from the test results.

1. Segments A, B, and C of the bridge deck, which had precast panels, demonstrated a better performance than segment D, which was cast in place. The prestressing force in the precast panels delayed/prevented the cracking of the deck and, therefore, improved its endurance under fatigue load cycles.

2. The deck developed a significant arching mechanism that led to a very high load resistance. Segment D had punching shear failures at a load of about 102 kips, which is slightly under the theoretical prediction of 111 kips evaluated with the method presented in Appendix C. The punching shear capacities of segments A, B, and C were higher than the prediction. This indicates the contribution of the prestressing force, which is ignored in the theoretical formula in Appendix C, to the punching shear strength. In summary, after 160,000 of fatigue load cycles, the strength of the deck was still at least 10 times the design truck load.

3. Segments A, B, and C showed comparable performances. Segments A and B, whose top reinforcement was selected according to the empirical method and the conventional method of AASHTO, respectively, had no bottom cracks, while segment C, whose top steel was selected with the proposed limit-state method, had bottom cracks developed in the positive moment regions. These cracks were, however, extensions of the cracks developed in segment D.

4. There was no visible difference in the performances of the south and north sides of the deck, which had CFRP prestressed panels and steel prestressed panels, respectively.

5. No reflection cracks were observed on the top surface of the deck right above the joints between the precast panels. The absence of lap splices at some panel joints did not seem to promote reflection cracks.

The use of the AASHTO empirical method for the design of the topping slab of a precast panel deck does not seem to jeopardize the deck performance under fatigue load cycles. The empirical method can lead to a significant reduction of the top reinforcement in such a deck. It will not only save construction costs, but will also prolong the life-span of a bridge deck that has steel reinforcement by reducing corrosion problems. Therefore, it is recommended that the empirical method be allowed for the design of the topping slab for precast panel decks.

The limit-state design method proposed in this project will result in a reinforcement quantity that is comparable to the empirical method of AASHTO. The former is, however, a more rational approach based on a rigorous analytical procedure. With more calibration and evaluation, this method can be adopted in the design practice.

APPENDIX A. SIMPLIFIED ANALYSIS OF SLAB-ON-GIRDER DECKS

Cao and Shing (1999) have proposed a simplified analysis method to analyze slab-on-girder bridge decks with the consideration of differential girder deflections. In this method, differential girder deflections are approximated using an orthotropic plate model. This allows for the consideration of the effects of stiffness, spacing of the girders, and span length of the bridge on girder deflections. By combining the effects of the negative moment for a slab on rigid girders and the positive moment induced by differential girder deflections, the maximum negative bending moment in the deck can be determined. For calculation of the negative moment of a slab on rigid girders, a three-girder deck subjected to a wheel load at the middle of each span can be modeled as a single span slab simply-supported on one end, fixed on the other, and subjected to a wheel load at midspan. For the secondary positive bending moment induced by the differential deflection of the girders, an analysis of an infinitely wide simply-supported slab subjected to a prescribed deflection at the midspan is considered. The controlling factors in these calculations are the magnitude of the wheel load, the span-to-length ratio, and the stiffness ratio for the two bending directions. The following section provides a summary of the analysis procedure. The solution derived here can also be conservatively extended to a deck with more than three girders, where the maximum negative bending moment is expected to be over a girder next to the exterior girder.

Maximum Negative Bending Moment in Slabs on Flexible Girders

The Simplified Analysis Method allows for the determination of the maximum negative bending moment per unit width in a deck with consideration of differential girder deflections. It is calculated by the following equation:

$$M_t = M_1 + K_d M_o \qquad\qquad (A.1)$$

where M_1 = maximum negative bending moment in a deck with rigid girders, K_d = negative bending moment reduction factor and M_o = maximum positive bending moment in a simply-supported deck. The equations and concepts behind the computation of each of these variables are presented in the succeeding sections.

Maximum Positive Bending Moment in Slabs

The maximum positive bending moment (M_o) can be computed based on the formulation derived by Westergaard (1930) for an infinitely wide simply-supported slab with a load at the midspan. This load is considered to have a finite area.

$$M_o = \left[\frac{(1+v)\ln(4S/\pi c_1)+1}{4\pi}\right]P \qquad\qquad (A.2)$$

where v = Poisson's ratio, S = span length of the slab, P = magnitude of wheel load, and c_1 = equivalent diameter of the wheel load as given by the following equation.

$$c_1 = \begin{cases} 2\left(\sqrt{0.4d_1^2 + t^2} - 0.675t\right) & \text{for } d_1 < 3.45t \\ d_1 & \text{for } d_1 \geq 3.45t \end{cases} \qquad\qquad (A.3)$$

where t = thickness of the slab and d_1 = actual diameter of the wheel load. Article 3.30 of the AASHTO 16th Edition (AASHTO 1996) specifies a rectangular tire area of 0.01P (IN^2) and a length-to-width ratio of 1:2.5, where the length is considered to run in the direction of traffic and

P equals the wheel load in pounds. By equating a circular load footprint to this area, the equivalent diameter (d_1) of the wheel load can easily be determined.

In a continuous deck, the positive bending moment is less than that of a simply-supported slab. On the other hand, with the introduction of girder deflections, an increase in this positive bending moment will result. This slight increase, however, does not totally offset the reduction created by continuity. As a result, the positive bending moment in a continuous deck can be conservatively calculated by Equation A.2.

Maximum Negative Bending Moment in Slabs on Rigid Girders

To calculate the maximum negative moment in a slab supported on three rigid girders, it is reasonably accurate to assume that a concentrated load is applied at the middle of each span. The actual wheel spacing in an axle of an HS-20 truck will result in a smaller moment. This more conservative moment can be calculated by considering a slab that is fixed on one end and simply-supported on the other three sides, subjected to a point load at midspan. The maximum negative moment can be found by superimposing the two load cases in Figures A.1(a) and A.1(b) and allowing no rotation at the fixed edge.

The maximum negative bending moment in the slab occurs at x=S/2 and y=0 and is given by the following equation:

$$M_1 = -K_1 P \tag{A.4}$$

where

$$K_1 = \frac{S}{L} \sum_{m=1,3,5,\ldots}^{\infty} K_m \tag{A.5}$$

$$K_m = \sinh\frac{m\pi S}{2L} \bigg/ \left\{ \cosh^2\frac{m\pi S}{2L}\left[\frac{m\pi S}{2L}\left(\tanh^2\frac{m\pi S}{2L} + \coth^2\frac{m\pi S}{2L} \right) \right.\right.$$

$$\left.\left. -\frac{m\pi S}{2L} - \tanh\frac{m\pi S}{2L} - \coth\frac{m\pi S}{2L} \right] \right\} \tag{A.6}$$

in which P = magnitude of point load, S = span length (center-to-center spacing between girders) and L = width of slab (distance between abutments or supports).
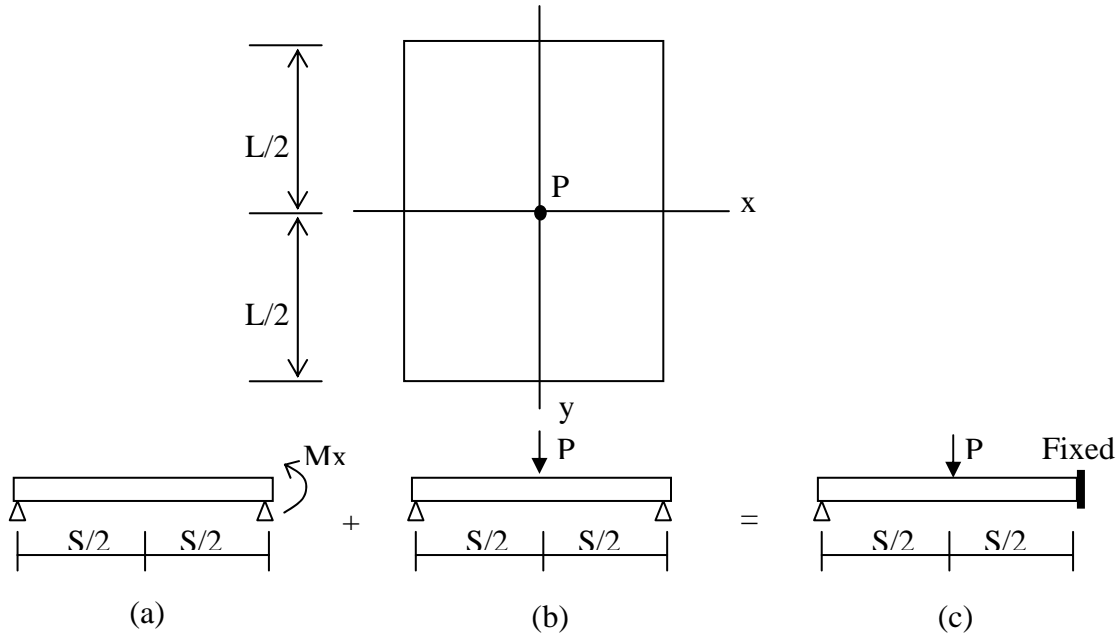

Figure A.1 – Slab Analysis: (a) Simply-supported Slab Subjected to Bending Moment along One Edge; (b) Simply-supported Slab Subjected to Point Load at Midspan; (c) Slab Subjected to Point Load at Midspan with One Edge Fixed and One Edge Simply-supported (Cao and Shing 1999).

However, Cao and Shing (1999) have shown that M_1 can be approximated conservatively by the following equations as shown in Figure A.2:

$$M_1 = \begin{cases} -0.2146P & \text{for S/L} \leq 0.75 \\ -0.064\left(4.1-\dfrac{S}{L}\right)P & \text{for S/L} > 0.75 \end{cases} \tag{A.7}$$
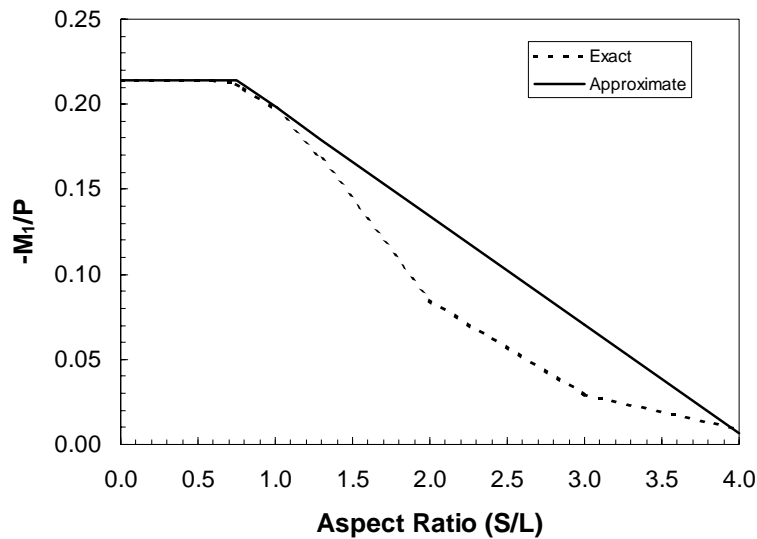
Figure A.2 – Exact and Approximate Slab Maximum Negative Bending Moments (Cao and Shing 1999)

Negative Bending Moment Reduction Factor

Cao and Shing (1999) have established a coefficient K_d, termed the negative bending moment reduction factor to account for differential girder deflections. When applied to the maximum positive bending moment, M_o, in a simply-supported slab, it provides the reduction allowed for the maximum negative bending moment due to girder deflections as shown in Equation A.1. This factor has been derived analytically and modified based on curve-fitting in order to create a function more in agreement with the results of finite element analysis of slab-on-girder decks. As is evident, the influence of girder deflections largely depends on the position of the load from the girder supports. A load at midspan between roller supports will produce minimum negative moments as opposed to a load near the supports.

The reduction factor derived by Cao and Shing (1999) is given as follows:

$$K_d = K_{do} \sin \frac{\pi d}{L} \tag{A.8}$$

where

$$K_{do} = 0.2176 \left(\frac{L}{S}\right)^2 \sqrt{\frac{D_x}{D_y}} e^{-\frac{\pi \alpha S}{2L}} \left[\left(\frac{1}{\alpha}\cos\frac{\pi \beta S}{2L} + \frac{1}{\beta}\sin\frac{\pi \beta S}{2L}\right) \right.$$
$$\left. -\left(\frac{1}{\alpha}\cos\frac{3\pi \beta S}{2L} + \frac{1}{\beta}\sin\frac{3\pi \beta S}{2L}\right) e^{-\frac{\pi \alpha S}{L}}\right] \tag{A.9}$$

$$D_x = \frac{E_c t^3}{12\left(1 - v_c^2\right)} \tag{A.10}$$

$$D_y = \frac{E_g I_{gc}}{S} \tag{A.11}$$

$$I_{gc} = \frac{E_c}{E_g\left(1 - v_c^2\right)}\left(\frac{S t^3}{12} + S t e_2^2\right) + I_g + A_g e_1^2 \tag{A.12}$$

$$\alpha = \left[\frac{1}{2}\left(\sqrt{\frac{D_y}{D_x}} + 1\right)\right]^{\frac{1}{2}} \tag{A.13}$$

$$\beta = \left[\frac{1}{2}\left(\sqrt{\frac{D_y}{D_x}} - 1\right)\right]^{\frac{1}{2}} \tag{A.14}$$

in which e_2 = distance between the neutral axis of the composite section and the mid-height of the slab, as shown in Figure A.3, e_1 = distance between the neutral axis of the composite section and the neutral axis of the girder, E_c = modulus of elasticity of concrete, E_g = modulus of elasticity of girder, v_c = Poisson's ratio of the concrete slab, t = thickness of the slab, I_{gc} = moment of inertia of the composite section, A_g = area of the girder, S = span length of slab, and d = distance of the load from the nearest abutment (or support).
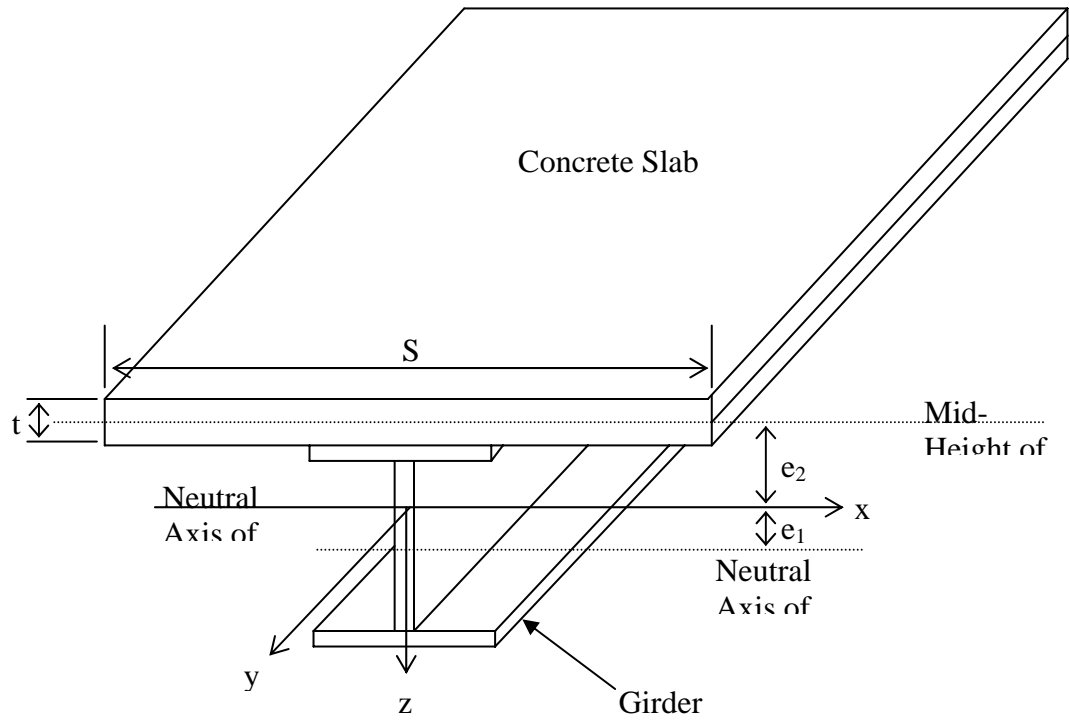
Figure A.3 – T-Beam Section of Deck (Cao and Shing 1999)

APPENDIX B. CALCULATION OF ARCHING CAPACITY

Many researchers have attempted to consider the arching mechanism to account for the enhancement of load-carrying capacity in slabs. The method proposed by Rankin and Long (1997) exhibits a sound theoretical foundation and is yet simple enough for practical applications. This method was first introduced by McDowell et al. (1956). An illustration of the behavior of a concrete slab under the effects of arching as described by Rankin and Long is shown in Figure B.1.

Based on kinematics and the nonlinear stress-strain properties of concrete, the ultimate load that can be carried by a bridge deck can be computed using the following procedure.
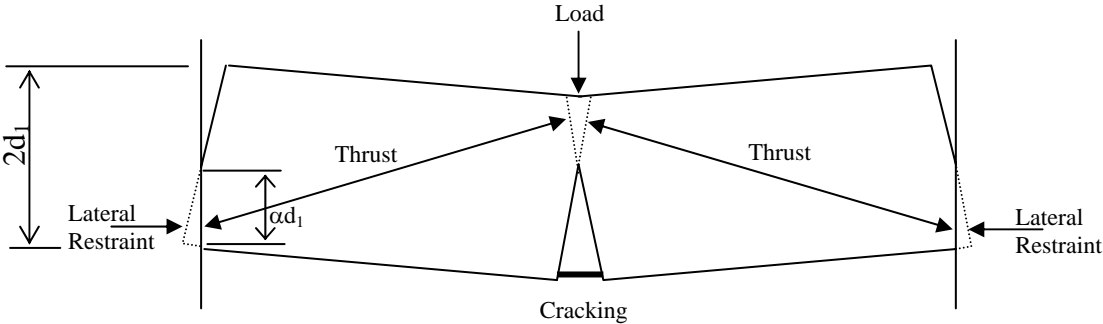

Figure B.1 – Arching Action in Reinforced Concrete Slab Strip (Rankin and Long 1997)

Determination of Arching Moment

This method introduces two parameters, R and u, for determining the distribution of stress at the contact areas. The parameter, R, provides a basis for measuring the slenderness of the member, and u provides a basis for quantifying the deflection as normalized by the depth of the member.

$$R = \frac{\varepsilon_c L_r^2}{4d_1^2} \tag{B.1}$$

$$u = \frac{w}{2d_1} \tag{B.2}$$

where ε_c = the yield strain of the equivalent elastic-plastic stress-strain relation of concrete, which will be explained later, w = midspan deflection, L_r = half span of rigidly restrained slab, and d_1 = half depth of section available for arching.

Because of the bending, the depth of the member available for arching must be reduced by the depth of the compression zone in the concrete required to balance the counteracting tensile force in the reinforcement. The depth available to contribute to the arching capacity can be estimated as:

$$d_1 = \frac{1}{2}\left[h - \left(\rho^+ + \rho^-\right)\frac{f_y d}{0.85 f'_c}\right] \tag{B.3}$$
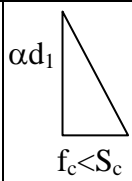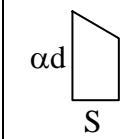
where h = actual depth of the section, ρ^+ = positive reinforcement ratio, ρ^- = negative reinforcement ratio, f'_c = compressive strength of concrete, and d = effective depth of the slab.

The normalized arching moment can be calculated with the formulations in Table B.1 and is defined as:

111

$$M_r = \frac{4M(u)}{S_c d_1^2} \tag{B.4}$$

where $M(u)$ = arching moment at deflection u, and S_c = compressive strength of concrete using the equivalent elastic-plastic stress-strain curve.

Table B.1 – Arching Moment Equations (Rankin and Long 1997)

R	u	Stress Distribution	M_r

$R \geq 0.5$
  $R < 0.5$
	$u \geq 0$
	  $0 \leq u \leq 1 - \sqrt{1 - 2R}$
		αd_1
		 $f_c < S_c$
			$\frac{8u}{3R}\left(1 - \frac{5u}{4}\right)\left(1 - \frac{u}{2}\right)^2$

$R < 0.5$	$1 - \sqrt{1 - 2R} \leq u < \sqrt{2R}$	αd S	$4\left(1 + \frac{R}{2} + \frac{3u^2}{4} - 2u - \frac{R^2}{3u^2}\right)$

In Table B.1, αd_1 = depth of contact area expressed as proportion of half depth of the member where

$$\alpha = 1 - \frac{u}{2} \tag{B.5}$$

In order to determine the maximum normalized arching moment, the equations in column four can be differentiated with respect to u and set equal to zero, resulting in the following:

$$20u^2 - 32u + 8 = 0 \tag{B.6}$$

$$6u - 8 + \frac{8R^2}{3u^3} = 0 \tag{B.7}$$

112

These equations were solved for u with given values of R. The resulting u values are then substituted back into the original equations in the table giving the maximum values of M_r. This leads to the following expressions for M_r^{max}:

$$M_r^{max} = \begin{cases} \dfrac{0.3615}{R} & \text{for } R > 0.26 \\ 4.3 - 16.1\sqrt{3.3x10^{-4} + 0.1243R} & \text{for } 0 < R < 0.26 \end{cases} \qquad (B.8)$$

Subsequently, the maximum arching moment resistance can be calculated from Equation B.4 by assuming a maximum concrete stress $S_c = 0.85f'_c$.

$$M_a = \frac{0.85M_r^{max}f'_c bd_1^2}{4} \qquad (B.9)$$

where b is the effective width of the slab.

Equivalent Trapezoidal Stress Distribution

Rankin and Long's model is based on an idealized elastic-plastic stress-strain relation for concrete. With this assumption, concrete stress will increase linearly with respect to strain until the concrete strain reaches ε_c as shown in Figure B.2. Once this strain is achieved, concrete becomes plastic. ε_c is calculated as follows:

$$\varepsilon_c = 2\varepsilon_u(1 - \beta_1) \qquad (B.10)$$

where ε_u = ultimate strain in the concrete and β_1 = the ratio of the depth of the equivalent compression zone to the distance from the extreme compression fiber to the neutral axis per rectangular stress block theory. This equation is derived by equating the area under the elastic-plastic curve to that of a rectangular stress block as shown in Figure B.2.

By relating the parameters of the equivalent rectangular stress block to a parabolic stress-strain curve of concrete, the following formula has been obtained for ε_c by Rankin and Long.

$$\varepsilon_c = \left(-400 + 414f'_c - 15.7{f'_c}^2\right) \times 10^{-6} \qquad\qquad (B.11)$$

where f'_c = the 28-day compressive strength of concrete given in ksi.
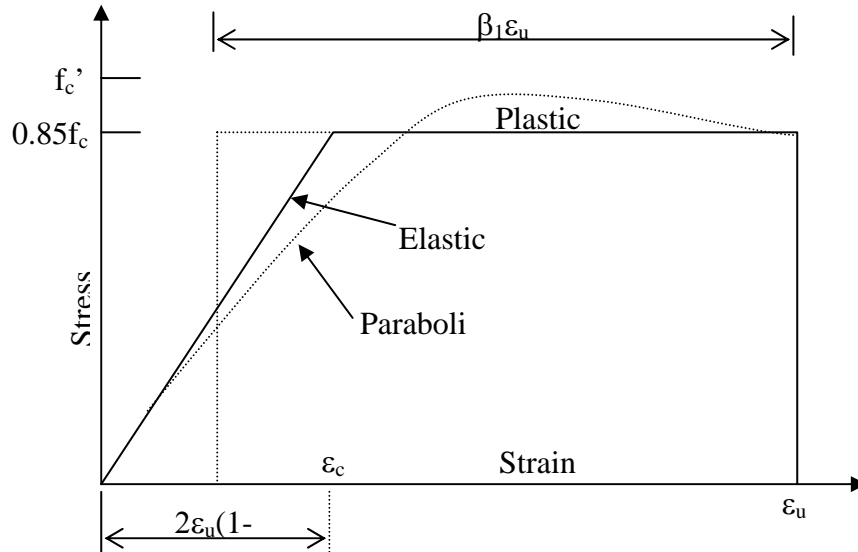

Figure B.2 – Idealized Stress-strain Relationships for Concrete (Rankin and Long 1997)

Lateral Restraint

The degree of lateral restraint plays a major role in the arching mechanism. Since the restraints of a deck slab are never perfectly rigid, the full effects of arching cannot be achieved. In order to analyze this reduction, a slab strip with less than rigid restraints can be modeled by a three-hinged arch with elastic spring restraints as seen in Figure B.3(a). The same arch with rigid restraints is shown in Figure B.3(b). To account for this situation, Rankin and Long have proposed a relation between the span length of a rigidly supported arch to that of an elastically restrained arch that will result in the same load-deformation relation.

$$L_r = L_e\left[\left(\frac{E_c A}{KL_e}\right) + 1\right]^{\frac{1}{3}} \qquad\qquad (B.12)$$

where L_e = half span of the elastically restrained strip, E_c = modulus of elasticity of concrete, A = effective area of arch leg given by d_1 times the width of the section b and K = stiffness of elastic spring restraint.
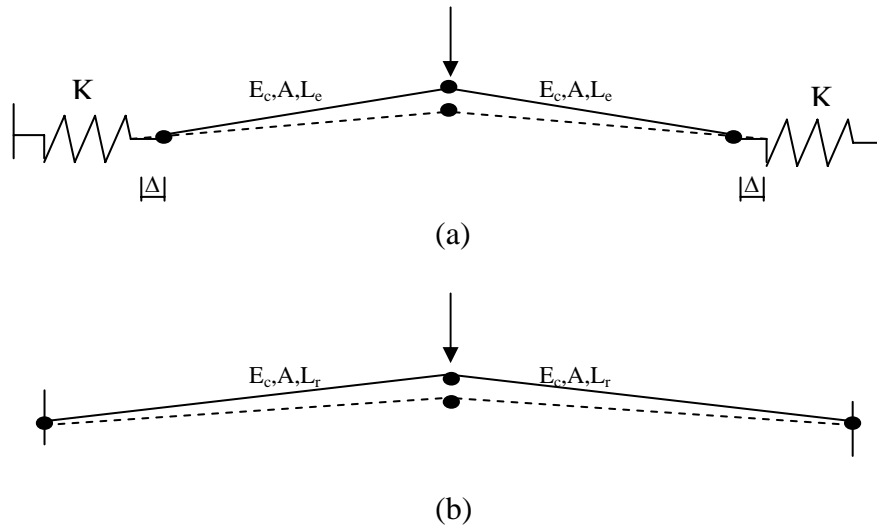

Figure B.3 – Equivalent Three-hinged Arches: (a) Elastically-restrained Arch; (b) Rigidly-restrained Arch (Rankin and Long 1997)

The relation presented in Equation B.12 shows that when the restraint stiffness equals the stiffness of the arch leg (i.e., $K = E_cA/L_e$), the maximum arching moment constitutes approximately 50-80% of the arching moment for a rigid restraint depending on the slenderness of the member.

Interaction of Bending and Arching Action

The interaction between the bending moment capacity produced by the reinforcement and the arching capacity can be estimated by considering the components separately. The bending moment is calculated using the simple beam theory:

$$M_b = \rho f_y d^2 \left(1 - 0.6\rho \frac{f_y}{f'_c} \right) \tag{B.13}$$

where M_b = bending moment capacity, ρ = reinforcement ratio, f_y = yield strength of reinforcement, d = effective depth of reinforcement and f'_c = compressive strength of concrete.

The ultimate load capacity can then be calculated as the sum of the load resisted by both bending and arching with the assumptions that the maximum arching moment develops after the yielding of the reinforcement and the bending deformation necessary for yielding can be neglected.

The ultimate load-carrying capacity of a slab due to bending and the arching mechanism can be calculated as:

$$P_p = P_b + P_a \tag{B.14}$$

where

$$P_b = k \left(M_b^+ + M_b^- \right) \tag{B.15}$$

$$P_a = k M_a \tag{B.16}$$

in which M_b^+ = the bending moment resisted by the positive reinforcement, M_b^- = the bending moment resisted by the negative reinforcement, and M_a = the moment resisted by the arching mechanism. The k factor depends on the load type and is determined by the equilibrium condition of the member. If the member is subjected to a uniform loading condition, k = 8/L. If a point load is applied at the midspan of the member, k = 4/L, where L is the span length.

APPENDIX C. PUNCHING SHEAR CAPACITY

The punching shear analysis method presented here is based on the work of Tsui, Burns

and Klingner (1986). Although it does not directly consider boundary restraints, it does allow

for varying failure angles. The failure angle can be determined experimentally with the

application of a rectangular load. Then, by summing the vertical components of the tensile

forces on the failure plane of this rectangular footprint and applying the principle of equilibrium,

the punching shear capacity can be determined.

Calculation of Punching Shear Capacity

The equation adopted by both ACI 318-99 (ACI 1999) and the AASHTO 16th Edition

(AASHTO 1996) for the determination of the punching shear capacity of a deck has proven

extremely conservative when compared to experimental results. The equation is expressed as

follows:

$$V_c = \left(2 + \frac{4}{\beta_c} \right) \sqrt{f'_c} b_o d \le 4 \sqrt{f'_c} b_o d \qquad (C.1)$$

where V_c = the punching shear strength (LBS) of the deck, β_c = ratio of the long side of the

loaded area to the short side, b_o = perimeter (IN) of the critical section taken to be at mid-depth,

d = the distance (IN) from the extreme compression fiber to the centroid of the tension

reinforcement, and f'_c = the compressive strength (PSI) of concrete.

The above equation assumes that the punching shear failure angle is 45 degrees. The 45-

degree assumption was found to be too conservative by Tsui et al. (1986). They have proposed

the use of a more general equation that takes into account the anticipated angle of failure (θ).

This formula is derived for a rectangular loading area, assuming that the failure surface

propagates downward at the same angle on all sides to a depth equal to the average effective depth of the section as detailed in Figure C.1.
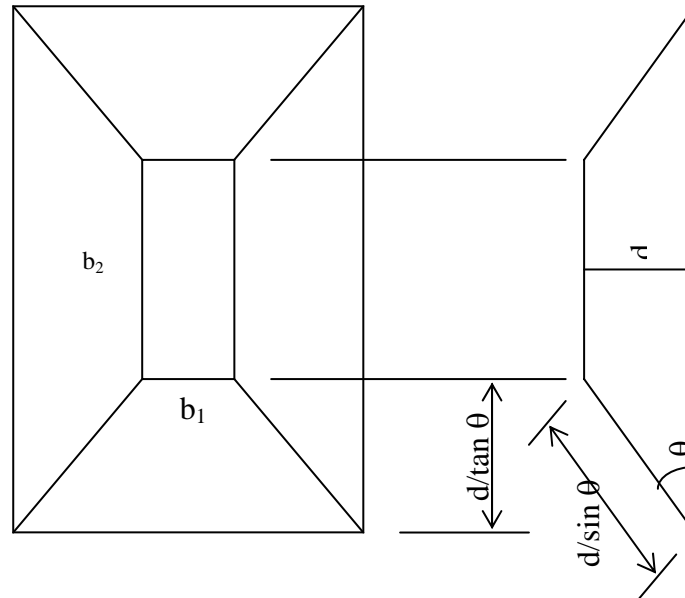

Figure C.1 – Plan and Sectional View of Failure Angle and Surface for General Model for Punching Shear (Tsui et al. 1986).

The formula is expressed as follows:

$$V_c = \frac{2d}{\tan\theta}\left(b_1 + b_2 + \frac{2d}{\tan\theta}\right)f_t$$ (C.2)

where b_1 = the length of the short side of the loaded rectangular area, b_2 = the length of the long side of the loaded rectangular area, d = the average distance from the extreme compression fiber to the centroid of the tension reinforcement, and f_t = the ultimate tensile strength of concrete given by the following equation.

$$f_t = \left(2 + \frac{4}{\beta_c}\right)\sqrt{f'_c} < 4\sqrt{f'_c}$$ (C.3)

REFERENCES

1) AASHTO (1998), *Standard Specifications for Highway Bridges - LRFD.* 2nd Ed., American Association of State Highway and Transportation Officials, Washington, D.C.

2) AASHTO (1996), *Standard Specifications for Highway Bridges.* 16th Ed., American Association of State Highway and Transportation Officials, Washington, D.C.

3) ACI Committee 440 (2000), *Guide for the Design and Construction of Concrete Reinforced with FRP Bars - Draft Document.* American Concrete Institute, Farmington Hills, MI.

4) ACI Committee 318 (1999), *Building Code Requirements for Reinforced Concrete (ACI 318-99).* American Concrete Institute, Farmington Hills, MI.

5) Borlin, K. A. (2001), "Bridge Deck Design Accounting for Girder Deflections, Arching Action and Punching Shear Capacity." *Master Thesis*, Department of Civil, Environmental, and Architectural Engineering, University of Colorado, Boulder, CO.

6) Cao, L. and Shing, P. B. (1999), "Simplified Analysis Method for Slab-on-Girder Highway Bridge Decks." *Journal of Structural Engineering,* ASCE, Vol. 125, No. 1, pp. 49-59.

7) Cao, L., Allen, J. H., Shing, P. B., and Woodham, D. (1996), "Behavior of RC Bridge Decks on Flexible Girders." *Journal of Structural Engineering,* ASCE, Vol. 122, No. 1, pp. 11-19.

8) deV. Batchelor, B., Hewitt, B. E., Csagoly, P. and Holowka, M. (1972), "Investigation of the Ultimate Strength of Deck Slabs of Composite Steel/Concrete Bridges." *Transportation Research Record No. 664,* TRB, National Research Council, Washington, D.C., pp. 162-170.

9) deV. Batchelor, B., Hewitt, B. E. and Csagoly, P. (1978), "Investigation of the Fatigue Strength of Deck Slabs of Composite Steel/Concrete Bridges." *Transportation Research Record No. 664,* TRB, National Research Council, Washington, D.C.

10) Dolan, C. W., Hamilton, H. R., Bakis, C. E., and Nanni, A. (2000), "Design Recommendations for Concrete Structures Prestressed with FRP Tendons." *Report No. DTFH61-96-C-00019*, Federal Highway Administration, Washington, D.C.

11) Mahmoud, Z. I., Rizkalla, S. H., and Zaghloul, E. R. (1999), "Transfer and Development Lengths of Carbon Fiber Reinforced Polymers Prestressing Reinforcement", *ACI Structural Journal*, Vol. 96, No. 4, pp. 594-602.

12) McDowell, E. L., McKee, K. E., and Sevin, E. (1956), "Arching Action Theory of Masonry Walls." *Journal of the Structural Division,* Proc. ASCE, Vol. 82, No. ST2, pp. 915-1 to 915-18.

13) Ontario Ministry of Transportation & Communications (1979), *The Ontario Highway Bridge Design Code.* Toronto, Ontario, Canada.

14) Ontario Ministry of Transportation & Communications (1991), *The Ontario Highway Bridge Design Code.* Toronto, Ontario, Canada.

15) Rankin, G. I. B. and Long, A. E. (1997), "Arching Action Strength Enhancement in Laterally-Restrained Slab Strips." *Structures and Buildings,* Vol. 122, No. 4, pp.461-467.

16) Tsui, C. K., Burns, N. H., and Klinger, R. E. (1986), "Behavior of Ontario-Type Bridge Deck on Steel Girders: Negative Moment Region and Load Capacity." *Report No. 350-3*, Center for Transportation Research, Bureau of Engineering Research, University of Texas, Austin, TX, pp. 71-87.

17) Westergaard, H. M. (1930), "Computations of Stresses in Bridge Slabs due to Wheel Loads." *Public Roads*, March, 1-23.

18) Zylstra, R., Shing, P. B., and Xi, Y. (2001), "Evaluation of FRP Prestressed Panels/Slabs for I-225/Parker Road Project." *CDOT Report No. CDOT-DTD-R-2001-14*, Colorado Department of Transportation, Denver, CO.